Experimental investigation of the weldability of high strength aluminium alloys using friction spot welding

Jeroen Vercauteren

Supervisors: Prof. dr. ir. Wim De Waele, Dr. ir. Koen Faes (BIL)

Master's dissertation submitted in order to obtain the academic degree of
Master of Science in Electromechanical Engineering

Department of Electrical Energy, Metals, Mechanical Constructions & Systems
Chair: Prof. dr. ir. Luc Dupré
Faculty of Engineering and Architecture
Academic year 2016-2017

GHENT
UNIVERSITY

Experimental investigation of the weldability of high strength aluminium alloys using friction spot welding

Jeroen Vercauteren

Supervisors: Prof. dr. ir. Wim De Waele, Dr. ir. Koen Faes (BIL)

Master's dissertation submitted in order to obtain the academic degree of
Master of Science in Electromechanical Engineering

Department of Electrical Energy, Metals, Mechanical Constructions & Systems
Chair: Prof. dr. ir. Luc Dupré
Faculty of Engineering and Architecture
Academic year 2016-2017

GHENT
UNIVERSITY

Preface

In this preface, I would like to take the opportunity to express my gratitude to the following people, who have helped and supported me during the course of this master dissertation.

Dr. ir. Koen Faes of the Belgian Welding Institute who granted me the opportunity to work on one of his projects. I want to thank him for his dedicated help, support and advice during the daily research. He was always available for advice and eager to help.

Prof. dr. ir. Wim De Waele for his guidance, strong involvement and critical point of view. The energy and passion he showed for my work was truly motivating.

Ir. Irene Kwee of the Belgian Welding Institute for her support with Design of Experiments and the interest she showed in my experimental results.

Gert Oost and ing. Michel De Waele of the Belgian Welding Institute for their assistance during the preparations of the metallographic samples and hardness measurements. Besides the professional assistance, they made the work enjoyable.

The Belgian Welding Institute for supplying materials and means and all its employees. It has been an enjoyable time working in this friendly setting.

Furthermore, I would like to thank my fellow students and friends for the support; especially Barbara Simoen for her daily motivation, Cedric De Beule for proofreading this work and Stef De Wilde for being a supportive roommate.

Finally, I thank my parents, for allowing me to continue studying and supporting me throughout my academic career.

Jeroen Vercauteren, June 2017

Experimental investigation of the weldability of high strength aluminium alloys using friction spot welding

By Jeroen Vercauteren

Master's dissertation submitted in order to obtain the academic degree of Master of Science in Electromechanical Engineering

Faculty of Engineering and Architecture

Academic year 2016-2017

Supervisors: Prof. dr. ir. Wim De Waele, Dr. ir. Koen Faes (BIL)

Department of Electrical Energy, Metals, Mechanical Constructions & Systems
Chair: Prof. dr. ir. Luc Dupré

Abstract

In this master dissertation, the weldability of high strength aluminium alloy EN AW-7075-T6 using friction spot welding is investigated. Lightweight high-strength alloys are nowadays very popular in transport and aeronautic applications. A solid-state welding technique to join such materials in overlap configuration is friction spot welding. Materials can be joined without melting the material or adding extra mass to the system. A three-component tool is plunged into the workpiece material and a bond is formed by frictional heat and plastic work. The surface has, in contrast to friction stir spot welding, a flat finish without the presence of a keyhole. The objective of this research is to investigate the influence of the welding process parameters on the weld quality. The parameters rotational speed, plunge depth and joining time were varied according to a design of experiments approach. The weld quality was evaluated using metallographic inspection and imperfection dimensions were quantified. Furthermore, the softening of the weldment was inspected using microhardness testing and surface temperature measurements. The strength of the welds was evaluated by means of lap shear and cross-tension tests. It is concluded that an increasing joining time and plunge depth are beneficial for the mechanical and microstructural weld quality. A lower rotational speed results in a larger and more fine-grained nugget area and hence increases the loading capacity.

Keywords: friction spot welding, refill FSSW, EN AW-7075-T6, parameter study

Experimental investigation of the weldability of high strength aluminium alloys using friction spot welding

Jeroen Vercauteren

Supervisor(s): Dr. ir. Koen Faes, Prof. dr. ir. Wim De Waele

***Abstract*: Friction spot welding is a recent solid-state welding technique, well suited for spot-joining lightweight materials in overlap condition. Aerospace and transport industries show great interest in this technique to join high-strength aluminium alloys, but published research is still limited. In this work, the relation between process parameters and weld quality is investigated for EN AW-7075-T6 material. Techniques used are metallographic qualification, measuring of temperature profiles, hardness measuring, lap shear testing and cross-tension testing. The welding parameters of interest have been optimized; a weld with a lap shear strength of 8.74 ± 1.32 kN and a cross-tension strength of 2.57 ± 0.29 kN has been produced.**

***Keywords:* friction spot welding, EN AW-7075-T6, parameter study**

I. Introduction

High strength aluminium alloys gain importance in industry, especially in automotive and aeronautic fields. Joining of these materials is an important step in the production of components or structures. Many joining techniques exist such as fusion welding, riveting, bolting, etc. Nevertheless, researchers keep looking for more efficient alternative techniques as each joining technology has its disadvantages.

Friction spot welding (FSpW) offers a solution to most of the issues concerning lightweight materials. FSpW is a solid-state welding process well suited for spot-joining lightweight materials in overlap configuration. It differs from the friction stir spot weld (FSSW) process in the ability to refill the keyhole created by the tool plunging and hence eliminates its major disadvantages: stress concentration and corrosion danger at the keyhole. Friction spot welding is seen as a green manufacturing method because no additional filler material is required and there is no waste material [1]. The goal of this work is the evaluation of the weldability of high-strength aluminium alloys using friction spot welding. In previous work [2], the weldability of alloy EN AW-7475-T761 has been evaluated; this study focuses on aluminium alloy EN AW-7075-T6.

II. Friction spot welding

A. Process description

The friction spot welding process is a solid-state spot joining technology to join sheets in overlap condition. The solid-state property implies that the working temperature does not exceed the melting temperature of the materials. The joint is fully generated by frictional heat and plastic work whereby a metallurgical bond is formed. The non-consumable tool consists of three components: a concentric clamping ring, a sleeve and a pin. All three components act independently in the axial direction. The pin and sleeve can rotate around their axis in the same direction. The function of the clamping ring is to fix the sheets rigidly in overlap configuration by pressing them against a backing anvil while the welding process takes place.

The four process stages are depicted in Figure 1. In the first stage, the clamping ring fixes the plates while the pin and the sleeve start rotating against the upper plate. As from the second stage the sleeve plunges into the material while rotating at a high rotational speed. Meanwhile, the pin rises, creating a cavity of the exact required volume for the plasticised material. The sleeve displaces the material underneath it and forces it into the cavity provided by the pin rise. Between the second and the third stage, the sleeve reaches a pre-defined depth. The frictional heat and mechanical work delivered by the stirring, bond the sheets at their interface. In the third stage, tool and sleeve translation reverse. The plasticised material that accumulated under the pin is pushed back into the keyhole created by the sleeve plunging. When retreating the complete tool in stage four, a flat surface is visible.

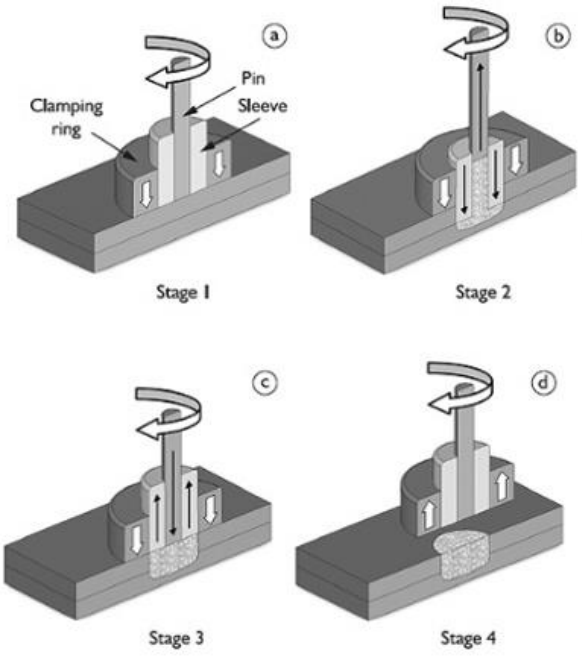

Figure 1: Friction spot welding sleeve plunge stages [3]

The process, and thus the weld quality, is controlled by several welding parameters. This work focusses on three parameters: rotational speed, plunge depth and joining time. The rotational speed (RS) of the pin and the sleeve controls the

material flow. A critical, and very material dependent parameter is the plunge depth (PD). This is the maximum depth that the sleeve plunges into the material, measured from the top surface of the upper sheet. A third process parameter is the joining time (JT) which consists of three sub-parameters: plunge time (PT), dwell time (DT) and retraction time (RT). These time parameters are graphically visualized in Figure 2. The total joining time influences the amount of heat input, the plunge time and retraction time determine the rate of plastic deformation of the weld zone. Related parameters are the plunge rate (PR) and retraction rate (RT).

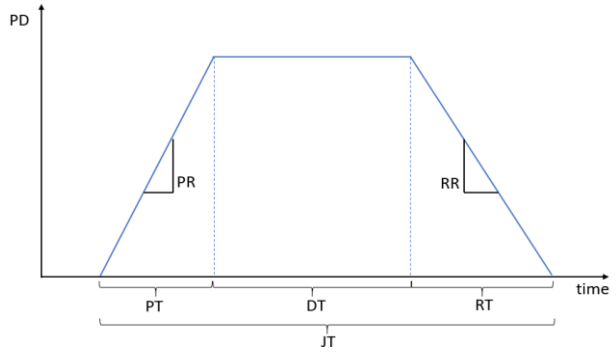

Figure 2: Plunge depth versus time and the different time parameters composing the joining time

B. *Weld cross-section*

A friction spot weld consists of different microstructural regions, called weld zones. Figure 3 shows the stir zone (SZ) and the thermo-mechanically affected zone (TMAZ). A third weld zone, the heat-affected zone (HAZ), is not clearly visible on the optical microscope image. All weld zones differ in microstructure and mechanical properties from the base material (BM) as a result of the welding process. The SZ is the centre of the weld and has approximately the same width as the sleeve diameter. It is characterized by refined and equiaxed grains as a result of dynamic recrystallization. This is the effect of the high strain rate and the high local temperatures during the stirring process [4]. Next to the SZ, the TMAZ exists as a transitional region between the SZ and the HAZ. This zone is formed by moderate deformations and temperatures. The microstructure is characterized by elongated and deformed grains caused by the material flow. As the TMAZ is a transition region between the SZ and the HAZ, it is hard to define the boundaries. The boundary between the TMAZ and the HAZ is defined as the location with the minimum hardness but cannot be indicated on a metallographic cross-section. The HAZ is the first zone that is not affected by plastic deformations, but solely by the thermal cycle. Far enough from the weld centre, all effects from the welding process on the microstructure disappear. This is where the HAZ ends and the BM starts

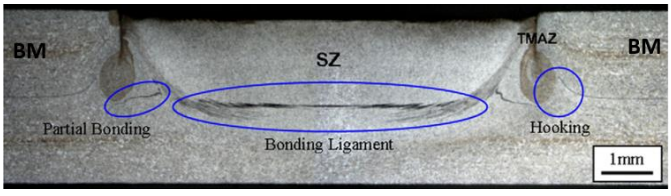

Figure 3: Typical cross-section of a FSpW weld in EN AW-6181-T4 [5]

Three geometrical features are often reported in metallographic inspection: hooking, partial bonding and bonding ligament. The location and appearance of these geometrical features are indicated in Figure 3. The hook feature is a transitional zone between the completely bonded regions and separated interfaces. It is suggested that its formation arises from the plastic upward bending of the interface due to tool penetration into the lower sheet. The bonding ligament is a region of good adhesion between the upper and lower sheet material [5]. It is located underneath the stir zone and forms the strongest metallurgical bond in the weld. However, the presence of the bonding ligament is not always visible in all materials. Finally, the partial bonding zone is a transition region between the hooking and the bonding ligament with minor bonding strength.

Apart from the features described above, imperfections related to improper welding parameter combinations can occur such as lack of mixing, void inclusions or incomplete refill. All these imperfections are located along the path of the sleeve plunge and thus associated with the material flow. Incomplete refill can partly be assigned to the extrusion of material into the tolerance gap between the clamping ring and the sleeve [6].

III. Experimental Study

A. *Materials and equipment*

The experiments were performed using commercial friction spot welding equipment RPS 100 (Harms & Wende, Germany). Overlap welds were produced in EN AW-7075-T6 sheet material with a thickness of 1.6 mm. The weld cross-section was inspected under an Olympus MX51 optical microscope in non-etched and etched state. Transverse microhardness measurements at half the upper sheet thickness were performed on a Struers Duramin A300 machine at a load of 0.5 kgf and with a spacing of 0.5 mm. Temperature profiles were obtained during the welding process using a K-type thermocouple attached at the workpiece upper surface at 14 mm away from the weld centre. Two destructive strength testing procedures were performed on a tensile machine Instron model 8801: a lap shear test at a displacement rate of 10 mm/min and a cross-tension tests at a displacement rate of 1 mm/min.

B. *Experimental weld matrix*

Three parameters of interest were varied according to the values given in Table 1. Other process parameters were kept constant to exclude their influence on the weld quality. The plunge and retraction rate were fixed at 0.8 mm/s and the clamping pressure at 3.5 bar. The dwell time follows from the joining time. Not all combinations were performed, but selections were made using design of experiments techniques: full factorial design and box-behnken design.

Table 1: Process parameters of interest and their tested range

Joining time (s)	6 – 7 – 8 – 9 – 10
Plunge depth (mm)	1.6 – 2.0 – 2.2 – 2.4
Rotational speed (rpm)	1000 – 2000 – 3000

IV. Results

A. Metallographic evaluation

The typical microstructural zones and features discussed above were all observed in the metallographic cross-sections. The influence of different welding parameters on the cross-section appearance is investigated by varying one parameter at a time. In each cross-section, the depth of the incomplete refill imperfection and the total area percentage of imperfections (incomplete refill, voids, non-bonded interface, tool misalignment, etc.) were measured.

For an increase in joining time, fewer imperfections are present and the incomplete refill imperfection is remarkably shallower. Furthermore, the stir zone microstructure shows finer grains due to the increased heat input and time for dynamic recrystallization. Besides the varying depth of the stir zone, the plunge depth has a large influence on the presence of interface imperfections. For a plunge depth which is equal to the upper plate thickness, interface imperfections such as a non-bonded interface and a partial bonding are more frequently observed.

The rotational speed has a large influence on the weld nugget size and appearance as depicted in Figure 4. For a lower rotational speed, the weld nugget reaches much deeper into the lower sheet. Moreover, the grain structure is much finer with a distinctive vertical band of coarse grains at the weld centre. At higher rotation speeds, the stir zone is much coarser and does not reach deeper than the tool plunge depth. The reason for this phenomenon is not yet completely understood since the material undergoes a complex process of microstructural changes, plastic deformation and precipitation state changes.

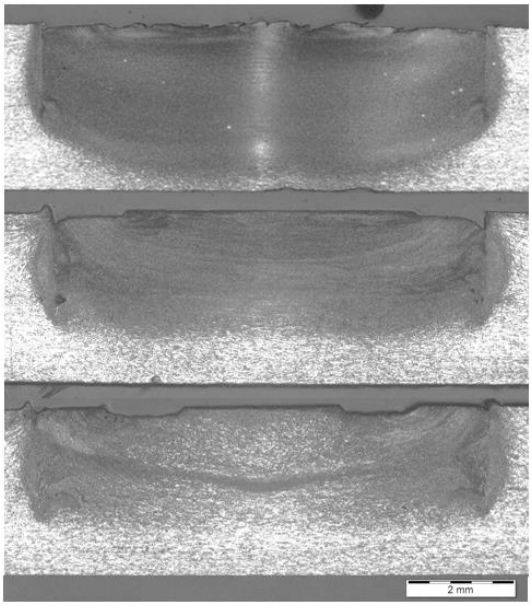

Figure 4: Cross-sectional overview of welds produced at varying RS: 1000 rpm (top), 2000 rpm (middle) and 3000 rpm (bottom); fixed parameters: JT=8 s, PD=2mm

B. Softening of the weldment

To investigate the influence of the welding parameters on the softening of the weldment, temperature measurements during processing and microhardness measurements are compared. The maximum temperatures that were recorded at the surface at 14 mm away from the weld centre ranged from 150 °C to 263 °C.

For a longer joining time, the peak temperature is higher which can be attributed to the increased heat input. This trend is also visible in the transverse hardness profile given in Figure 5. For the lowest joining time, and thus the lowest heat input, the width of the HAZ is smaller and the minimum hardness is higher. The W-shaped hardness profile is very typical for a friction spot weld. At the left, the base material shows a constant hardness value. Going to the right, the hardness decreases in the HAZ, with a minimum at the boundary between the HAZ and the TMAZ. This softening is attributed to the coarsening of the grains and the precipitates in the HAZ. The average hardness reduction obtained is 35 %. The stir zone is recognizable by the plateau profile and has an elevated hardness compared to the TMAZ as a result of the dynamic recrystallization.

The rotational speed has a similar influence on the softening of the weldment. For higher rotational speeds, the heat input is higher as a result of the additional frictional heat in the same time unit. Hence, higher peak temperatures are reached at a high rotational speed. The HAZ is for this case wider and has a larger hardness reduction. The opposite is true for a low rotational speed of 1000 rpm.

Finally, welding with a higher plunge depth increases the workpiece temperature. This can be explained by the increased friction surface and the large volume of plastically deformed material. Conclusions from the hardness measurements were less clear but based on literature [7], it is expected that a higher plunge depth leads to more softening.

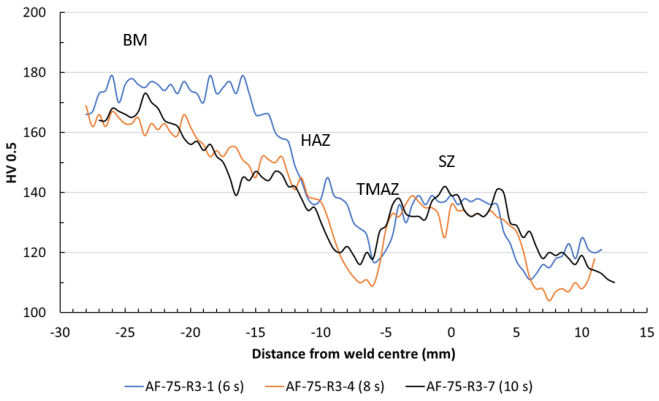

Figure 5: Hardness profile at half upper plate thickness for varying JT; PD=1.6 mm, RS=1000 rpm

C. Weld strength and failure mode

Lap shear tests and cross-tension tests were executed and interpreted according to a design of experiments approach. This helped identifying the main and interaction parameter effects on the weld strength. The same conclusions were made for the lap shear test and the cross-tension test, although the welds were loaded in a completely different direction. As expected, the cross-tension test showed lower strength values since a lap joint is not designed to take up normal forces. The plunge depth has the largest influence. It is concluded that the minimum plunge depth of 1.6 mm, equal to the upper plate thickness, should be avoided. The typical interface imperfections that occur with this low plunge depth, are detrimental for the weld

strength. A deeper plunge depth is observed as beneficial for both lap shear and cross-tension loading. This positive influence can be attributed to the increased load bearing nugget size. Similarly, an increase in joining time led to higher strength values as depicted by the trendline in Figure 6. The data points represent an average value of different welding combinations with a certain joining time. Error bars are added to show the variability on the trend. A plateau value of the strength is reached at a joining time of 8 s. Further increase of the joining time only results in a negligible strength increase. Again, this influence can be related to the decrease in weld imperfections at longer joining times.

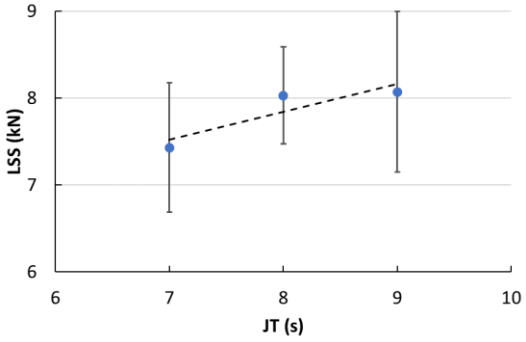

Figure 6: Influence of the joining time on the lap shear strength: mean value, standard deviation and trend line

The interaction between plunge depth and joining time was also identified as a significant effect. When both a deep plunge depth and a long joining time are combined, the weld strength increases strongly. Only when these two parameters were optimized, the effect of the rotational speed became detectable. The strongest welds were produced at a rotational speed of 1000 rpm. This parameter setting was related with the largest load bearing nugget, the finest grains and the smallest HAZ. All these characteristics contribute to a strong weld. The strongest weld was produced at a rotational speed of 1000 rpm, a joining time of 8 s and a plunge depth of 2.4 mm. A lap shear strength of 8.74 ± 1.32 kN and a cross-tension strength of 2.57 ± 0.29 kN were obtained.

The failure mode of the specimens was also recorded and related to the welding parameters. Three different failure modes were distinguished: through-nugget failure (N), plug pull-out at the upper sheet (PU) and plug pull-out at the lower sheet (PL). The visual appearance of the fracture surfaces is given in Figure 7. A fourth failure mode was observed as the combination of a plug pull-out in the upper and in the lower sheet, resulting in a complete nugget removal. The weakest welds failed in a through-nugget failure, while the strongest failed by a plug pull-out at the lower sheet. The failure path indicates the weakest link of the joint. In a through-nugget failure, the original sheet interface of the welded sheets acts as the weakest bonding location. This type of failure mode especially occurred in welds produced at a low plunge depth and a high rotational speed. These two settings result in a weak bonded interface. Welds that showed a higher lap shear strength, failed in a plug pull-out type failure. In these type of failures, the bond along the softened sleeve plunge path acts as the weakest link instead of the bonding ligament. This is attributed to the higher heat input that was used to produce these welds and the resulting softened TMAZ. For strong welds produced at a longer joining time, a deeper plunge depth and a slower rotational speed, the failure mode shifted form plug pull-out at the upper sheet to plug pull-out failures at the lower sheet. In these cases, the strong joint fails through the lower sheet although it has not been penetrated by the tool over its complete thickness. Hence, the bonded interface and the sleeve plunge path act stronger than the lower sheet material.

Figure 7: Weld appearance at upper (top) and lower (bottom) sheet corresponding to a failure mode: PU (left), PL (middle) and N (middle)

V. Conclusions

The influence of the welding parameters on the weld quality of EN AW-7075-T6 using friction spot welding has been derived. The weld quality was assessed by metallographic examination, microhardness testing, lap shear testing and cross-tension testing. It is concluded that a longer joining time, a deeper plunge depth and a slower rotational speed are beneficial for the weld strength. The best parameter combination discovered in this work is a joining time of 8 s, a plunge depth of 2.4 mm and a rotational speed of 1000 rpm. This combination results in a weld with few imperfections, a large load bearing nugget and a trade-off between hardness reduction and weld strength.

Acknowledgements

This work has been carried out as a part of a master dissertation at Ghent University in cooperation with the Belgian Welding Institute.

References

[1] T. Rosendo, M. Tier, J. Mazzaferro, C. Mazzaferro, T. R. Strohaecker, and J. F. Dos Santos, 'Mechanical performance of AA6181 refill friction spot welds under Lap shear tensile loading', *Fatigue Fract. Eng. Mater. Struct.*, vol. 38, no. 12, pp. 1443–1455, Dec. 2015.

[2] T. Kolba, W. De Waele, and K. Faes, 'Experimental investigation of the weldability of aluminium alloys using friction spot welding', master dissertation at Ghent University, Gent, 2016.

[3] 'Friction spot welding | www.bil-ibs.be'. [Online]. Available: http://www.bil-ibs.be/en/friction-spot-welding. [Accessed: 02-Nov-2016].

[4] A. Gerlich, G. Avramovic-Cingara, and T. H. North, 'Stir zone microstructure and strain rate during Al 7075-T6 friction stir spot welding', *Metall. Mater. Trans. -Phys. Metall. Mater. Sci.*, vol. 37A, no. 9, pp. 2773–2786, Sep. 2006.

[5] T. Rosendo *et al.*, 'Mechanical and microstructural investigation of friction spot welded AA6181-T4 aluminium alloy', *Mater. Des.*, vol. 32, no. 3, pp. 1094–1100, Mar. 2011.

[6] Y. Q. Zhao, H. J. Liu, S. X. Chen, Z. Lin, and J. C. Hou, 'Effects of sleeve plunge depth on microstructures and mechanical properties of friction spot welded alclad 7B04-T74 aluminum alloy', *Mater. Des.*, vol. 62, pp. 40–46, Oct. 2014.

[7] Z. Shen, Y. Chen, J. S. C. Hou, X. Yang, and A. P. Gerlich, 'Influence of processing parameters on microstructure and mechanical performance of refill friction stir spot welded 7075-T6 aluminium alloy', *Sci. Technol. Weld. Join.*, vol. 20, no. 1, pp. 48–57, Jan. 2015.

Contents

Chapter 1 Introduction 1
Chapter 2 Friction Spot Welding 2
2.1 Process description 2
2.2 Welding parameters 4
2.3 Setup 5
Chapter 3 Welding Tool 6
3.1 Durability 6
3.2 Tool base material 8
3.3 Tool coatings 10
3.4 Summary and conclusions 11
Chapter 4 Weld quality 12
4.1 Geometrical zones and features 12
4.2 Overview of mechanical properties 15
4.3 Summary and conclusions 16
Chapter 5 FSpW of high-strength aluminium alloys: a review 18
5.1 7xxx aluminium alloys 18
5.2 2xxx aluminium alloys 22
5.3 Summary and conclusions 24
Chapter 6 Experimental test procedures 25
6.1 Welding trials 25
6.2 Visual inspection 26
6.3 Metallographic examination 27
6.4 Temperature measurements 28
6.5 Microhardness measurements 30
6.6 Lap shear strength testing 31
6.7 Cross-tension strength testing 32
Chapter 7 Experimental weld matrix 34
Chapter 8 Evaluation of the weld appearance 39
8.1 Visual surface quality 39
8.2 Metallographic quality 40
8.2.1 Weld cross-section appearance 40
8.2.2 Influence of welding parameters 45
8.2.3 Observation of material flow patterns 50

8.2.4 Repeatability of the weld quality 51
8.3 Summary and conclusions 53
Chapter 9 Mechanical properties of the weld 54
9.1 Softening of the weldment 54
9.1.1 Temperature measurements 54
9.1.2 Hardness reduction 56
9.1.3 Summary and conclusions 60
9.2 Lap shear strength 60
9.2.1 Design of experiments: full factorial 60
9.2.2 Optimized design of experiments: Box-Behnken 64
9.2.3 Summary and conclusions 66
9.3 Cross-tension strength 67
9.3.1 Design of experiments: full factorial 67
9.3.2 Summary and conclusions 69
Chapter 10 Overall parameter influences 70
10.1 Influence of the joining time 70
10.2 Influence of the plunge depth 70
10.3 Influence of the rotational speed 71
10.4 Best performing weld 71
Chapter 11 Future work 73
Chapter 12 Conclusions 75
References 76
Appendix A: Welding conditions 79
A.1 Metallographic test samples 79
A.2 Hardness test samples 80
A.3 Strength test samples 81
A.3.1 Lap shear strength test samples 81
A.3.2 Cross-tension strength test samples 82
A.4 Temperature test samples 83
Appendix B: Cross tension clamps 85
Appendix C: SCAD paper 89

List of figures

Figure 1: FSSW process: (a) plunging, (b) stirring and (c) retracting phases [11] 2
Figure 2: Three-component tool used in FSpW [7] 3
Figure 3: Friction spot welding sleeve plunge stages [14] 3
Figure 4: Typical visual appearance of a friction spot weld in EN AW-7475-T761 [15] 4
Figure 5: Plunge depth versus time and the different time parameters composing the joining time ... 5
Figure 6: Friction spot welding machine RPS100 at BWI [14] 5
Figure 7: Three-component tool: clamping ring, sleeve and pin (from left to right) [17] 5
Figure 8: Gap loading between concentric tool components 6
Figure 9: The wear problem with gap loading between the tool components [8] 7
Figure 10: Cross section of a weld surface with irregularities [8] 8
Figure 11: Typical cross-section of a FSpW weld in EN AW-6181-T4, adapted from [6]. 12
Figure 12: Differences in grain size and shape between adjacent weld zones [6] 13
Figure 13: Typical W-shaped hardness profile in EN AW-6181-T4 [6]. 13
Figure 14: Hook imperfection in SZ [42]. 14
Figure 15: Hook imperfection in TMAZ [42]. 14
Figure 16: Material flow velocity in FSpW process: (a) on surface during DT, (b) half cross-section during PT, (c) half cross-section during RT [43] 15
Figure 17: Imperfections in an EN AW-7075-T6 joint: (a) bonding ligament, (b) incomplete refill, (c) no mixing and (d) lack of mixing [41] 19
Figure 18: Cross section of the nugget thickness in EN AW-7075-T6 joint, obtained at various plunge depths and joining times [53] 20
Figure 19: Plug pull-out at the upper sheet [53] 20
Figure 20: Melting cracks in the SZ: liquation crack indicated by H [53] 21
Figure 21:Occurrence of annular groove: (a) without indentation (b) with 0.2 mm indentation [52]. 22
Figure 22: (a) Tearing at TMAZ/SZ interface, (b) Incomplete refill [48] 23
Figure 23: Surface quality classes: class 1 (left), class 2 (middle) and class 3 (right) 26
Figure 24: Non-etched cross-section (top) and area percentage of imperfections (bottom) 27
Figure 25: Sample holder containing three etched weld cross-sections 28
Figure 26: Thermocouple wire attached with epoxy glue 29
Figure 27: M3 tapped hole next to a weld to attach a thermocouple wire 29
Figure 28: Full map hardness indents (HV1) on specimen no. AF-75-R2-10 30
Figure 29: Transverse hardness indents (HV0.5) on specimen no. AF-75-H2-5 30
Figure 30: Lap shear specimen dimensions (mm) according to EN ISO 14273 31
Figure 31: Failure modes: PU, PL and N 32
Figure 32: Dimensions (mm) of one sheet of a cross tension specimen according to EN ISO 17272 ... 33
Figure 33: Cross tension clamping system: isometric (left) and exploded (right) view 33
Figure 34: Schematic overview of welding conditions in R1 series 35
Figure 35: Schematic overview of welding condition in R2 (●) and R3 (◆) series 36
Figure 36: Schematic overview of welding conditions in T1 and T2 series, according to a full factorial design 37
Figure 37: Schematic overview of welding conditions in T3 series, according to a Box-Behnken design 38
Figure 38: Surface irregularity on the weld surface, due to excessive heat input 39
Figure 39: Illustration of the tool misalignment on the cross-sectional overview (specimen no. AF-75-R3-1) 39
Figure 40: Completely etched cross-section (specimen no. AF-75-H2-5) 40

Figure 41: Metallographic cross-section of specimen no. AF-75-R2-12 41
Figure 42: Metallographic cross-section of specimen no. AF-75-R3-6 41
Figure 43: Stir zone and TMAZ present in specimen no. AF-75-R3-6 41
Figure 44: Surface indentation of the clamping ring and underlying affected zone in specimen no. AF-75-R2-6 42
Figure 45: Hook in TMAZ (specimen no. AF-75-R2-3) 43
Figure 46: Two hooks in SZ (specimen no. AF-75-R1-6) 43
Figure 47: Illustration of incomplete refill and voids present in the area subjected to tool plunging (specimen no.AF-75-R2-5) 43
Figure 48: Type 1 non-bonded interface, extending along a long curved distance within the stir zone (specimen no.AF-75-T3-10) 44
Figure 49: Type 2 non-bonded interface type 2, located in the centre along the interface, between 2 bonded interfaces (specimen no. AF-75-R2-7) (top), non-etched (left) and etched (right) detail. 45
Figure 50: Deep incomplete refill in a weld produced with JT=4 s (specimen no. AF-75-R1-2) 46
Figure 51: Varying JT: 6 s (top), 8 s (middle), 10 s (bottom); Fixed parameters: RS=2000 rpm, PD=1.6 mm 47
Figure 52 Mean area % of imperfections at varying JT and RS 47
Figure 53: Mean depth of incomplete refill at varying JT and RS 47
Figure 54: Partial bonding under the stir zone due to the limited plunge depth (specimen no. AF-75-R3-1) 48
Figure 55: Cross-sectional overview and detail of welds produced at varying RS: 1000 rpm (top), 2000 rpm (middle) and 3000 rpm (bottom); fixed parameters: JT=8 s, PD=2mm 49
Figure 56: Maximum actuator current of the spindle during a weld cycle, for varying RS 49
Figure 57: Mean area % of imperfections at varying JT and RS 50
Figure 58: Mean depth of IR at varying JT and RS 50
Figure 59: Striations, typically found in welds produced at a low rotational speed (specimen no. AF-75-R3-5) (left), banded zones, typically found in welds produced at a high rotational speed (specimen no. AF-75-R2-15) (right) 51
Figure 60: (Non-)etched cross-sectional overview of three repetitions (from top to bottom) of the same welding condition (specimen no. AF-75-R3-6) 52
Figure 61: Etched cross-sectional overview of three repetitions of the same welding condition (specimen no. AF 75-R2-10) 52
Figure 62: Surface temperature profile at 14 mm away from the weld centre for varying JT; Fixed parameters: PD=1.6 mm, RS=1000 rpm 54
Figure 63: Surface temperature profile at 14 mm away from the weld centre for varying RS. Fixed parameters: dashed line: JT=8 s, PD=2.4 mm; solid Line: JT=6 s, PD=1.6 mm 55
Figure 64: Maximum surface temperature at 14 mm away from the weld centre for varying PD. Fixed parameters: AF-75-R3-4/6: JT=8 s, RS=1000 rpm; AF-75-R3-7/9: JT=10 s, RS=1000 rpm 56
Figure 65: Typical W-shaped transverse hardness profile (specimen no. AF-75-R3-6) 57
Figure 66: Full hardness mapping (HV1) (specimen no. AF-75-R2-10) 57
Figure 67: Hardness profile, measured at half of the upper sheet thickness, for varying JT; fixed parameters: PD=1.6 mm, RS=1000 rpm 58
Figure 68: Hardness profile, measured at half of the upper sheet thickness, for varying RS; fixed parameters= JT=8 s, PD=2.4 mm 59
Figure 69: Hardness profile, measured at half of the upper sheet thickness, for varying PD; fixed parameters JT=8 s, RS=1000 rpm 59
Figure 70: Lap shear strength (kN) results for T1 series: error on the results (left) and mean values (right). 61

Figure 71: Main influences (JT and PD) on the LSS (kN) of T1 series, according to a full factorial design. 62
Figure 72: Interaction influences on the LSS (kN) of T1 series, according to a full factorial design 63
Figure 73: Correlation between failure modes and: LSS (left), welding parameters (right) 64
Figure 74: LSS (kN) results for T3 series: error on the results (left) and influence of the blocks (right)65
Figure 75: Main influences (JT and RS) on the LSS (kN) of T3 series, according to a Box-Behnken design 66
Figure 76: Correlation between failure modes and: LSS (left), welding parameters (right) 66
Figure 77: Cross-tension strength (kN) results for T2 series: error on the results (left) and mean values (right). 67
Figure 78: Main influences (JT and PD) on the CTS (kN) of T2 series, according to a full factorial design 68
Figure 79: Interaction influences on the CTS (kN) of T2 series, according to a full factorial design..... 68
Figure 80: Correlation between failure modes and: CTS (left), welding parameters (right) 69
Figure 81: Best performing weld: cross-section and details of interface (curve) and void (circle) in specimen no. AF-75-T1-7..... 72

List of tables

Table 1: Indicative summary of tool materials 9
Table 2: Nominal chemical composition of tool materials (mass%) [23]–[25], [27] 10
Table 3: Mechanical properties of tool materials at elevated temperature [23]–[25], [27] 10
Table 4: Mechanical properties of Al alloy FSpW overlap joints 17
Table 5: Composition of EN AW-7075-T6 in weight % [47] 18
Table 6: Mechanical properties of EN AW-7075-T6 [47] 18
Table 7: Composition of EN AW-2024-T3 in weight % [47] 22
Table 8: Mechanical properties of EN AW-2024-T3 [47] 22
Table 9: Surface quality classes 26
Table 10: Possible process parameter ranges 34
Table 11: Welding conditions in R1 series 35
Table 12: Welding conditions in R2 and R3 series 36
Table 13: Welding conditions in T1 and T2 series 37
Table 14: Welding conditions in T3 series 38
Table 15: Significant factors contributing to the LSS, according to the factorial design of the T1 series 61
Table 16: Significant factors in Box-Behnken design of T3 series 65
Table 17: Significant factors contributing to the cross-tension strength, according to the factorial design of the T2 series 68

List of abbreviations

BLL	bonding ligament length
BM	base material
CTS	cross tension strength
DLC	diamond-like-carbon
DT	dwell time
FSpW	friction spot welding
FSSW	friction stir spot welding
FSW	friction stir welding
HAZ	heat affected zone
IR	incomplete refill
JT	joining time
LSS	lap shear strength
N	through-nugget failure
PAZ	pin-affected zone
PD	plunge depth
PL	plug pull-out at lower sheet
PR	plunge rate
PT	plunge time
PU	plug pull-out at upper sheet
PUL	plug pull-out at lower and upper sheet
RFSSW	refill friction stir spot welding
RR	retraction rate
RS	rotational speed
RT	retraction time
SAZ	sleeve-affected zone
SZ	stir zone
TMAZ	thermo-mechanically affected zone
TWI	The Welding Institute

Chapter 1 Introduction

High-strength lightweight materials, such as some aluminium alloys, gain importance in industry, especially in automotive and aeronautic fields [1-3]. Transport accounts with 27% for the largest share of aluminium consumption [4]. During the last four decennia, cars have gained up to 5 times in aluminium content and it makes up to 75-80% of a modern aircraft structure [4]. Joining of these materials is an important step in the production of components or structures. Many joining techniques exist such as fusion welding, riveting, bolting, etc. Nevertheless, researchers keep looking for more efficient alternative techniques as each joining mechanism has inherent disadvantages [5]. Fusion welds can contain imperfections which deteriorate the mechanical strength of the bond. Furthermore, fusion welds in some high-strength lightweight alloys suffer from low weldability issues [6]. Mechanical fasteners add non-neglectable mass to the structure which is undesirable in lightweight applications.

Friction welding offers a solution to most of the issues concerning lightweight materials. This master dissertation focuses on the friction spot welding (FSpW) process, also referred to as refill friction stir spot welding (refill FSSW). It is a solid-state welding process well suited for spot-joining lightweight materials in overlap configuration. A three-component non-consumable rotating tool plunges into both sheets which have to be welded, which soften from the frictional heat. The joint is generated by the mechanical work and frictional heat input of the rotating tool at the interface between sheets where a metallurgical bond is formed. Friction spot welding is regarded as a green manufacturing method because no additional filler material is required and no waste material is produced [5, 7]. The welding process has a high opportunity for mass production lines as the welding time is short and the process can easily be automated.

Main issue of the process is the lack of published research on joining high-strength lightweight materials and hence its limited use in industrial applications. Furthermore, the welding tool is easily contaminated upon joining these materials. The material of interest for this master dissertation is EN AW-7075-T6, a high strength aluminium alloy typically used in aircraft applications. This work will investigate the influence of the process parameters rotational speed, joining time and plunge depth on the weld quality. The ultimate goal is to get a deeper understanding of the process and to get control of the weld quality. Chapter 2 will introduce the welding process and the controllable welding parameters. Chapter 3 will propose alternative tool materials since there is a strong need for tool improvement. The typical microstructure and strength values of a friction spot weld will be discussed in Chapter 4, while Chapter 5 focusses specifically on published results of some high-strength aluminium alloys. Chapter 6 will give an overview of the measurement procedures and Chapter 7 of the performed welding conditions in this dissertation. Chapter 8 and Chapter 9 respectively discuss the metallographic and mechanical results obtained. Finally, Chapter 10 combines all results in a parameter influence summary.

Chapter 2 Friction Spot Welding

2.1 Process description

The friction spot welding (FSpW) process is a solid-state spot joining technology to join sheets in overlap condition. The solid-state nature of the process implies that the working temperature does not exceed the melting temperature of the materials. The joint is fully generated by frictional heat and plastic work whereby a metallurgical bond is formed. FSpW is a rather recent technique as it was invented by the GKSS research centre in 1999 [8]. Often this technique is also referred to as refill friction stir spot welding (RFSSW) as it originates from the friction stir spot welding (FSSW) and friction stir welding (FSW) process.

FSW is a solid-state joining technique to weld abutting or overlapping plates. A rotating non-consumable tool plunges into the material and softens the workpiece locally by frictional heat. The material plasticizes and is stirred by the rotating tool which translates along the weld line. This procedure seems rather straightforward, but a proper design of the stirring tool is of major importance to enhance the material flow [9]. Omitting the translational movement along the workpiece leads to a spot joining process: friction stir spot welding.

Friction stir spot welding joins thin sheets in overlap configuration by plunging a rotating tool into the sheets. When the tool reaches a pre-defined depth, it is retracted from the workpiece, leaving a keyhole. The procedure is visualized in Figure 1 and consists of three distinctive steps. Firstly, the tool starts rotating at a high rotational speed and plunges into the upper sheet, which results into expelling of the material. This is called the plunging stage. When the tool is at the pre-defined depth, often near the sheet interface, the tool continues rotating and stirring the material. In this stirring stage, the solid-state joint is formed by frictional heat and plastic work. In the final retracting stage, the tool retracts from the workpiece and leaves behind a keyhole [10]. This typical keyhole is the major disadvantage of the process. The spot weld is prone to stress concentrations which reduce the mechanical properties. Furthermore, fluids can accumulate in the keyhole resulting in corrosion of the weld.

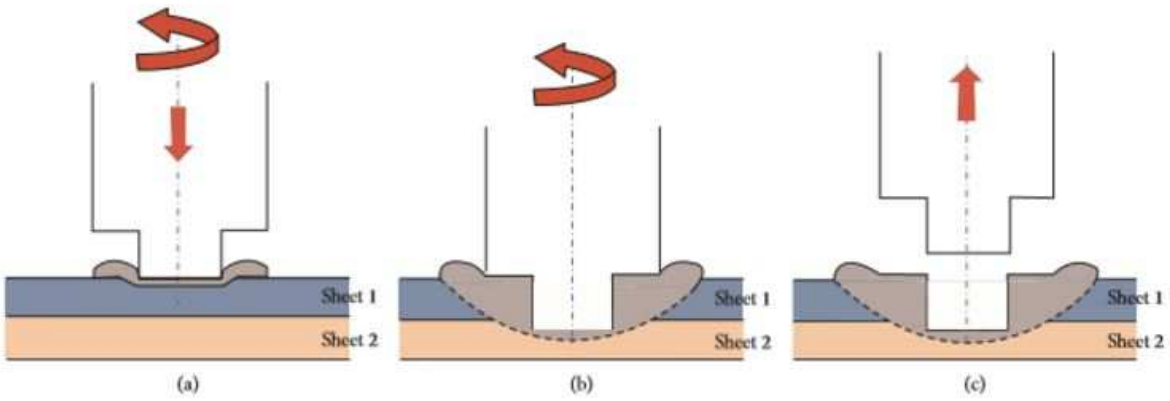

Figure 1: FSSW process: (a) plunging, (b) stirring and (c) retracting phases [11]

Friction spot welding offers a solution to this issue by refilling the keyhole in the last stage of the welding process. A three-component tool is required to achieve this refill step. The non-consumable tool is schematically represented in Figure 2 and consists of a concentric clamping ring, a sleeve and a pin. All

three components act independently in the axial direction. The pin and sleeve can rotate in the same direction. As the pin and sleeve plunge in the material, a circumferential thread is applied to improve the material flow [12]. The function of the clamping ring is to fix the sheets rigidly in the overlap configuration by pressing them against a backing anvil, while the welding process takes place.

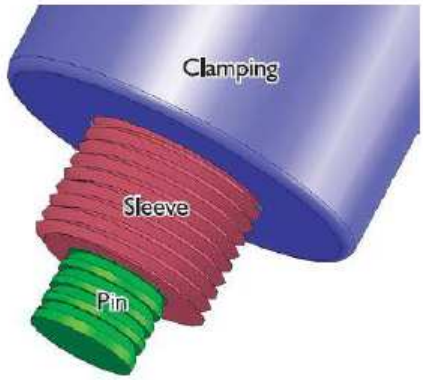

Figure 2: Three-component tool used in FSpW [7]

The four process stages are depicted in Figure 3. In the first stage, the clamping ring fixes the plates while the pin and the sleeve start rotating against the upper plate. In the second stage, the sleeve plunges into the material, while rotating at a high rotational speed. At the same time, the pin rises, creating a cavity of the exact required volume for the plasticised material. The sleeve displaces the material underneath and forces it into the cavity provided by the pin rise. Between the second and third stage, the sleeve reaches a pre-defined depth. The frictional heat and mechanical work delivered by the stirring results in the bonding of the sheets at their interface. In the third stage, the tool and sleeve translation reverse. The plasticised material that was accumulated underneath the pin is pushed back into the keyhole which was created by the sleeve plunging. During the fourth stage, the complete tool retreats and a flat surface without visual imperfections is visible. A typical visual appearance of such a spot weld is shown in Figure 4. The three concentric rings of clamping ring, sleeve and pin are clearly visible. Besides the sleeve-plunge technique described above, also a pin-plunge technique exists. In this variant, the pin plunges into the workpiece while the sleeve creates the cavity for the displaced material. The sleeve-plunge variant is dominantly used in practice since the larger weld diameter results in stronger joints [13].

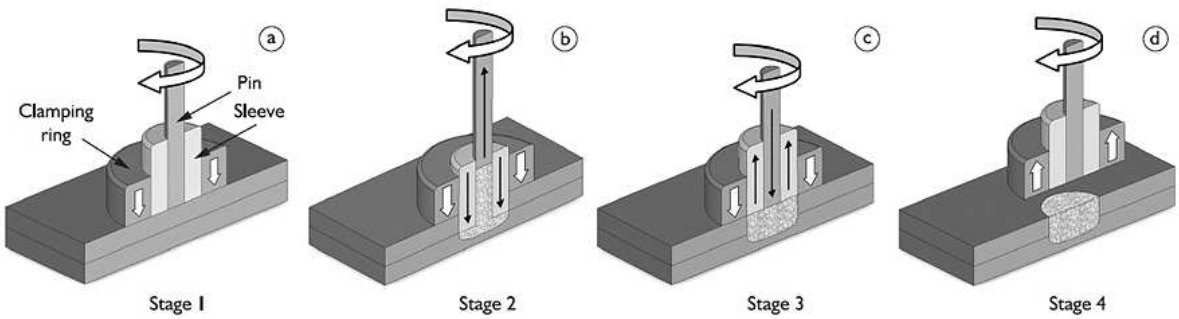

Figure 3: Friction spot welding sleeve plunge stages [14]

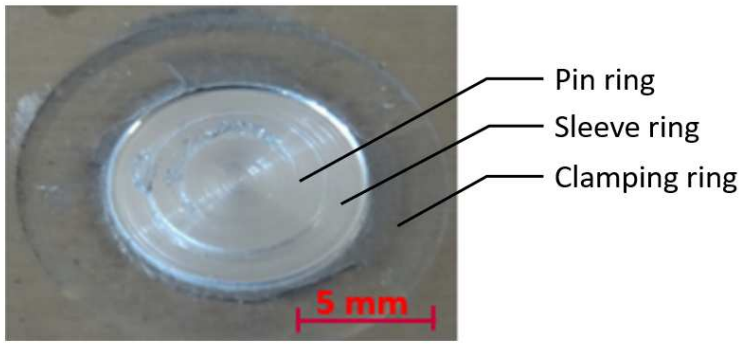

Figure 4: Typical visual appearance of a friction spot weld in EN AW-7475-T761 [15]

It is clear that friction spot welding has a high potential to become an important joining technique for lightweight materials that encounter low weldability issues with fusion techniques, or in weight-critical applications. Moreover, this process offers many advantages such as a lower energy consumption, eco-friendliness (no generated fumes or waste), no filler materials required, a good surface quality, fast and easy automation [7].

2.2 Welding parameters

The process, and thus the weld quality, is controlled by certain parameters. Finding the optimal parameter setting for a specific alloy type is the ambition of many researchers. This section briefly discusses the most important process parameters and their influence on the weld quality.

The rotational speed (RS) of the tool, pin and sleeve, is important in the FSpW process. The upper value is limited by the machine capacity, while the lower value is restricted by a minimum required heat input. The amount of heat input determines the softening of the workpiece material. The softer the material, the easier the tool can plunge into it. The more heat is delivered, the larger the heat affected zone around the weld nugget.

A critical [12], and very material dependent parameter is the plunge depth (PD). This is the maximum depth that the sleeve can plunge into the material, measured from the top surface of the upper sheet. Consequently, the plunge depth is restricted to the total thickness of the overlap configuration. The plunge depth is larger than the thickness of the upper sheet for most welds. For hybrid joints, the plunge depth is sometimes kept smaller than the upper sheet thickness, in order to avoid plunging into the lower material and hence possibly forming intermetallic phases [16].

A third process parameter is the joining time (JT), which influences the amount of heat input, similar to the rotational speed. It consists of three sub-parameters: the plunge time (PT), the dwell time (DT) and the retraction time (RT). These time parameters are graphically visualized in Figure 5. The plunge time and retraction time determine the rate of plastic deformation of the weld zone. Related parameters are the plunge rate (PR) and retraction rate (RR).

A final parameter is the clamping force used to fix both sheets during the process. This can be varied in a wide range but should stay within limits. A too low clamping force will result in a rotational movement

of the sheets during the welding process. A too high clamping force will plastically deform the upper sheet, especially when it is softened by the frictional heat.

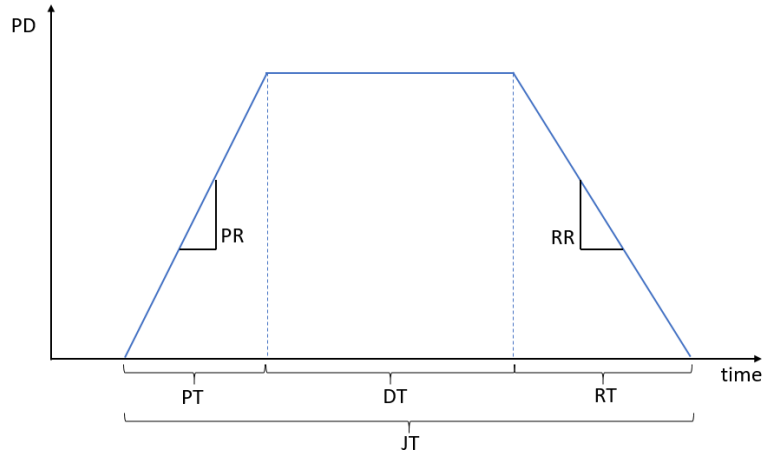

Figure 5: Plunge depth versus time and the different time parameters composing the joining time

2.3 Setup

In this section, the welding equipment is presented. The experiments are executed at the Belgian Welding Institute (BWI) on a friction spot welding machine of Harms & Wende, type RPS100 (Figure 6). The welding head can rotate at a maximum of 3300 rpm. The separate components of the welding tool are shown in Figure 7. The clamping ring, sleeve and pin have a nominal outer diameter of respectively 14.5, 9.0 and 6.0 mm.

Figure 6: Friction spot welding machine RPS100 at BWI [14]

Figure 7: Three-component tool: clamping ring, sleeve and pin (from left to right) [17]

Chapter 3 Welding Tool

3.1 Durability

The welding tool, or welding head, is the most important component of the friction spot welding machine. The tool and especially the sleeve are in close contact with the workpiece material. It experiences high axial forces, torques and thermal cycles. However, the most important problem is not immediately obvious from the schematic procedure description. The pin and sleeve are concentric within narrow tolerances, but still there remains a small ring-shaped gap between them. During welding, this gap is continuously filled with plasticized base material of the workpiece and hence a higher torque is required to rotate the tool components as the welding processes advances [8]. In literature, this is referred to as the gap loading. Figure 8 schematically shows this phenomenon, the gap dimensions are exaggerated for illustrative purposes.

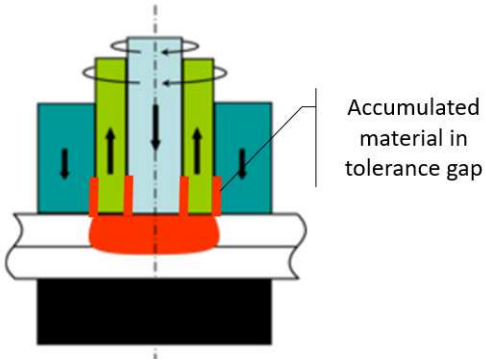

Figure 8: Gap loading between concentric tool components

Problems have been encountered due to this phenomenon in a previous master dissertation: squeaking noises and shutdown of the motors due to too high overload currents [18]. Even failure of the sleeve has occurred due to the exerted torque at the sleeve top, while the sleeve bottom was sticking to the fixed clamping ring [17]. To limit the accumulation of plasticized material, a circumferential thread is machined at the bottom of the pin and sleeve. This should reduce the height of material contamination and prevent more material from entering the gap [8]. This phenomenon of gap loading is an important cause of tool wear. The filling of the tolerance gap results in a higher needed torque, in order to maintain a constant rotational speed. The additional friction increases the temperature of both the tool and the workpiece material. The softened base material can now flow more easily into the gaps and wears out the tool components abrasively. This results in an increase of the gap spacing and hence the gap loading increases as well. This cycle of increasing tool wear is visualized in Figure 9. It has been measured that the largest wear is located at the outer surface of the sleeve, between the rotating sleeve and fixed clamping ring [8].

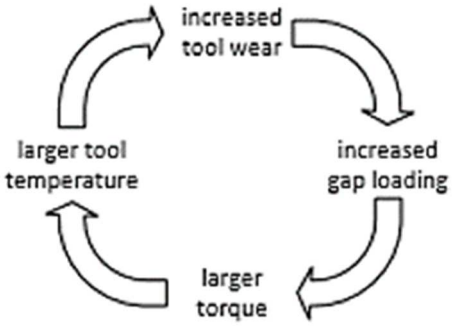

Figure 9: The wear problem with gap loading between the tool components [8]

Until now, the only measure to solve this problem is cleaning of the tool surfaces after a certain number of welds or trying to limit the wear rate by optimising the welding parameters. In [19], the influence of setting parameters on the tool durability for welding of an EN AW-6082-T6 aluminium alloy is investigated. The required force and torque were indirectly measured based on the actuator currents. The research revealed that a higher rotational speed requires less torque current and hence a lower torque. This can be explained from the fact that the workpiece material is more softened due to the increased frictional heat. As mentioned above, this extra softening of the workpiece will gradually lead to gap loading and eventually require an additional torque. For very low rotational speeds, a very irregular current and torque behaviour was measured, hence this operation mode should be avoided. In the same work, the influence of plunge rate and retraction rate is also investigated. The plunge rate should occur relatively slow to limit the required torque, as the material is not softened yet. The retraction rate is less sensitive for an optimal value of minimal forces, as the plasticized material is already in a softened state. Nevertheless, the retraction rate can have a large influence on the weld filling quality. An increase of the total joining time is always beneficial if a certain weld strength is required. However as stated before, the excessive heat supply is disadvantageous for the hardness properties of the weld.

The increasing tool wear has a high influence on the machine reliability. It can lead to a shutdown of the welding machine for maintenance or replacement of a failed tool. The weld quality and appearance is also affected by the state of the tool. A schematic of the different observed surface irregularities is given in Figure 10. Two surface irregularities are attributed to the use of a worn-out tool [8]. Firstly, two burrs appear at the location of the widened ring-shaped gaps between the three concentric tool components. Material that has filled the gaps, remains there until the tool is retracted from the workpiece material. The more severe the wear is, the wider and higher the burrs appear. Additional flattening processes can be necessary to obtain a flat weld surface. Secondly, a notch at the sleeve-clamping ring interface is seen as a result of a reduced inner sleeve length. The bottom of the sleeve is worn out at the internal diameter of the sleeve component. When retracting the sleeve, the longer outer sleeve leaves a circular notch. A third surface irregularity was observed, but the exact cause is not yet clear. A zero-level drift of the sleeve and pin, which means that the bottom surfaces are not in-plane when idle, results in an elevated pin plateau [8]. It is suggested that adhesion forces between tool and workpiece cause this zero-level drift when retracting the tool. [8]

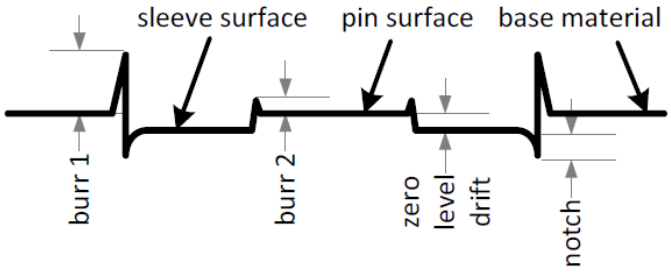

Figure 10: Cross section of a weld surface with irregularities [8]

One positive aspect related to tool wear is that there is no reported dependency with lap shear strength [8]. The increased temperature with increasing tool wear can even improve the metallurgical bonding of the surfaces. This independency of the joint strength on the tool wear is a major advantage for industrial applications.

3.2 Tool base material

Rather than the use of the welding tool, the tool material has a large influence on the tool wear and behaviour. Possible tool material classes are discussed below. They have to withstand the harsh process conditions and therefore should satisfy the following requirements [20]:

- Elevated-temperature strength: the material should keep its strength at temperatures approaching the workpiece liquidous temperature.
- Thermal fatigue resistance: an automated friction spot welding process consists of multiple heating and cooling cycles.
- Low tool reactivity: the material should not react with the environment (corrosion) or the workpiece material (adhesion).
- High fracture toughness: especially the first tool – workpiece contact (impact) during the plunging step can lead to failure for a brittle material.
- Low coefficient of thermal expansion: when pin and sleeve expand, tolerances will change.
- Machinability: at least a circular groove should be machinable.
- Affordable cost because the tool lifetime is finite.

Tool steels are the most widely used tool materials in friction stir welding of aluminium alloys [21]. Often, they are air- or oil-hardened to maintain their strength at elevated temperatures. Moreover, they are easily machinable and available at low cost. The most cited tool steel in literature is AISI H13 (EN: X40CrMoV5-1). It is a chromium-molybdenum hot work steel that is air-hardened to improve its hot strength and hot hardness. Moreover it shows a good thermal fatigue and wear resistance in friction stir welding of aluminium alloys and even oxygen-free copper [20].

Nickel- and cobalt - based alloys can be used as tool material to stir weld stronger workpiece materials such as high-strength aluminium alloys and copper. As they were initially designed for aircraft engines, they offer high strength, ductility, good creep resistance and corrosion resistance [21]. One should be aware that these alloys gain their strength by precipitation and therefore the working temperature has

to remain under the precipitation temperature in order to avoid over-aging [20]. A disadvantage is the low machinability for some type of alloys.

When processing high-melting point materials, **refractory metals** such as tungsten, molybdenum, niobium and tantalum can offer a solution. Consisting of a single phase, they maintain their strength to nearly their melting point temperature [21]. Disadvantages are the high cost, low machinability and excessive tool wear. Highly wear resistant materials can be found in machining applications. **Carbides** are often used in machining tools for their excellent wear resistance at elevated temperatures. WC or WC-Co tools are used in friction stir welding of Ti-alloys and steel [21]. In [22], a cemented carbide tool is optimized to FSW 980 MPa tensile strength steels. By applying a specially tuned TiAlN coating, the tool life was increased from several hundreds of spots for a conventional tool to 7000 spots. The most polyvalent friction stir tool material is polycrystalline cubic boron nitride (**PCBN**) which was originally developed for turning and machining of tool steels [21]. Owing to its high mechanical and thermal performance, it is used in friction stir welding of stainless steels [20]. However, the cost and low fracture toughness are disadvantages. An overview of the aforementioned tool materials is given in Table 1.

Table 1: Indicative summary of tool materials

	Hot strength	Hot hardness	Wear resistance	Machinability	Low cost	Workpiece materials
Tool steel	+	+	-	+++	++	Al, Mg, Cu
Ni/Co based alloy	++	+	+	+	+	Al, Cu alloy
Refractory metals	+++	+++	--	-	-	Cu, Ti, Ni, steel
Carbides	+++	++	++	-	--	Al, Ti, steel
PCBN	+++	++	++	--	---	Stainless steel

Regarding the workpiece materials used in this master dissertation, high-strength aluminium alloys, a number of tool material classes suffice. Based on Table 1, tool steels and Ni/Co based alloys are preferred as they combine a relative high hot strength and hardness with machinability. Tool steels, such as X40CrMoV5-1, can be used for FSpW of most aluminium alloys. EN ISO 4957 X40CrMoV5-1 is also known as Thermodur 2344 Superclean [23]. Previous master theses concerning this topic [17, 18] used a high performance molybdenum-vanadium alloyed hot-work tool steel named Uddeholm Hotvar [24] . Nowadays, at the Belgian Welding Institute, X45MoCrV5-3-1, a non-standardized steel from the Deutschen Edelstahlwerke GmbH, is used. This is also known as Thermodur 2999 Superclean [25]. For the high-strength aluminium alloys such as the 2xxx and 7xxx series, the use of tool steels is also possible but can result in excessive wear. TWI [26] suggests to opt for the nickel-cobalt alloy MP 159 [27] for these material families, as it is readily machined in its as-received state and can obtain the highest strength level via precipitation strengthening. A comparison between Hotvar, Thermodur 2344, Thermodur 2999 and MP159 is given in Table 2 and Table 3. The tool material used in this master dissertation, Thermodur 2999 Superclean, is a tool steel with improved properties at elevated temperatures. The maximum operation temperature is 650 °C as the hot hardness drops dramatically from there on.

As the working temperature for copper is several hundred degrees Celsius higher, TWI [26] suggests to use a W or WC tool.

Table 2: Nominal chemical composition of tool materials (mass%) [23]–[25], [27]

	Fe	C	Si	Mn	Cr	Mo	V	Ni	Co	Ti	Cb	Al
Uddeholm Hotvar	91.85	0.55	1.0	0.8	2.6	2.3	0.9	-	-	-	-	-
Thermodur 2344	90.50	0.40	1.0	0.4	5.3	1.4	1.0	-	-	-	-	-
Thermodur 2999	89.95	0.45	0.3	0.3	3.0	5.0	1.0	-	-	-	-	-
MP 159	9.00	-	-	-	19.0	7.0	-	25.5	35.7	3.0	0.6	0.2

Table 3: Mechanical properties of tool materials at elevated temperature [23]–[25], [27]

	Yield strength (MPa) at 20/500/600 °C	Hardness (HRC) at 20/600 ° C
Uddeholm Hotvar	1800/1250/800	56/55
Thermodur 2344	1300/950/600	54/50
Thermodur 2999	-	57/53
MP 159	1750/1600/1550	-

3.3 Tool coatings

In section 3.1, the mechanism of gap loading was explained. The plasticized material that fills the gap between the tool components increases the torque and forces required to perform the process. However, the most important problem is the adhesion of the workpiece material to the tool after retraction. This behaviour is called material transfer of the workpiece onto the tool. In hot forming [28] or dry machining [29] of aluminium, the material transfer of aluminium onto the tool steel is a well-known problem. In most applications, this is solved by lubricating the process, but this generates a non-eco-friendly waste flow of used lubricants. Therefore, research activities are oriented towards the application of coatings, of which some are interesting to evaluate in the friction spot welding process. The material transfer is based on 2 mechanisms: mechanical and chemical interaction [28]. The former covers the material transfer from a soft to a harder material by mechanical contact. The latter relies on adhesion and even appears in stationary conditions. The material transfer is dominated by the roughness peaks of both materials at lower temperatures (20-200 °C) , while it is dependent on the adhesion at higher temperatures (300-500 °C) [30, 31]. FSpW works in the high temperature region in normal operation. Adhesion increases with increasing temperature as the softening workpiece material highly plasticizes under the Hertzian contact stresses and consequently creating larger adhesion surfaces [30].

Much research has been done on finding the ideal coating for tools in different aluminium operations. Coatings that may be suitable for the FSpW tool can be found in processes with similar operating conditions. One possibility is to look into tool protection in dry machining operations of aluminium. Adhesion can be a problem without lubrication and working temperatures can increase due to friction.

Different studies concerning these processes investigate a diamond-like-carbon (DLC) coating. This hard coating material shows low friction and excellent anti-adhering properties. Moreover, the machining forces are lower compared to the bare tool material [29]. A DLC coating can be applied on different kinds of tool materials. A DLC-coating was suggested as a suitable coating for covering a cemented carbide in a dry milling process on EN AW-7075 [32]. DLC-coatings were also favoured as a coating on a cemented carbide tool machining EN AW-5052 [29]. Even for the protection of a DIN100C6 tool steel at elevated temperatures of 420°C and in contact with EN AW-5182, the DLC-coating resulted in the lowest amount of aluminium transfer [33]. DLC coatings can be classified into hydrogenated and non-hydrogenated types according to the hydrogen content. A study concluded that the hydrogenated DLC coatings had advantages in keeping the cutting forces low and limiting adhesion, while dry drilling in a 319 grade aluminium [34].

Another strategy is to look at coatings to protect die tools in aluminium die casting. Two coatings, TiAlN and CrN applied on the popular tool steel X40CrMoV5-1, were compared in terms of their adhesion to an EN AW-6060 aluminium alloy [31]. TiAlN shows the best results for lower working temperatures (20-300 °C), while CrN is more appropriate for higher working temperatures (400-500 °C). Nevertheless, a thin transfer film developed on both coating surfaces. A follow-up experiment looked into the friction behaviour of a CrN coating in an aluminium forming process using a perpendicular cross-cylinder test in a 25-500 °C range [35]. A much smaller aluminium transfer surface sticks to the CrN coating compared to the tool steel surface, but the coefficient of friction is similar for both at high temperatures. The AlCrN coating is a variant of the above mentioned CrN coating and showed negligible adhesion in an aluminium adhesion test (AAT) of a X40CrMoV5-1 tool steel onto a typical cast aluminium [36]. Another study also compared the soldering resistance of CrN and TiN coatings to pure aluminium, in order to find a suitable die coating material [37]. CrN coatings were superior, although its practical use relies on adhesion strength to the die bulk material. Solid/solid interaction of CrN coated HTCS steels against aluminium is successfully evaluated using a ball-on-disc configuration at a temperature of 450 °C [38]. On the other hand, another study claims that hard TiN coatings show an optimal combination of hardness, adhesion, soldering behaviour, oxidation resistance, and stress state [39].

3.4 Summary and conclusions

This chapter discussed the need for a suitable tool material since the tool head suffers from gap loading. Tool materials should maintain their strength and hardness at elevated temperatures. Moreover, they should be easily machinable and wear resistant. Friction spot machines are normally equipped with tool steel components since they are able to work in most of the light-weight materials. However, when the tool wear rate becomes too high, they should be replaced by Ni/Co alloys. Since the welding machine in this work is only used for experimental purposes, the tool steel Thermodur 2999 Superclean has been used. Adhesion of the workpiece material to the tool could possibly be reduced by applying a tool coating. Diamond-like-carbon coatings are favoured above (Al)CrN or Ti(Al)N coatings as a tool protection in dry milling [32] or hot forming [33] of aluminium. However, in die casting processes, (Al)CrN and Ti(Al)N are preferred. Since friction spot welding is a solid-state process, it is similar to hot forming processes. Hence, it is recommended to evaluate the performance of a diamond-like-carbon coating in further research.

Chapter 4 Weld quality

This chapter focusses on the visual appearance and mechanical properties of a friction spot weld. Different zones that can be distinguished in a cross-section of a typical weld are discussed with respect to their characteristics and formation. The mechanical properties, and thus the quality, of different reported welds will be summarized.

4.1 Geometrical zones and features

Figure 11 shows a typical cross-section of a weld made with the friction spot welding process. A friction spot weld consists of different microstructural regions, called weld zones. Figure 11 shows the stir zone (SZ) and the thermo-mechanically affected zone (TMAZ). A third weld zone exists, but is not clearly visible on the optical microscope image: the heat-affected zone (HAZ). All weld zones differ in microstructure and mechanical properties from the base material (BM) as a result of the welding process. The microstructures of the three weld regions are shown in detail in Figure 12. The SZ is the centre of the weld and has approximately the same width as the sleeve diameter. It is characterized by refined and equiaxed grains as a result of dynamic recrystallization. This is the effect of the high strain rate and the high local temperatures during the stirring process [40]. The finest grains are located at the same diameter as the sleeve-pin interface [41]. The workpiece material is severely stirred between these tool surfaces. Next to the SZ, the TMAZ exists as a transitional region between SZ and HAZ. This zone is formed by moderate deformations and temperatures as the name suggests. The microstructure is characterized by elongated and deformed grains caused by the material flow as visible in Figure 12 [6]. As the TMAZ is a transition region, it is hard to define the boundaries. The TMAZ changes gradually into the HAZ when retreating from the weld centre. The HAZ is the first zone that is not affected by plastic deformation. As the name suggests, the microstructure of this zone is influenced by the conducted heat from the welding process. Grain and precipitate coarsening has occurred due to the thermal treatment. Far enough from the weld centre, all effects from the welding process on the microstructure disappear. This is where the HAZ ends and the BM starts.

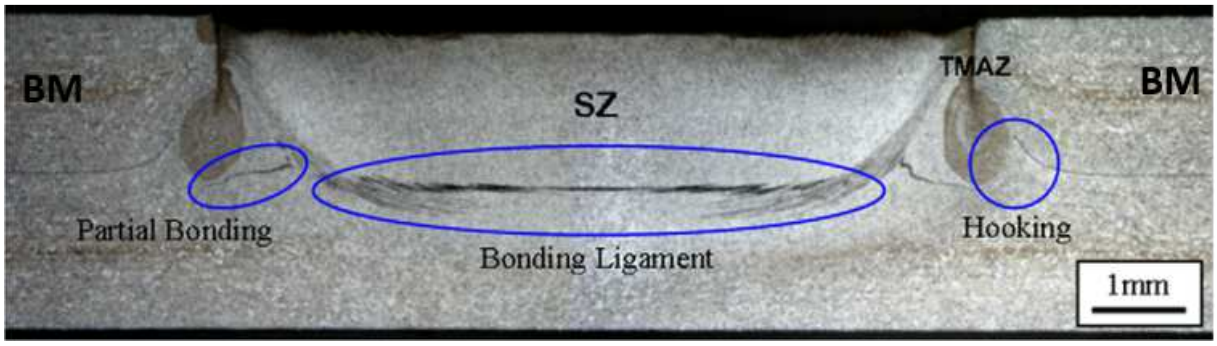

Figure 11: Typical cross-section of a FSpW weld in EN AW-6181-T4, adapted from [6].

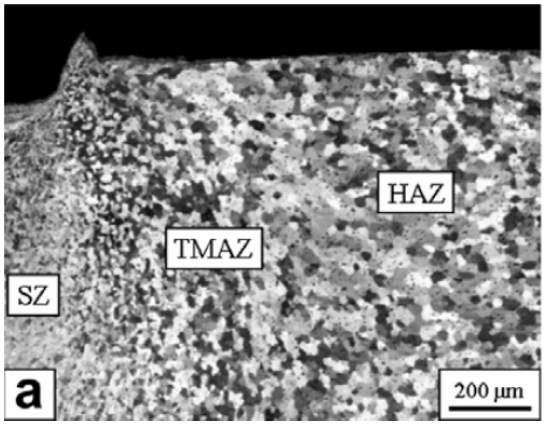

Figure 12: Differences in grain size and shape between adjacent weld zones [6]

The changes in microstructure influence the micro-hardness properties of the weld region. Many researchers perform hardness profile measurements at the mid-thickness of the upper plate to quantify the structural quality of the weld. Rosendo et al. [6] linked the different weld zones to distinctive trends in the obtained hardness profile. Heat-treatable alloys show a W-shaped hardness profile in the width direction of the weld as depicted for EN AW-6181-T4 in Figure 13. The material has a hardness value which changes in the weld region due to the different microstructures. The stir zone exhibits an increase in hardness value compared to the base material. This phenomenon has two strengthening contributions [6]. Firstly, the refined grains in the SZ locally increase the strength and hardness. Secondly, this zone is exposed to high temperatures for a long time as the centre of the weld has the slowest cooling rate. This causes dissolution of precipitates and their re-precipitation during cooling right after welding [6]. The hardness value drops in the TMAZ due to precipitate coarsening. In the mechanically deformed zone close to the SZ, this effect is partially compensated by strain hardening. Based on the continually decreasing hardness in the TMAZ, Rosendo et al. [6] defined the boundary between the TMAZ and the HAZ as the minimal hardness value and the boundary between the SZ and the TMAZ as the location where the hardness drops under the base material hardness. The material softening in the HAZ is a result of the thermal influence. The strength increase of the base material due to the cold rolling of the plate is partially neutralised in the HAZ by the heat from the welding process [6].

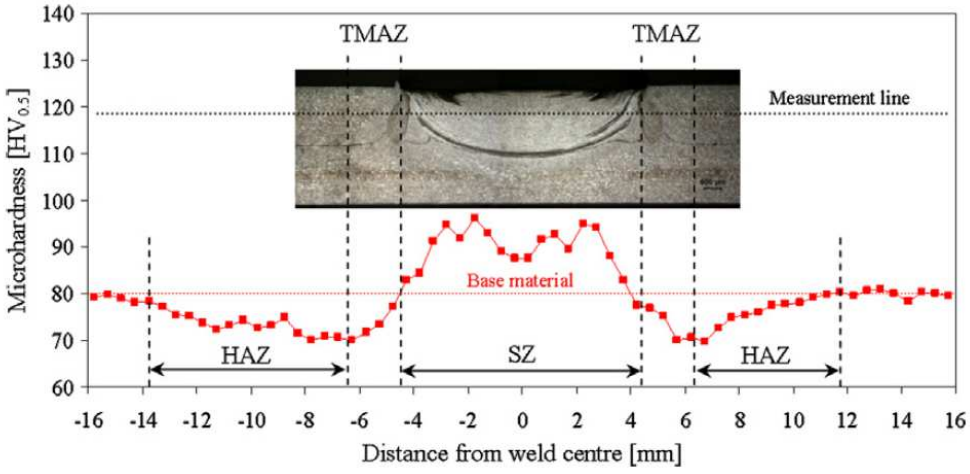

Figure 13: Typical W-shaped hardness profile in EN AW-6181-T4 [6].

Three geometrical features are often reported in metallographic inspection: hooking, partial bonding and bonding ligament. The location and appearance of these geometrical patterns are indicated in Figure 11.

The hook imperfection was defined as the partially metallurgical bonded region, a transitional zone between the completely bonded regions and the non-bonded ones [42]. Cao et al. [42] discovered two types of hook imperfections which differ in their location of occurrence. The first type of hook imperfection was located in the stir zone of the weld and is shown in Figure 14. It is believed that the hook shape is a result of the third stage in the welding process: the pin pushing the extruded material back into the created keyhole. The plasticized lower sheet material is pushed upwards at the sides by the retreating pin. This type of hooking occurred with a plunge depth smaller than the upper sheet thickness [42]. A second type of hooking appeared when the plunge depth was increased. This hook imperfection only appears in the TMAZ and has an upside down V-shape (Figure 15), as also reported in [6]. It is suggested that the formation of this hook type arises from the upward bending of the interface due to tool penetration into the lower sheet [42]. Figure 15 also shows a quantitative parameter to express the severity of the hook imperfection: the hook height. It is measured between the top of the hook and the original sheet interface. The final hook height is believed to be controlled by two factors: the amount of plasticized material and the upward material flow thread [42]. Hence, increasing the rotational speed and the joining time affect the first factor and increasing the plunge depth affects the second. The importance of hooking lies in the fact that the tensile shear strength decreases monotonically with increasing hook height [42].

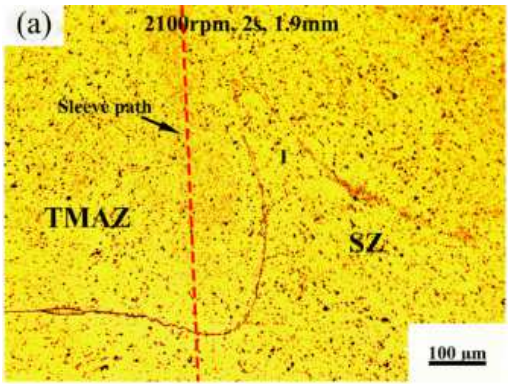

Figure 14: Hook imperfection in SZ [42].

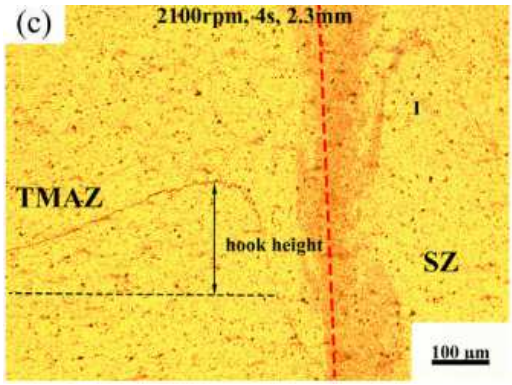

Figure 15: Hook imperfection in TMAZ [42].

The next weld feature to discuss is the bonding ligament. It is a region of good adhesion between the upper and lower sheet material [6]. It is located underneath the stir zone and forms the strongest metallurgical bond in the weld. The quantitative parameter coupled to the bonding ligament is the bonding ligament length (BLL) as defined by Tier et al. [12]. The BLL is proportional with the weld strength, a long bonding ligament results in a high-quality weld. Tier et al. [12] showed that a longer, flatter and stronger bonding ligament can be obtained in EN AW-5042-O for lower rotational speeds. For larger rotational speed, the bonding ligament is curved upwards and the effective BLL is smaller.

The final geometry indicated in Figure 11 is the partial bonding. Contrary to the bonding ligament, the partial bonding is a weaker bond between both sheets. It is a transition region between the hooking and the bonding ligament. Apart from the geometries described above, imperfections related to bad welding parameters can occur such as lack of mixing and incomplete refill [6].

This section dealt with the typical appearance of a friction spot weld. Many of the geometrical features and weld zones can be explained using the complex material flow during the welding process. Zhao et al. [43] simulated the material flow and compared this to experimental metallographic images. Figure 16 shows the velocity profile and scale during different stages of the welding process. Figure 16a shows that the material at the inner surface of the sleeve is stirred most, hence the finest grains arise there. The half cross-section in Figure 16b shows the sleeve-plunging stage. The material flows into the sleeve cavity from the periphery and the bottom of the sleeve, as marked by the red arrow. In Figure 16c, depicting the sleeve retreating stage, the material in the sleeve cavity is extruded by the pin and flows downwards out of the sleeve cavity. It then flows laterally and upwards to fill the gap left by the retreating sleeve. The upward flow near the outer edge of the sleeve explains the upward curving of the hook, the lateral elongation of the grains in the TMAZ and the U-shaped bonding ligament. [43]

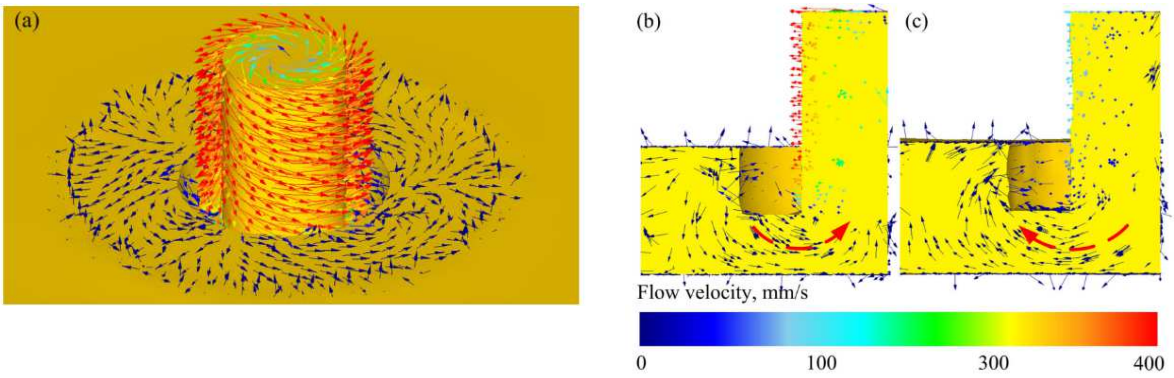

Figure 16: Material flow velocity in FSpW process: (a) on surface during DT, (b) half cross-section during PT, (c) half cross-section during RT [43].

4.2 Overview of mechanical properties

Already quite some research has been done on the FSpW joinability of aluminium alloys. Each researcher tried to optimize the welding parameters in order to achieve a high-quality weld. The quality of the weld is expressed in its mechanical properties with the most important ones being lap shear strength and hardness. Overlap spot joints are mostly tested in lap shear testing as this load mode resembles the expected application load. Published results of cross-tension tests on friction spot welds are very rare and show a lower strength when compared to lap shear tests [44]. Another important quality indicator is the hardness reduction in the weld nugget. As explained in section 4.1, the microstructure of the material changes in the weld compared to the base material. The maximum hardness reduction takes place at the boundary between the TMAZ and the HAZ. Table 4 summarizes published research of FSpW in aluminium and their mechanical results. As different aluminium alloys and different sheet thicknesses are used, the results are hard to compare. The final column contains the minimum shear load requirement for resistance spot welds in aluminium and magnesium alloys used in

aerospace applications [45]. All weld combinations pass the minimum requirement and hence are capable of replacing resistance welds.

4.3 Summary and conclusions

This chapter discussed the typical microstructural appearance of a friction spot weld. Distinct microstructural zones are present: stir zone, thermo-mechanically affected zone, heat affected zone and base material. Each region experienced different temperatures and deformations during processing which results in a typical W-shaped hardness profile. The original sheet interface of the welded components leads typical geometries: hooking, partial bonding and bonding ligament. Finally, an overview of mechanical properties of the weld such as lap shear strength and hardness reduction was given. The presence and influence of the different weld regions and geometries will be evaluated in the experiments of this master dissertation. The obtained mechanical properties will be compared to published results and minimum shear load requirements to validate the weld performance.

Table 4: Mechanical properties of Al alloy FSpW overlap joints

Materials	Thickness (mm)	Overlap area shear test (mm x mm)	Lap shear strength (kN)	BM hardness (HV)	Maximum hardness reduction (- %)	Ref	UTS (MPa)	Shear load requirements minimum; average. [kN per spot weld] [45]
2xxx								
EN AW-2024-T3 (Alclad)	2.0	46x46	7.50-10.68	110	16.0	[46]	359-510 [47]	4.560; 5.715
EN AW-2024-T3 (Alclad)	2.0	46x60	9.00	100-120	16.0	[44]	359-510 [47]	4.560; 5.715
EN AW-2024-T3	2.0	46x60	8.00-10.00	/	/	[13]	359-510 [47]	4.560; 5.715
EN AW-2024-T3	1.6	38x45	7.00-8.00	/	/	[18]	359-510 [47]	2.980; 3.635
EN AW-2024-T4 (Alclad)	1.5/2.0	50x60	9.36	140	10.0	[48]	359-445 [47]	2.725; 3.307
EN AW-2198-T8	3.2	35x60	14.70	150	23.0	[49]	450 [50]	9.430; 11.785
5xxx								
EN AW-5042-O	1.5	50x60	4.50-6.30	/	/	[12]	240-350 [47]	2.503; 3.135
6xxx								
EN AW-6061-T6	2.0	25x25	7.40-8.60	115	10.0	[42]	233-257 [47]	3.805; 4.760
EN AW-6181-T4	1.7	46x46	6.80	80	12.5	[6]	200 [50]	2.675; 3.390
EN AW-6181-T4	/	/	6.00-7.00	/	/	[51]	200 [50]	
EN AW-6181-T4	1.7	/	6.50	/	/	[7]	200 [50]	2.675; 3.390
EN AW-6082-T6	2.0	35x45	10.50	107	35.0	[17]	280-340 [47]	3.805; 4.760
7xxx								
EN AW-7B04-T74 (Alclad)	1.9	30x30	7.00– 11.90	165-175	18.0	[52]	498 [52]	4.115; 5.160
EN AW-7075-T6	2.0	40x40	7.03	140-150	17.0	[41]	434-580 [47]	4.560; 5.715
EN AW-7475-T761	1.6	38x45	7.00-8.00	/	/	[18]	455-503 [47]	2.980; 3.635
EN AW-7475-T761	1.6	35x45	5.38	150	16.0	[17]	455-503 [47]	2.980; 3.635
EN AW-7075-T6	1.6	35x45	/	180	22.0	[17]	434-580 [47]	2.980; 3.635
EN AW-7075-T6 (Alclad)	0.8	25x25	4.00-4.75	165-180	23.0	[53]	434-580 [47]	1.155; 1.445
Dissimilar								
EN AW-7475-T761/EN AW-2024-T3	1.6	38x45	8.00-10.00	/	/	[18]	455-503/ 359-510 [47]	2.980; 3.635

Chapter 5 FSpW of high-strength aluminium alloys: a review

This section reviews the state-of-the-art in friction spot welding of high-strength aluminium alloys of the 7xxx and 2xxx series.

5.1 7xxx aluminium alloys

This work will mainly focus on the EN AW-7075-T6 aluminium alloy and its weldability using friction spot welding. EN AW-7075-T6 is a precipitation hardened Al-Zn-Mg-(Cu) alloy that has been used extensively in highly stressed applications for its light weight and high strength. Composition and mechanical properties are presented in Table 5 and Table 6, respectively.

Table 5: Composition of EN AW-7075-T6 in weight % [47]

Al	Cr	Cu	Fe	Mg	Mn	Si	Ti	Zn	Other
87.2-91.4	0.18-0.28	1.2-2.0	0-0.5	2.1-2.9	0-0.3	0-0.4	0-0.2	5.1-6.1	0-0.15

Table 6: Mechanical properties of EN AW-7075-T6 [47]

Yield strength (MPa)	Tensile strength (MPa)	Failure strain (%)	Melting point (°C)
359-530	434-580	2-10	475-635

Up until now, only a limited amount of researches regarding the FSpW of EN AW-7075-T6 have been published [41], [53]. In a first study [41], 2.0 mm thick sheets were joined using a variety of welding parameters. The rotational speed and duration time were varied, which were 1500, 1750 and 2000 rpm, and 3 ,4 and 5 s, respectively. The plunge depth was kept constant, but is not mentioned. The general conclusion is that with the combination of lower rotational speed and shorter joining time optimal mechanical properties can be obtained. In contrast, a study of performing FSW on the same material states that for higher rotational speeds, the material may strengthen due to precipitation dissolution and natural aging [54]. However both studies agree that when working at a higher rotational speed, the joining time should also be extended [41]. It is important to notice that these results may not be very significant as many imperfections, such as hooking, voids, incomplete refill and lack of mixing, were present in the welds. Those are attributed to inappropriate processing parameters leading to poor material flow and plasticity of the base material [41]. Figure 17 shows the different observed imperfections. The bonding ligament is classified as an imperfection due to its banded structure. The sheet materials were covered with an Alclad layer, a thin layer of pure aluminium to improve the corrosion resistance. This surface layer formed bands in the bonding ligament and lowered the mechanical fusion at the weld interface [41]. The numerous voids that were present, also diminished the integrity of the weld. The produced samples were validated using a lap shear test and a cross-tension test. The strongest bonds were obtained at a rotational speed of 1500 rpm and a joining time of 3 s. For these parameters, the maximum strength measured in the lap shear test and cross-tension test was 7.0 kN and 2.6 kN, respectively [41]. The fracture followed a nugget shear fracture path in the lap shear test and the cross-tension test. The shear fracture started at the hook effect and took place along the

boundary between the upper and lower sheets through the nugget of the weld [41]. This fracture mode confirms the poor quality of the weld.

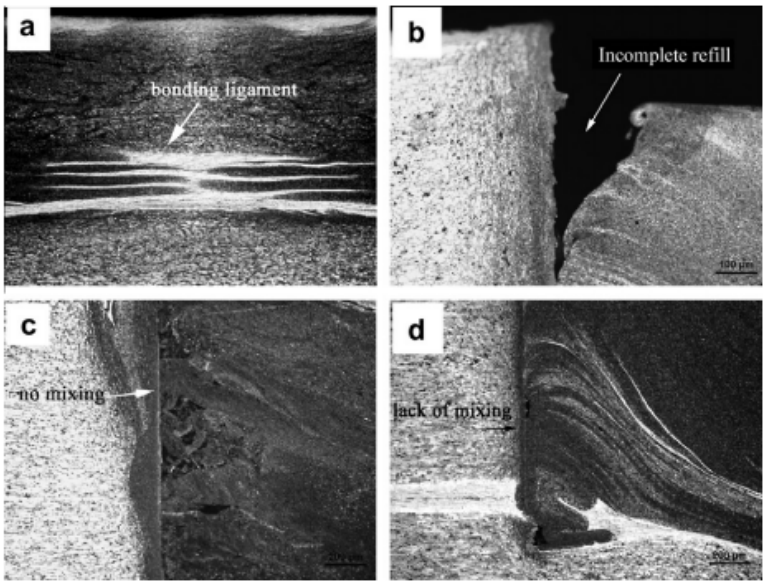

Figure 17: Imperfections in an EN AW-7075-T6 joint: (a) bonding ligament, (b) incomplete refill, (c) no mixing and (d) lack of mixing [41]

In a follow-up research on EN AW-7075-T6 [53], 0.8 mm thick sheets were joined at a relatively high rotational speed of 2100 rpm, which was higher than the previous study. The joining time and plunge depth were varied over 3.0 and 3.5 s, respectively 0.85, 0.95 and 1.1 mm. The joining time can be considered relatively long compared to the previous research as the sheet thickness is less than half. The best result was obtained for the highest plunge depth and joining time and this corresponded to the largest nugget thickness, due to the increased amount of material volume that was subjected to heating and dynamic recrystallization [53]. This combination of parameters also resulted in the smallest hook. Figure 18 shows the weld cross sections corresponding to the different parameter combinations. The increasing stir zone area with increasing plunge depth and joining time is clearly visible. In contrast to other research studies, the hook had no significant effect as nucleation site, since the non-bonded interface did not end within the hook feature [53]. The strongest bond, which attained a force of 4.7 kN, failed by a plug type fracture as shown in Figure 19. The fracture initiated near the end of the non-bonded region, labelled as B and hence not in the hook region. The propagation of the crack travelled along the minimum hardness zone. The high heat input that followed from this parameter combination had also some other effects: decreased hardness in TMAZ and the occurrence of molten films in the stir zone [53]. Coarsening of the grain size and precipitates caused the extra hardness reduction in the TMAZ, but the typical W-shape remained. A temperature of 471 °C was measured during the plunging and retreating stages. These thermal cycles imply that dissolution of precipitates will occur and the dissolution of some precipitates will not be completed before the melting temperature is reached [53]. This led to the formation of liquid films and liquation cracks which are visible in Figure 20. It has been shown that a temperature of 527 °C is possible during FSSW of EN AW-7075-T6, which is higher than the incipient melting point [55]. Local molten films dissolved rapidly in the high temperature stir zone and when the spot weld cooled to room temperature following welding, evidence of local melting was

observed [56]. Even in FSpW, eutectic films are reported along the grain boundaries [43]. They appeared as black lines in the stir zone and indicated that local melting had occurred during processing.

Research on 1.6 mm thick EN AW-7075-T6 was started in last year's master dissertation, but insufficient decent samples could be investigated to conclude any influence of the welding parameters. The following parameter values were suggested to perform a parameter analysis: rotational speeds of 1500-2000-2500 rpm, dwell times of 0-1-2 s, plunge depths of 1.8-2.2-2.7 mm, plunge time and a retraction time of 2 s [17].

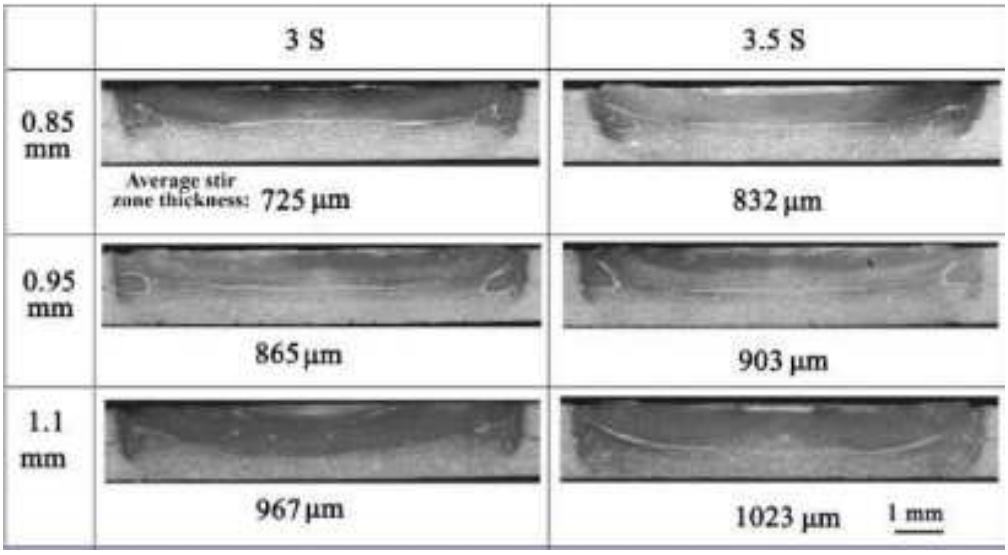

Figure 18: Cross section of the nugget thickness in EN AW-7075-T6 joint, obtained at various plunge depths and joining times [53]

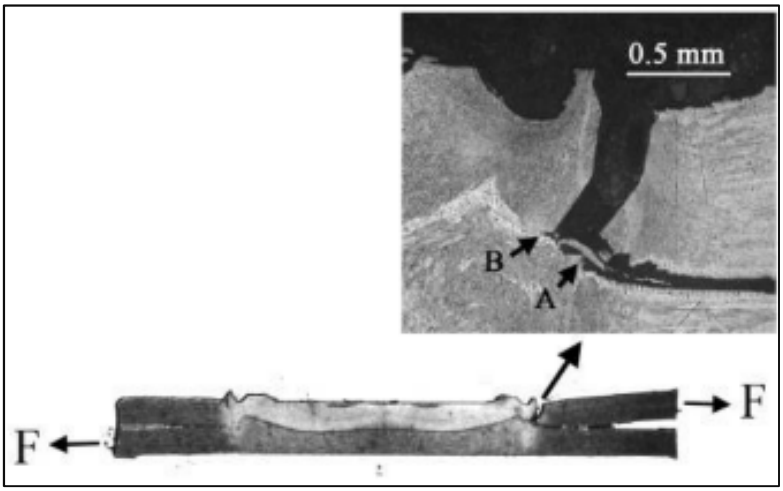

Figure 19: Plug pull-out at the upper sheet [53]

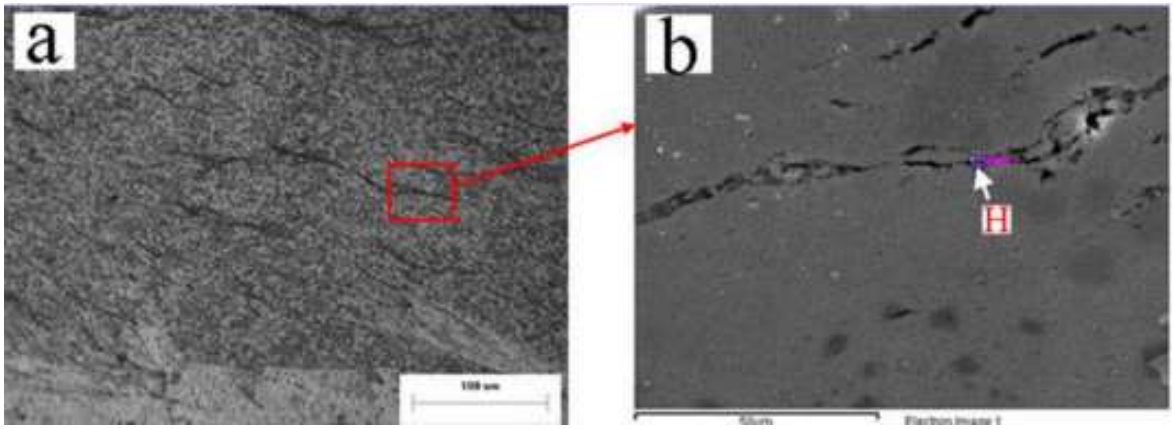

Figure 20: Melting cracks in the SZ: liquation crack indicated by H [53]

Friction spot welding of EN AW-7475-T761 has already been investigated as a dissertation topic at the Belgian Welding Institute [17, 18]. Some conclusions are discussed below. Rotational speed seems to have little influence on the weld quality as long as it stays in the range of 1000-2000 rpm [18]. The joining time has the largest influence and is recommended as 10 s for a 1.6 mm thick sheet. Lower durations result in a poor or absent bonding ligament [18]. Both dissertations disagree on the influence of plunge depth, but agree that it should be at least equal to the sheet thickness. The individual effect of the plunge time, the dwell time and the retraction time, which is almost never discussed in literature, was investigated. The plunge time seems rather irrelevant, the dwell time should be sufficiently long in order to create a bonding ligament, but the retraction time is most important. To refill the keyhole and to form a good final structure, the retraction time should compose around 50% of the total joining time [18].

An Alclad EN AW-7B04 aluminium alloy, which is derived from EN AW-7075 aluminium alloy [43], is used in a FSpW process with 1.9 mm thick sheets [52]. The fixed parameters are a rotational speed of 1500 rpm and a plunge and retraction rate of 1 mm/s, combined with zero dwell time. The plunge depth is varied over 2.0, 2.5, 3.0, and 3.5 mm and thus the joining time becomes 4, 5, 6 and 7 s accordingly. The lap shear strength is strongly dependent on the plunge depth and reaches a maximum of 11.9 kN at a value of 3 mm and hence a joining time of 6 s [52]. This behaviour can be explained by the microstructure. At a low plunge depth, the hook penetrates into the stir zone and diminishes the effective bonding area. At a higher plunge depth, the vertical material flow bends the hook upwards out of the stir zone. For the highest plunge depth value of 3.5 mm, the hook becomes too significant and harmful. The effect of the Alclad layer is also dependent on the plunge depth. A larger plunge depth results in a more dispersed pattern of the Alclad material throughout the stir zone and thus lowers the level of stress concentration. Furthermore, the hardness profile, which is typically W-shaped, is also affected by the welding parameters selected. An increasing plunge depth and joining time adds extra heat and softens the HAZ. For the highest plunge depth-value of 3.5 mm, the softened weld starts to affect the lap shear strength. All strong welds failed in a tensile-shear mixed mode [52]. The crack first initiates at the hook and grows vertically and around the periphery of the weld (tension mode), and finally the crack propagates through the stir zone (shear mode). A final observation is the occurrence of an annular groove for an increase in plunge depth. This means that the keyhole cannot be fully refilled due to a loss of material. This material is lost between the sleeve and clamping ring where it forms the

annular groove. This effect was compensated by applying a 0.2 mm surface indentation at the end of the weld procedure in order to achieve a complete refill (Figure 21) [52].

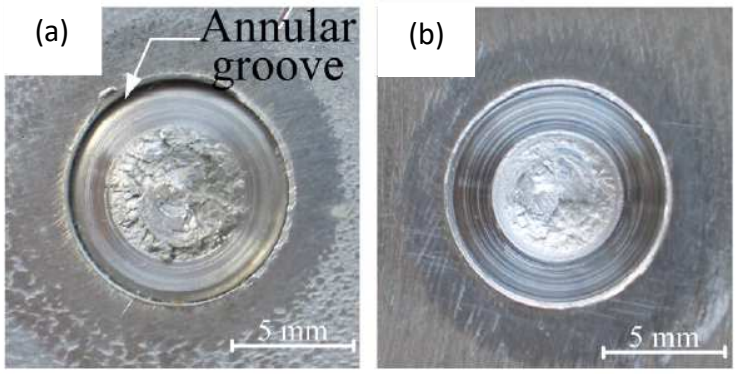

Figure 21:Occurrence of annular groove: (a) without indentation (b) with 0.2 mm indentation [52]

5.2 2xxx aluminium alloys

The 2-series aluminium alloys are well-known for their high strength over a wide range of temperatures. Classified as high-performance materials, they are frequently used in aerospace and aircraft applications. They are heat treatable like the 7-series but the main constituent is copper instead of zinc. Unfortunately, this material class also suffers from low weldability and is considered non-weldable by the conventional arc welding processes. The most convenient alloy in research and aerospace is EN AW-2024-T3. The composition and mechanical properties of this Al-Cu-Mg alloy are presented in Table 7 and Table 8.

Table 7: Composition of EN AW-2024-T3 in weight % [47]

Al	Cr	Cu	Fe	Mg	Mn	Si	Ti	Zn	Other
90.8-94.7	0-0.1	3.8-4.9	0-0.5	1.2-1.8	0.3-0.9	0-0.5	0-0.15	0-0.25	0-0.15

Table 8: Mechanical properties of EN AW-2024-T3 [47]

Yield strength (MPa)	Tensile strength (MPa)	Failure strain (%)	Melting point (°C)
248-372	359-510	8-15	502-638

In contrast to the 7-series, the weldability of the EN AW-2024 alloy using FSpW has been investigated by different researchers. In most cases, the researchers used a sheet material covered with an Alclad layer. This Alclad layer has a negative influence on the quality of the weld. Alclad islands with lower mechanical properties are formed in the stir zone, resulting in a non-uniform microstructure and strength distribution [46]. The bonding ligament, which is the bonded zone between the two plates, is entirely composed of pure aluminium which easily results in non-uniform stress distributions [48]. In the present work, sheets without this protective layer are used and there will not be given any further attention to these side effects.

Several studies inspect the metallographic cross-section of the weld. Inherent imperfections as hooking are always present and cannot be avoided, only diminished [48]. Other imperfections, mostly resulting from insufficient material flow, such as tearing, voids and incomplete refills were present. Tearing and voids often appear at the TMAZ/SZ interface as metallurgical bonding takes places along this edge after tool retraction. Tearing (Figure 22a) can be attributed to the insufficient metallurgical bond which cannot sustain the tensile stresses upon cooling. High forces, temperature and time are required to form a sound metallurgical bond. Unfortunately, the TMAZ/SZ interface is parallel to the axial force and thus the radial forces applied by the sideways material flow are not that high. Incomplete refill (Figure 22b) can also partly be attributed to the tensile stress generated upon cooling. The shrinkage forces enlarge the incomplete refill gap. Another reason is that material is extruded into the tool gap, known as gap loading [48].

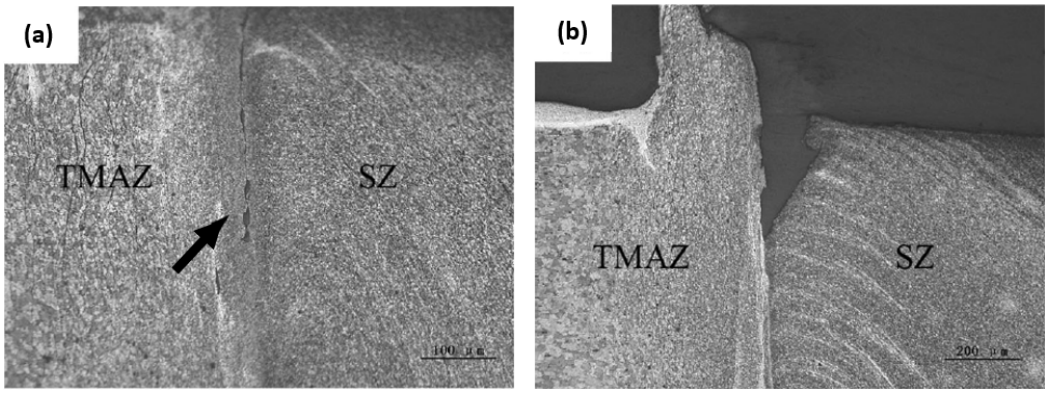

Figure 22: (a) Tearing at TMAZ/SZ interface, (b) Incomplete refill [48]

The stir zone always exists of finer grains as a result of dynamic recrystallization. However, the microstructure in the SZ can be classified into a pin-affected zone (PAZ) and a sleeve-affected zone (SAZ) [57]. In the SAZ, the material was violently stirred by the sleeve. Meanwhile, the material in the PAZ is not directly stirred by the pin or sleeve [48]. This results in coarser grains in the PAZ, although still much finer than the base material.

The search for optimal welding parameters always returns in friction spot welding research. In [13], the rotational speed (1900/2400/2900 rpm) and joining time (4.8/5.8/6.8 s) were varied. No dwell time was used and the plunge depth was constant (2.5 mm for a 2.0 mm sheets). Using design of experiments, a statistical approach, the parameters required to obtain a maximum lap shear strength were identified. The maximum value of 10.1 ±0.1 kN was achieved for a rotational speed of 2400 rpm and a joining time of 6.8 s. The effect of rotational speed was limited and the weld strength only increased from the lowest to the medium value of joining time. However, the interaction between both parameters is interesting. Only at the highest rotational speed, interaction was noticed with a clear optimum for the medium joining time. For the short joining time, an increase in rotational speed will lead to a higher weld strength because more heat was being generated by friction, which increases the nugget area. For a longer joining time, an increase in rotational speed will lower the weld strength as the heating efficiency already was quite high. The increase in heat input lowers the heating efficiency as slipping of the tool occurs. This is known as the slip/stick transition [13]. The influence of plunge depth and plunge rate is investigated in [46]. The plunge depth should be chosen such that the sleeve plunges in the lower sheet

for 25 % of the lower sheet thickness. This is in good agreement with the common practice of 30 % penetration of the bottom sheet in FSW [46]. Lower plunge rates are mostly beneficial for the shear performance, although in some parameter combinations this can differ. The lap shear strength seems to decrease when only the rotational speed is increased because of a softer stir zone and a widened HAZ [48]. However, an optimum is reached for the rotational speed, based on a cross-tension test [57].

The choice of the welding parameters is also related to the fracture mechanism. Two main failure mechanisms exist in lap shear testing: through the weld fracture and plug pull-out [13].The former consists of a crack path through the stir zone and actually fails in pure shear at the bonding ligament. The nugget is horizontally split in half and each half is still connected to the specimen sheets. The latter consists of a crack path perpendicular to the sheet interface and follows the weak plunge depth path. The complete weld nugget remains welded to one of both sheets, while a hole is left in the other sheet. Both failure mechanisms often start at the hooking imperfection. The shear fracture often corresponds to high rotational speed manufacturing of the weld. At higher speeds, the material is more stirred and the extra frictional heat improves the metallurgical bond at the TMAZ/SZ interface. The bonding ligament will consist of coarser grains and will hence be more prone to a failure through the weld nugget. At low rotational speeds, the bond at the TMAZ/SZ interface will be of minor quality as the limited material flow results in tearing and voids at the interface. The crack will prefer this interface for propagation [48]. In peel or cross-tension testing, the fracture modes are slightly different. As the weld is not loaded in shear, the through the weld fracture does not take place and all fractures propagate through the thickness. Again, two fractures modes are observed: plug pull-out along the TMAZ/SZ interface or complete nugget removal along the TMAZ [57]. The former mode appears at lower rotational speeds for the reasons discussed above. The latter mode takes place in the softened TMAZ because of the high heat input.

5.3 Summary and conclusions

This chapter discussed the influence of the processing parameters on the weld quality in high-strength aluminium alloys. Different researches state different optimal process parameters since the sheet thickness and material differs. Overall conclusions are that the rotational speed has a minor influence on the weld strength. The plunge depth however is of great importance and should be kept about 25 % in the bottom sheet. The influence of the joining time is less clear, but the interaction between the rotational speed and the joining time is a strong point of discussion since they both control the heat input. Furthermore, the distinction between different failure modes was made: through-nugget and plug pull-out failures. This work will focus on the influence of the process parameters using a design of experiments approach. The obtained strength values, hardness profiles and failure modes will be compared to this state-of-the art review.

Chapter 6 Experimental test procedures

Previous chapters were based on a review of published researches. They explained the process and the possibilities to control its joint quality. Typical observations were discussed in detail and compared for different materials. The most important challenges of this process were stated and some solutions were suggested. This chapter is the start of the experimental part of this master dissertation. It gives an overview of the different techniques and procedures used to qualify the weld. Testing different weld aspects will allow to obtain more insight into the influence of the welding parameters on the weld quality.

6.1 Welding trials

In this research, the workpiece material EN-AW-7075-T6 with sheet thickness 1.6 mm has been used. The composition and mechanical properties of this high-strength aluminium alloy have already been presented in section 5.1. All welds were produced with the RPS100 machine as described in section 2.3. The welding is semi-automatic and can be performed by anyone after a short training. The movement of the tool components can be programmed in the interface, while the clamping pressure has to be set manually at the pressure gauge. Additional clamping pliers are used to prevent the workpiece material from lifting together with the clamping ring when the tool head retracts. The upper sheet tends to stick to the clamping ring due to a limited indentation. The clamping of the workpiece should be sufficiently rigid to avoid bending of the specimen between the clamping pliers and the clamping ring upon retraction. The user interface allows the operator to program and save a certain welding procedure. The movement of the tool components is programmed in discrete steps. In each step a desired depth of the pin and the sleeve, a rotational speed and a step duration are set. The duration is the time that it takes to go from the previous to the current state. Pin and sleeve always move according to a certain ratio in order to respect the conservation of volume of the displaced plasticized material. This ratio is computed and fixed as 1.023 by the machine manufacturer. Positive depth values indicate a position inside the workpiece material, the zero depth starts at the upper sheet surface.

At start-up, the tool components first rotate for 30 seconds to warm up the tool. To reduce cold start effects on the weld quality, three dummy welds were always produced after start-up before producing any experimental test specimens. This ensures that the tool temperature is at a nominal state for all the test samples. The tool head is water cooled during the process, which makes it possible to weld at a fast rate without overheating the machine. Besides eliminating cold start effects on the test results, warming up of the tool is necessary to produce welds with certain parameters. Producing welds at a slow rotational speed of 1000 rpm is not recommended when the tool head is cold. It requires too much torque to rotate the sleeve at this slow speed as the material hardly softens. This condition has led to several alarm warnings stating that the spindle actuator measures an overcurrent. Fortunately, these alarms did not lead to a machine failure, as the warning limit was set to 80% of the maximal allowable current.

As thoroughly explained in Chapter 3, the tool suffers from gap loading. This contamination phenomenon of the tool head is an intrinsic problem of the friction spot welding technique. Workpiece material that has filled the tolerance gaps between the tool components can never leave this area again

during any stage of the process. Three different cleaning programs are pre-programmed in the machine software to mechanically clean the tool: pin-cleaning, sleeve-cleaning and combined cleaning. The majority of the material is removed from the tool during sleeve-cleaning as this removes the accumulated material between clamping ring and sleeve. One millimetre thick aluminium rings have been removed from this wide tolerance gap. Mechanical cleaning was executed every 15 welds, or sooner if needed, to avoid excessive tool contamination or tool failure. When the pin or sleeve are contaminated at the bottom, hence not only between the tolerance gaps, chemical cleaning is necessary. The tool components are submerged in NaOH, which dissolves the adhered material from the tool. Chemical cleaning was required three times during this master dissertation, but mostly due to the use of incorrect parameter combinations or tool settings.

Despite the good maintenance of the machine, a problem with the zero-setting occurred. The zero-setting is the relative position of the three tool components. This setting is used as a reference for all tool movements. The zero-setting should be chosen such that the produced weld has a flat unlevelled surface. After producing about 100 welds, irregular weld surfaces were created. The zero-setting was no longer correct and impossible to reset. Chemical cleaning and disassembling of the tool head were required to solve this problem. After reassembling, the zero-setting was recalibrated and flat welds could be produced again. Important to note is that the perfect zero-setting is different for different workpiece materials.

6.2 Visual inspection

The first quality test is a visual inspection of the weld surface. Weld surfaces can contain imperfections, which are mostly related to tool problems. Situations that can lead to an imperfect surface are sticking of material to the tool, poor refill at the clamping ring-sleeve interface and wrong zero-setting. To qualify the surface quality, a score from 1 to 3 was given. Table 9 gives an overview of the different classes and Figure 23 shows typical weld surfaces.

Table 9: Surface quality classes

1	Surface without imperfections
2	Surface with minor imperfections and/or small circumferential grooves
3	Surface with large imperfections and/or large circumferential grooves

Figure 23: Surface quality classes: class 1 (left), class 2 (middle) and class 3 (right)

6.3 Metallographic examination

The microstructure of the workpiece material has severely changed during the welding process. The influence of the different parameters is visible in a metallographic image. Section 4.1 already gave an overview of the typical regions of interest that can be examined. Before metallographic examination is possible, a couple of steps needs to be performed: cutting, embedding, polishing and etching. The produced welds are cut along the centre of the weld nugget. The cross-sections are then placed into specimen mounting cups and embedded in an epoxy. A mixture of CaldoFix resin and hardener is used. At room temperature, a curing duration of 1-2 days was required. Subsequently, the metallographic samples were ground to remove any epoxy traces from the cross-section surfaces. Afterwards, several polishing steps were applied to remove all micro-scratches. Every polishing step requires a finer polishing clot and suspension. When the cross-section is perfectly polished, investigation under the Olympus MX51 optical microscope is possible.

Each sample is first inspected in the non-etched condition as this facilitates the detection of imperfections. The total area percentage of imperfections in the cross-section is calculated afterwards. Figure 24 shows a non-etched cross section with several imperfections and a coloured version with detected imperfections in red. The total area percentage of imperfections is calculated as the percentage red of the complete rectangle. Only imperfections with a minimum area of 0.002 square millimetres are taken into account to exclude small porosities inherent to the parent material. The global percentage of imperfections gives an indication of the overall weld quality, but does not take into account that some imperfections are more dangerous than others. Sharp, fine imperfections like a non-bonded interface, lead to higher stress concentrations than spherical voids. Additional measurements were performed on two types of imperfections: the depth of the incomplete refill and the width of the non-bonded interface.

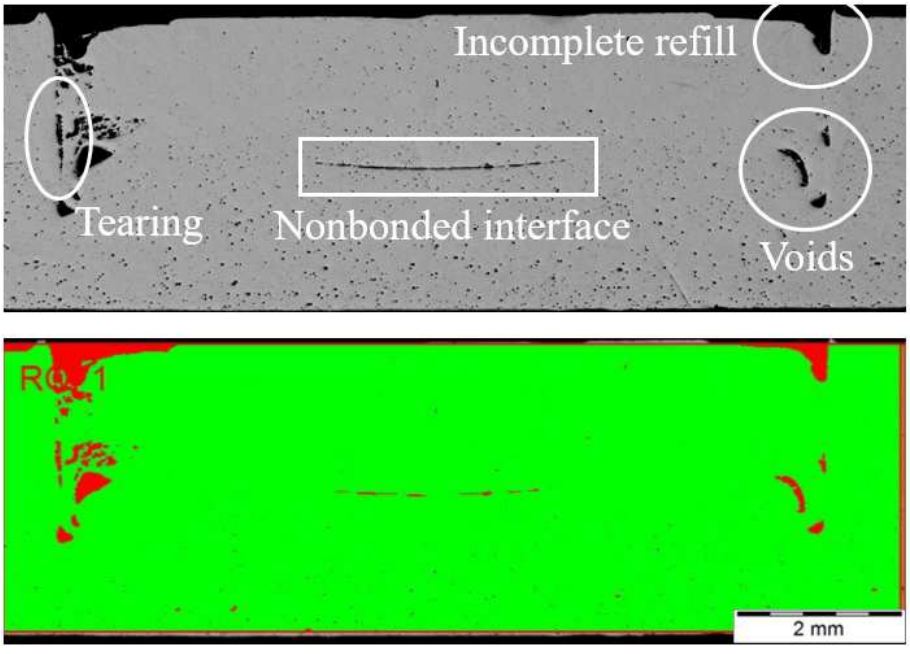

Figure 24: Non-etched cross-section (top) and area percentage of imperfections (bottom)

Subsequently, the samples were etched using Keller's reagent to reveal the weld microstructure. Figure 25 shows an embedded and etched sample with three weld cross-sections. Due to the large variety in grain sizes in the weld, the etching duration is very crucial. Different regions were inspected with special interest for imperfections and material flow patterns.

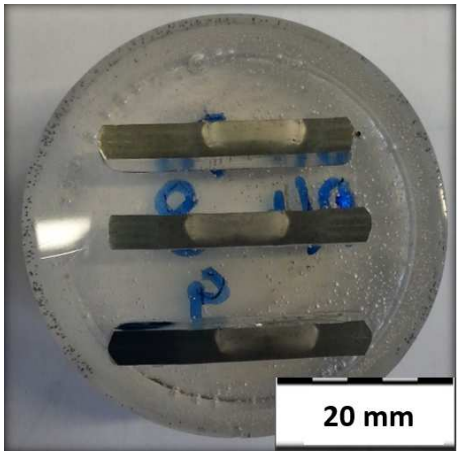

Figure 25: Sample holder containing three etched weld cross-sections

6.4 Temperature measurements

Heat supply is very important in welding. Unfortunately, this cannot be controlled directly but should result from a good combination of controllable welding parameters. Consequently, it is interesting to investigate the influence of controllable welding parameters on the temperature distribution during welding. Logging the temperature in the stir zone is a difficult task as some practical problems arise.

Firstly, the stir zone itself is not reachable with any kind of thermocouples as they would get destroyed by the stirring of the welding tool. Attaching a thermocouple to the bottom of the weld nugget is not possible either. The workpiece material is clamped between clamping ring and backing anvil and hence the bottom of the workpiece is unreachable. The closest place one can attach a thermocouple to is right next to the clamping ring. Other contactless measurements such as infrared thermography suffer from the same impracticalities. The region of interest, the welding nugget, is always covered by the clamping ring and backing anvil.

Secondly, the attachment of a temperature measurement device on an aluminium alloy is not evident. Normally, thermocouple wires are spot-welded to the workpiece in order to achieve a strong and small electrical contact. However, trying to spot-weld thermocouple wires to the aluminium workpiece resulted in very brittle contacts, which failed upon the slightest force. Since the conventional connection method was not successful, an alternative attachment method was used. The thermocouple wires were connected to the workpiece with high thermally conductive epoxy glue having an elevated working temperature. The thermocouple wires were placed against the workpiece material and fixed with Fisher Elektronik WLK 5 glue. A sample with connected thermocouple wire is shown in Figure 26. The blue epoxy glue covers the thermocouple wire and fixes it firmly to the substrate. A hook is bent at the end of the thermocouple wire to ensure a point measurement. Two welds are placed right next to the glue. Since the glue is smeared out, the measurement point is relatively far away from the weld centre.

Unfortunately, this alternative connection method was not successful either. Upon heating of the sample and the epoxy, the glue expanded and lifted the thermocouple from the workpiece resulting in a signal loss. Upon cooling and contraction of the glue, the thermocouple re-made contact. Hence, the highest and most interesting temperatures were not recorded.

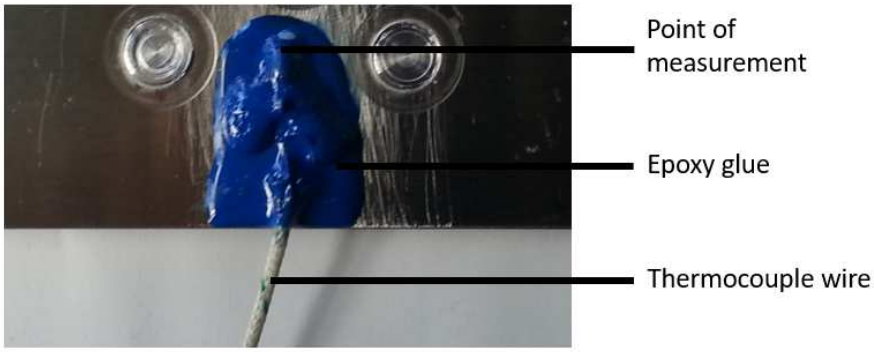

Figure 26: Thermocouple wire attached with epoxy glue

As a final alternative, the thermocouple wires were bolted to the workpiece material using a metric M3 bolt and corresponding washer. Both thermocouple wires were clamped between the washer and the workpiece. The disadvantage is that the thermocouple also measures the temperature of the washer instead of the workpiece alone. A possible future improvement could be to replace the washer by an electrically insulating alternative. However, it is recommended to focus on other connection techniques for the thermocouple wire so that it can be located closer to the weld centre. Figure 27 shows the location of the tapped hole where the thermocouple wire was connected. The weld is placed as closely as possible to the washer. All temperature measurements are logged at a distance of 13 to 15 mm from the weld centre at the upper sheet surface. The temperature was measured with a K-type thermocouple and processed using LabVIEW.

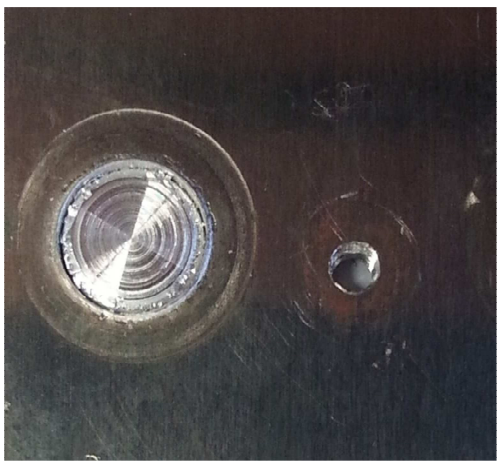

Figure 27: M3 tapped hole next to a weld to attach a thermocouple wire

6.5 Microhardness measurements

The different microstructural zones investigated during metallographic investigation should be linked to a difference in hardness. Since the tensile strength and hardness of a material are related, softening of the workpiece material should be limited. To quantify the change in hardness, microhardness measurements are performed. Full hardness map measurements are executed to quantify the hardness value in all locations across the weld cross-section. Transverse measurements give more insight into the hardness reduction at different distances from the weld centre. The full hardness maps were obtained using the Leco AMH43 Automatic Micro-Indentation Hardness Testing System of Laboratory Soete of Ghent University. A microscopic image of a characterized weld cross-section is given in Figure 28. The hardness is automatically obtained at every indentation. After calibration, the testing system makes and measures all indentations autonomously. The indentations for the full hardness map were produced with a force of 1kgf. Transverse hardness measurements are executed manually as the amount of indentations is limited. These tests are performed on the Struers duramin A300 machine of the Belgian Welding Institute. A load of 0.5 kgf is used on this machine and the indentations are separated by 0.5 mm. Figure 29 shows the transverse indentations across the weldment. The transverse is located at mid-thickness of the upper sheet such that all distinctive zones of the weld are tested. Notice that the weld is placed asymmetrically along the cross-section, to ensure that the measurements reach the base material.

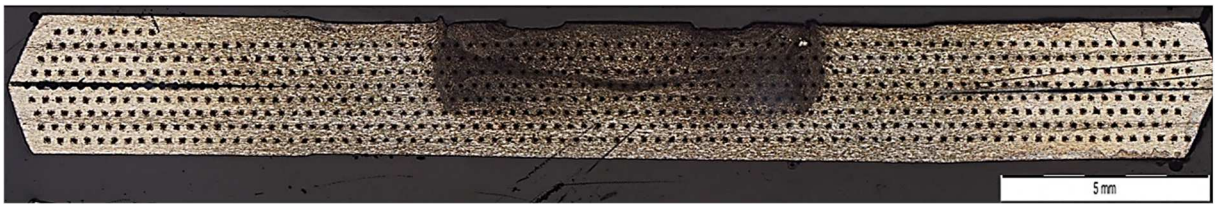

Figure 28: Full map hardness indents (HV1) on specimen no. AF-75-R2-10

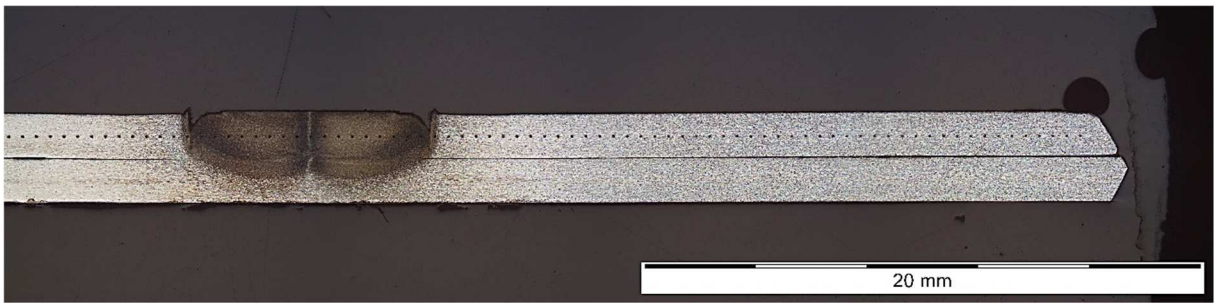

Figure 29: Transverse hardness indents (HV0.5) on specimen no. AF-75-H2-5

6.6 Lap shear strength testing

The most practical quality test for an overlap weld is a lap shear strength (LSS) test. This standardized testing method resembles the typical load application for lap joints. The lap shear tests were performed according to EN ISO 14273. The test samples were cut in the specified dimensions and then joined with a prescribed overlap length. A technical drawing of the lap shear specimen is given in Figure 30. To ensure a full shear loading, shims of the same material and thickness were placed between the tensile clamps. Otherwise the misalignment between the two plates would induce an extra bending moment. The lap shear tests were performed on a conventional tensile machine Instron model 8801. All tests were performed at a displacement rate of 10 mm/min. To evaluate the variation in the results, each welding condition was repeated three times. The evolution of tensile strength and displacement were recorded over time. The maximum lap shear strength and the displacement at failure are used as output parameters of these experiments.

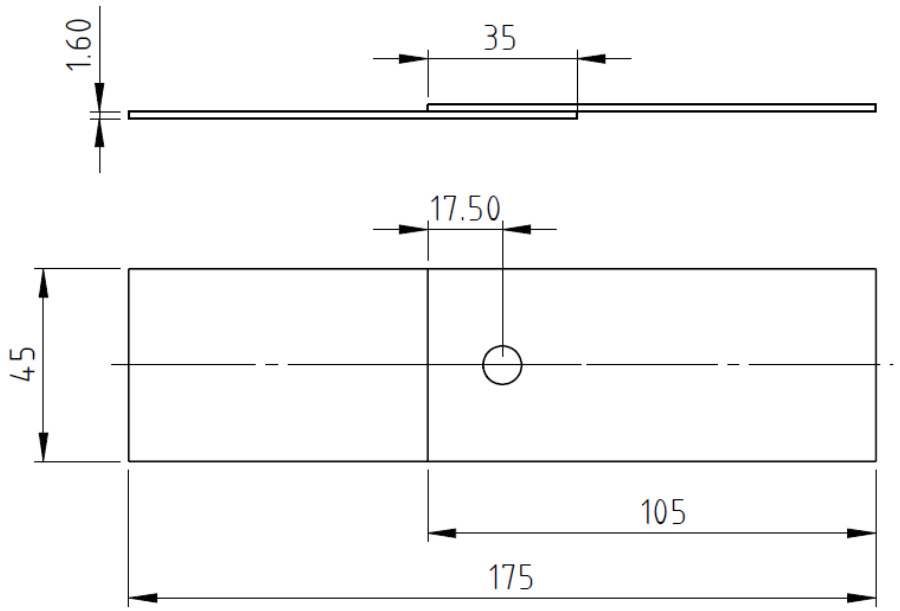

Figure 30: Lap shear specimen dimensions (mm) according to EN ISO 14273

A qualitative output parameter of these strength tests is the failure mode of the specimen. Three different modes are distinguished: plug pull-out at the upper sheet (PU), plug pull-out at the lower sheet (PL) and through-nugget failure (N). Figure 31 shows these three distinctive failure modes. In the two cases of the plug pull-out, the nugget is removed from one of the two sheets but is still attached to the other sheet. The failure has occurred circumferentially around the weld nugget in the weakest sheet. In the case of a through-nugget failure, the weld nugget is sheared in half at the original sheet interface. Both sheets are still joined to one part of the weld nugget. It is important to note that real failure modes can be a combination of these three types, for example a combination of through-nugget failure and plug pull-out or plug pull-out from both sheets.

	plug pull-out at upper sheet	plug pull-out at lower sheet	through-nugget failure
Upper sheet			
Lower sheet			

Figure 31: Failure modes: PU, PL and N

6.7 Cross-tension strength testing

Lap shear tests have shown results with large variation in the past [17]. Therefore, an alternative strength test is introduced in this work. Cross-tension testing appears less frequently in published research about FSpW, but it is a proven method to test spot joints. The loading is totally different than in lap shear testing. Since the applied loading is not the strongest loading direction of an overlap joint, it is expected that the cross-tension strength (CTS) will be lower. The strength tests were performed according to EN ISO 14272. The test samples were cut in the specified dimensions and provided with clamping holes. A technical drawing of one sheet that is part of a cross tension specimen is given in Figure 32. A second identical sheet is spot welded perpendicular on top of the other sheet forming a cross with an overlapping area of 50x50 mm². The spot joint is centred at this overlap. During the cross-tension test, the two sheets are lifted from each other until failure occurs. A good clamping of the sheets is important to avoid as much as possible bending contributions. Moreover, it should be possible to perform these tests on a conventional tensile bench. Hence, a design of a clamping system was highly required. Based on a conceptual sketch in EN ISO 14272, the clamping system of Figure 33 was designed. The technical drawings can be found in Appendix B. The exploded view explains the assembly and use of the clamping system. The cross-tension specimen (white crossed sheets) is clamped between clamping blocks through the clamping holes. The long rods at the clamping blocks are used to fix the structure into the tensile bench. Upon applying force, both clamping blocks are pulled apart and the cross-tension specimen breaks at the only connection: the FSpW joint. The cross-tension tests were also performed on the conventional tensile machine Instron model 8801, but a less powerful load cell was installed. All tests were performed at a slower displacement rate of 1 mm/min. These precautions are made because the expected strength is much lower than with the lap shear tests. To evaluate the variation in the results, each welding condition is repeated three times. The evolution of tensile strength and piston displacement are recorded over time. The maximum cross tension strength and the

displacement at failure are used as output parameters of these experiments. The failure modes are classified as explained in section 6.6.

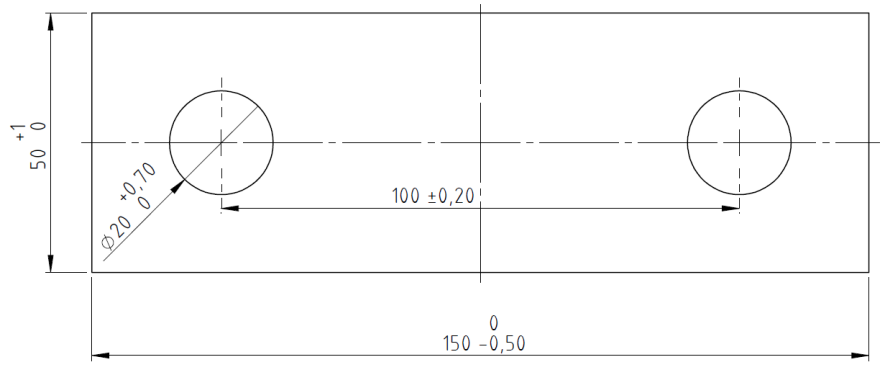

Figure 32: Dimensions (mm) of one sheet of a cross tension specimen according to EN ISO 17272

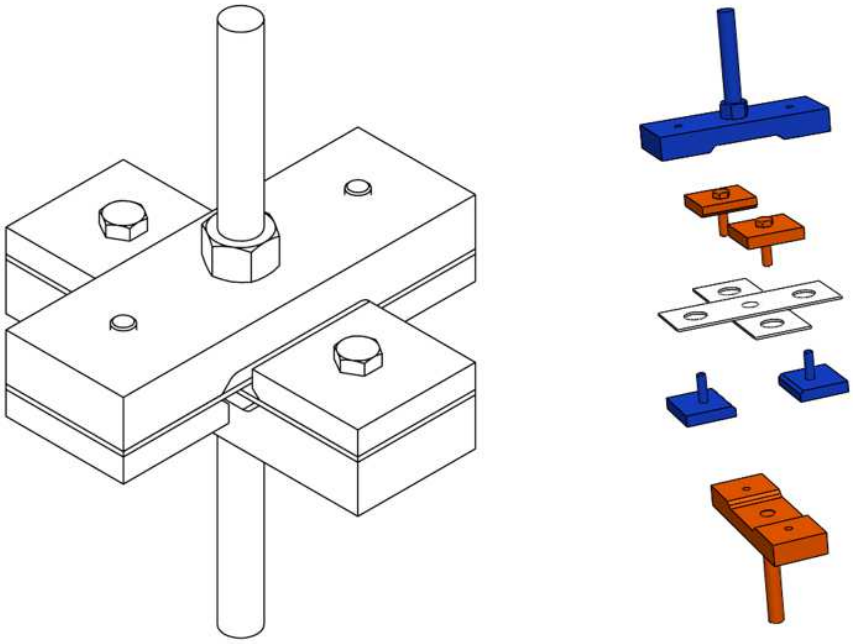

Figure 33: Cross tension clamping system: isometric (left) and exploded (right) view

Chapter 7 Experimental weld matrix

This chapter introduces the experimental weld matrix, an overview of all welding conditions that have been tested during the course of this research.

A welding condition is a set of process parameters that are used to produce a certain weld. The process parameters of interest have been discussed in section 2.2, as well as their relative importance. Based on published research, three parameters were chosen as design factors: rotational speed, joining time and plunge depth [6, 49]. The remaining parameters were kept constant for all weld conditions. The plunge rate and retraction rate were both set at a value of 0.8 mm/s, which should be sufficiently slow according to [52]. The clamping pressure was obtained by trial-and error and fixed to a value of 3.5 bars. This provided a sufficiently strong clamping, without excessive plastic deformation of the workpiece surface. The dwell time follows after short calculation from the joining time, plunge depth and plunge/refill rate. The typical parameter limits have been discussed in section 2.2, however without taking the limits of the welding machine into account. The combination of both boundary conditions leads to the ranges presented in Table 10.

Table 10: Possible process parameter ranges

RS (rpm)	500 – 3300
JT (s)	2 – 15
PD (mm)	t - 2t, where t = sheet thickness

Since one of the goals of this master dissertation is the investigation of suitable welding parameters, the welding conditions have been optimized over time during this research. A set of welding conditions used in successive optimization steps is called a series. The different series are labelled starting with the code 'AF-75' which stands for AluFrix, an acronym for aluminium friction welding, and which refers to the workpiece material EN AW-7075-T6. This code is followed by a character indicating the sample purpose: 'R' for metallographic testing, 'T' for strength testing, 'H' for hardness testing and 'TM' for temperature measurements. The last part of the sample name is the number of the welding combination, uniquely related to the different parameter settings. Note that the different welds in a series have been welded in a statistically randomized order, so to exclude any secondary effects of the welding environment. A complete overview of all produced weld samples during the course of this master dissertation is given in Appendix A. In the remainder of this section, a schematic and tabular overview of each series are given.

First some preliminary test welds (R0 series) were produced to validate the selected constant values for the plunge rate, the retraction rate and the clamping pressure. Afterwards, the first test matrix (R1 series) was constructed based on the limited published research on EN-AW-7075-T6 [17, 41, 53]. Table 11 and Figure 34 give an overview of the experimental welding conditions of the R1 series (1 to 9). The nine combinations have all been evaluated by metallographic inspection. Note that for this test series, the dwell time is chosen as varying factor. A range of the dwell time of 0-4 s together with the chosen range of plunge depth results in a range of the joining time of 4-10 s. For further test series, the joining time will be used instead of the dwell time, since this is more proportional to the total heat input. Energy input is an important factor in the control of welding processes.

Table 11: Welding conditions in R1 series

Welding condition	RS (rpm)	DT (s)	PD (mm)
AF-75-R1-1/3	1500	0	1.6/2.4
AF-75-R1-5/7		4	
AF-75-R1-2/4	2500	0	
AF-75-R1-6/8		4	
AF-75-R1-9	2000	2	2.0

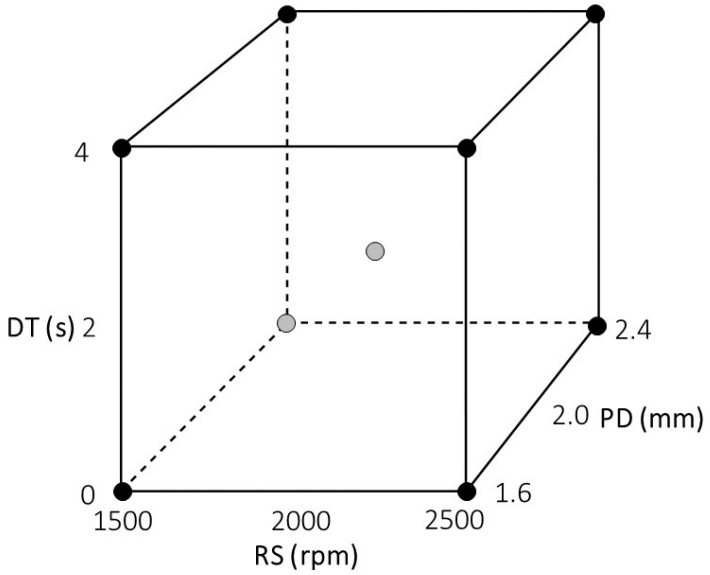

Figure 34: Schematic overview of welding conditions in R1 series[1]

The parameter settings for the second series of welds (R2) were shifted compared to the first one (R1). Some careful conclusions were made to omit the lowest joining times. The rotational speed was shifted to higher values. Sequentially, a third series (R3) was added to also include the rotational speed of 1000 rpm. Earlier, this low rotational speed was not considered as this resulted in tool failures in the past. Table 12 and Figure 35 give an overview of both R2 and R3 series. Again, all 27 samples were investigated under the optical microscope without performing any replications.

Weld samples used for hardness or temperature measurements are a selection of series R2 and R3. No new parameter combinations are used for this purpose. The sample name then contains the character 'H' or 'TM' as discussed above. An overview of the hardness and temperature samples can be found in Appendix A.

[1] The grey colour of some welding conditions is only for improved visual-spatial ability, without further meaning.

Table 12: Welding conditions in R2 and R3 series

Welding condition	RS (rpm)	JT (s)	PD (mm)
AF-75-R2-1/3/5	2000	6	1.6/2.0/2.4
AF-75-R2-7/9/11		8	
AF-75-R2-13/15/17		10	
AF-75-R2-2/4/6	3000	6	
AF-75-R2-8/10/12		8	
AF-75-R2-14/16/18		10	
AF-75-R3-1/2/3	1000	6	
AF-75-R3-4/5/6		8	
AF-75-R3-7/8/9		10	

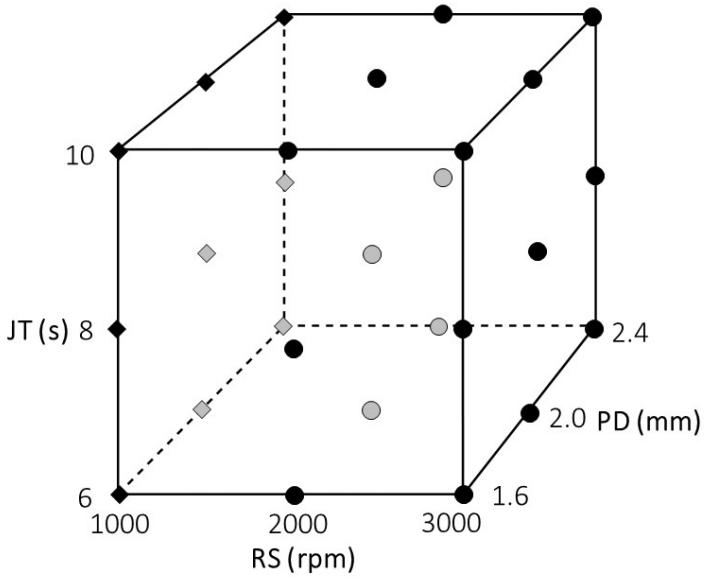

Figure 35: Schematic overview of welding condition in R2 (●) and R3 (◆) series[2]

Based on microstructural and hardness investigations of the above-mentioned series, weld matrices for strength testing purpose were designed. To limit the required number of samples, a design of experiments (DoE) approach was opted. A design of experiments is a statistical method to determine the most influencing factors for certain output parameters (also called responses). The choice of parameter combinations is mathematically supported and scientifically proven. In a design of experiments, the number of tests is limited, without losing crucial information about the response. The commercial software Minitab [58] was used to design and validate the results. For the first lap shear (code T1) and cross-tension strength (code T2) design, a full factorial design was used. Table 13 and Figure 36 give an overview of the experimental welding conditions used in this design. Eight welding conditions are located at the cube vertices, and a ninth condition is located at the centre. The circled numbers in Figure 36 indicate the sample number used to identify the welds. The sample number can

[2] The grey colour of some welding conditions is only for improved visual-spatial ability, without further meaning.

be found in the sample name following the code 'AF-75-T1' or 'AF-75-T2'. The purpose of the design in Figure 36 is to extract as much as possible information from the design in Figure 35. This reduced design is able to detect the same trends and conclusions about the influencing parameters and their interactions with less experiments. To reduce the variability in the process and the testing procedures, all welding combinations are repeated three times. Since the centre point is of great importance in validating the linearity of the design, it is repeated six times. As an example, replicates are named AF-75-T1-1.1 through AF-75-T1-1.3; or in the case of centre points: AF-75-T1-9.1 through AF-75-T1-9.6. All replicates are separated in blocks which are produced successively. A block contains ten welds (8 vertices and 2 centre points) of which only the centre point is replicated once. In short, all welding conditions are produced once before replicating. By separating replicates in blocks, secondary trends of the welding process can be detected e.g. changes in the environment or machine temperature. As with all produced welds, the sequence in a block is statistically randomized by Minitab. The same design is applied to both the first lap shear test (T1) and the cross-tension test (T2).

Table 13: Welding conditions in T1 and T2 series

Sample name	RS (rpm)	JT (s)	PD (mm)
AF-75-T1/2-1/5	1000	6	1.6/2.4
AF-75-T1/2-3/7		10	
AF-75-T1/2-2/6	3000	6	
AF-75-T1/2-4/8		10	
AF-75-T1/2-9	2000	8	2.0

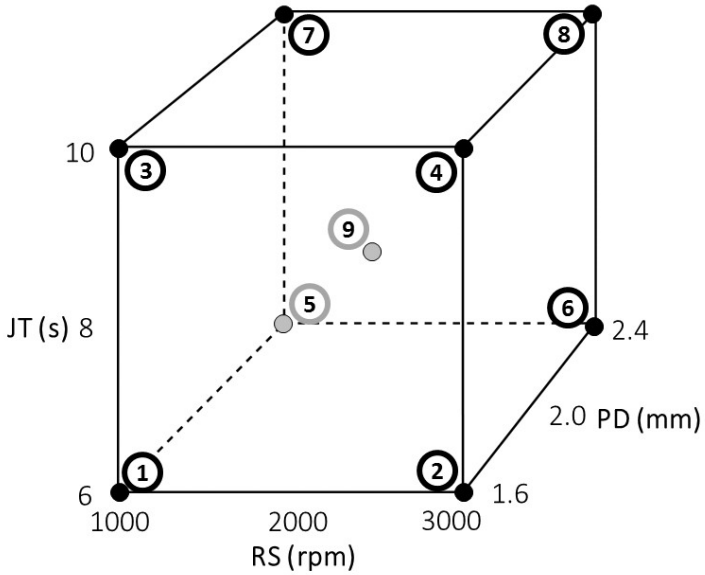

Figure 36: Schematic overview of welding conditions in T1 and T2 series, according to a full factorial design[3]

[3] The grey colour of some welding conditions is only for improved visual-spatial ability, without further meaning.

One disadvantage of the full factorial design is that it expects the data to be linear over the parameter range. A more advanced design is called Box-Behnken. It is an experimental design for the response surface methodology that allows to model quadratic relationships. This design is used for a follow-up series of lap shear tests (T3). Table 14 and Figure 37 show the welding conditions used in this Box-Behnken design. The welding conditions are positioned on the edges of the cube instead of at the vertices. The range of the welding parameters is shifted to a more optimal region based on the results achieved with the full factorial design. Similar to the previous design, the experiments are again divided into blocks and repeated three times.

Table 14: Welding conditions in T3 series

Sample name	RS (rpm)	JT (s)	PD (mm)
AF-75-T3-1	1000	7	2.2
AF-75-T3-5/7		8	2.0/2.4
AF-75-T3-3		9	2.2
AF-75-T3-9/11	2000	7	2.0/2.4
AF-75-T3-13		8	2.2
AF-75-T3-10/12		9	2.0/2.4
AF-75-T3-2	3000	7	2.2
AF-75-T3-6/8		8	2.0/2.4
AF-75-T3-4		9	2.2

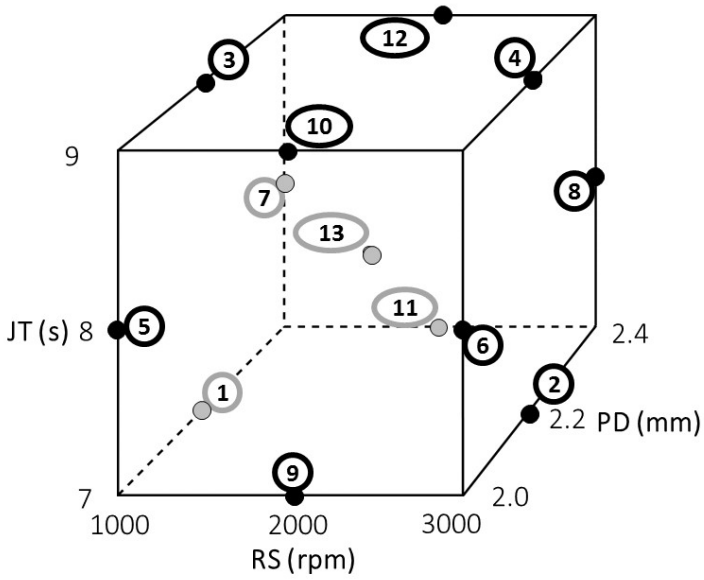

Figure 37: Schematic overview of welding conditions in T3 series, according to a Box-Behnken design[4]

[4] The grey colour of some welding conditions is only for improved visual-spatial ability, without further meaning.

Chapter 8 Evaluation of the weld appearance

This chapter will discuss the weld appearance which is evaluated using visual and metallographic inspection. Different geometrical features will be linked to the welding parameters.

8.1 Visual surface quality

The surface quality of the weld is investigated visually using a three-level score as explained in section 6.2. Most of the time the welds were scored with the best score, so few correlations were discovered. However, a distinctive feature of surface irregularity (see Figure 38) was more frequently detected for welds with high heat input. The weld surface seems to be smeared out and a circular island with a smaller diameter than the pin is located at the centre. Moreover, the deep and brown oxidized indentation of the clamping ring is related to softening of the workpiece material during processing. Apart from this, the weld surface quality was mainly influenced by the tool zero-setting and the tool contamination. Figure 39 shows a metallographic cross-section of a weld produced with a tool misalignment. The zero-settings of pin and sleeve were not correctly set and the height difference between both components was therefore visible on the cross-sectional overview. The sleeve has not retracted as much as it should prior to retraction of the tool head. The pin has not completely refilled the keyhole as the weld surface is still higher than the surrounding base material surface. This problem was attributed to adhesion forces between the tool component and the workpiece in [8].

Figure 38: Surface irregularity on the weld surface, due to excessive heat input

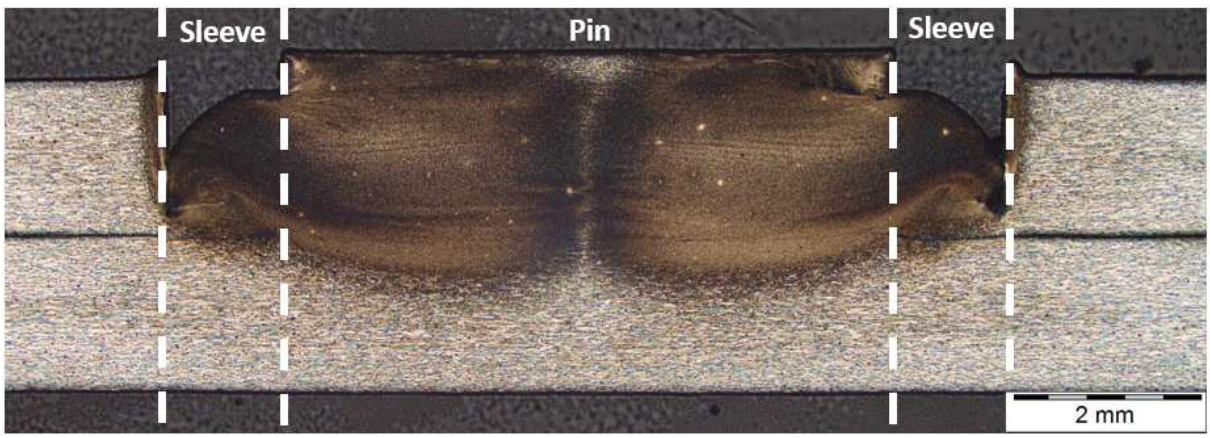

Figure 39: Illustration of the tool misalignment on the cross-sectional overview (specimen no. AF-75-R3-1)

8.2 Metallographic quality

This section will discuss the metallographic results. The weld cross-sections have been studied with special attention for imperfections, flow patterns and different microstructural zones. Correlations between these features and the welding parameters are discovered. Firstly, the presence of these features will be shown. Next, the influence of the welding parameters will be discussed and finally the repeatability of the process will be evaluated.

8.2.1 Weld cross-section appearance

Section 4.1 discussed some typical etched cross-sections observed in literature. Figure 40 shows a completely etched cross-section from a metallurgical sample. The region of interest is the black coloured weld nugget. The metallographic cross-section shows that further away from the weld, the sheets are still separated. As discussed in literature, the black stir zone is surrounded by microstructural zones affected by heat and mechanical work. Far away from the weld zone, the workpiece is composed of the base material.

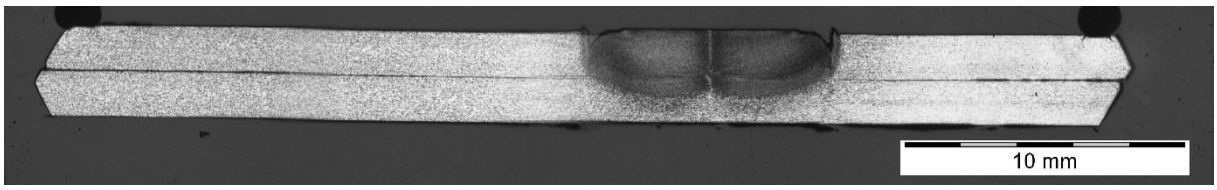

Figure 40: Completely etched cross-section (specimen no. AF-75-H2-5)

Figure 41 and Figure 42 show two weld nuggets in more detail. The black horizontal lines at the sides are added to indicate the original sheet interface. Firstly, large differences in the microstructure of these two welds are observed. However, despite these large differences, similar zones appear in every weld. The stir zone is clearly horizontally confined within the straight vertical dashed lines. The dashed lines are placed along the sleeve plunge path and thus represent the total outer diameter of the sleeve. Within the stir zone, the bonding ligament is indicated with an arrow. The bonding ligament is not always clearly visible in all cross-sections but is distinguished as a band of finer grains near the original sheet interface. The bonding ligament in Figure 42 is harder to observe as the entire stir zone is excessively refined. The observed boundary layers do not resemble the ones presented in literature [41], since in the present work material without an Alclad layer was used. Alclad is a protective layer of pure aluminium at the surface which mixes at the bonding interface during the process. Due to the absence of this protective layer, this weld is completely composed of one alloy. Next to the stir zone, the thermo-mechanically affected zone is located. Similar as described in literature [12, 42], this zone is semi-spherical and consists of deformed grains. Figure 43 shows a detail of the transition from the stir zone to the thermo-mechanically affected zone, which also illustrates the large difference in grain size over this short distance. The straight vertical line at the left of Figure 43 indicates the sleeve plunge path. At the left from this line, a part of the stir zone is visible. At the right of that line, the semi-circular part of the TMAZ is visible, with deformed and reoriented grains along its periphery. Gradually, the grains orient back to their horizontal positions and will eventually be non-distorted in the HAZ. The fine horizontal line at the lower right hand-side of Figure 43 indicates the interface where the two sheets are no longer

connected. In good quality welds, this interface terminates within the TMAZ and does not proceed into the stir zone.

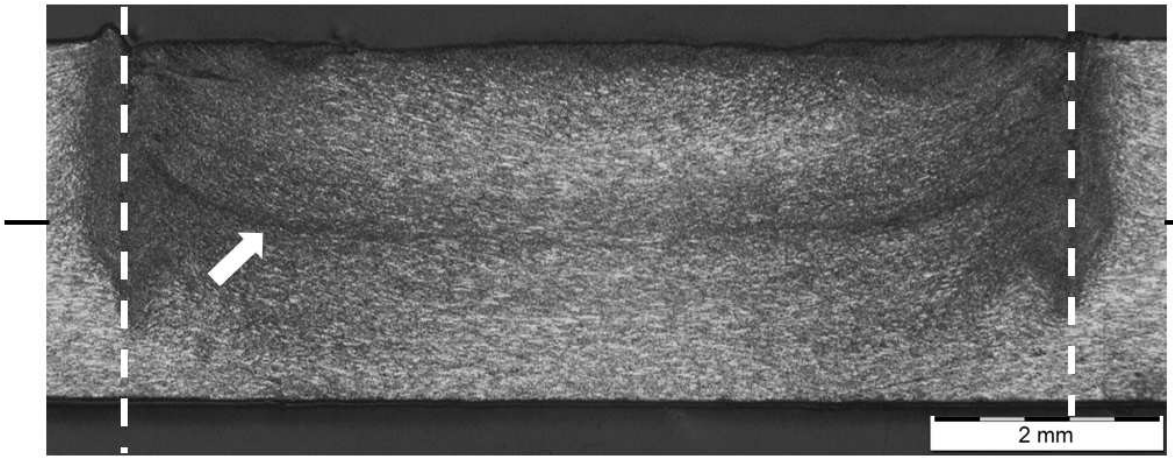

Figure 41: Metallographic cross-section of specimen no. AF-75-R2-12

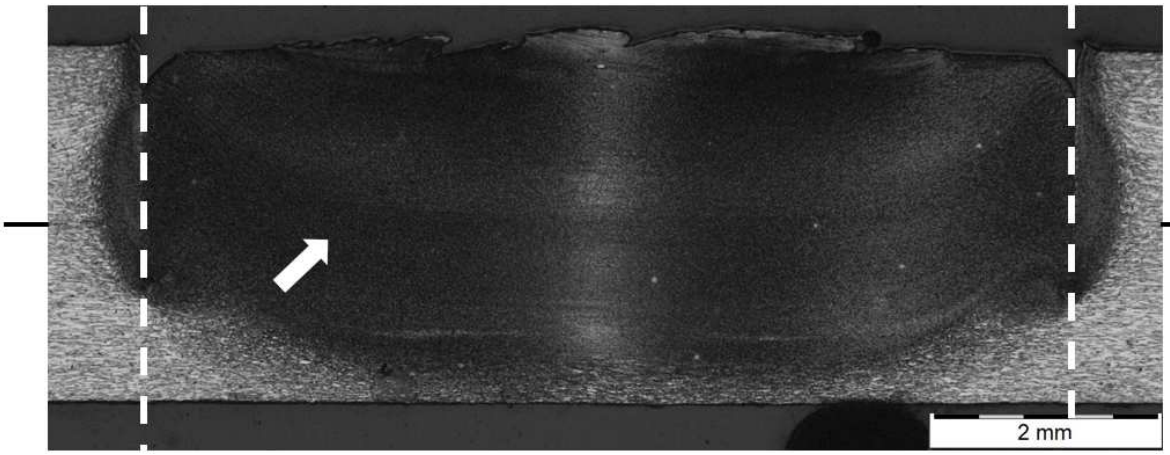

Figure 42: Metallographic cross-section of specimen no. AF-75-R3-6

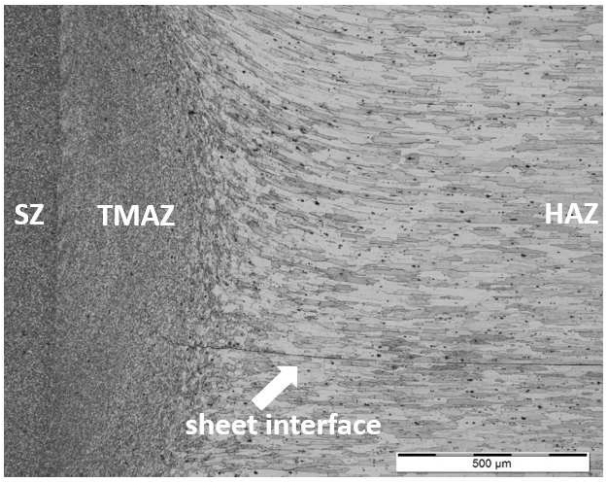

Figure 43: Stir zone and TMAZ present in specimen no. AF-75-R3-6

One final remark on the affected zones outside the stir zone has to be made regarding the clamping ring. The clamping pressure is set at a constant value for all welding combinations. However, a weld produced with a higher heat input will result in more softening. Consequently, the clamping ring will leave a visible indentation as illustrated in Figure 44. The dashed lines indicate the outer diameter of the clamping ring and the stir zone. For welds created with a high heat input, the microstructural zone under the clamping ring is visually affected. This is attributed to the plastic deformation caused by the indentation of the clamping ring and the heat that is entrapped between the clamping ring and backing anvil during the welding process. In order to reduce the entrapment of heat and hence also reduce the heat affected zone, a possible solution could be diminishing the outer clamping ring diameter. However, the indentation will be larger due to the increased surface pressure.

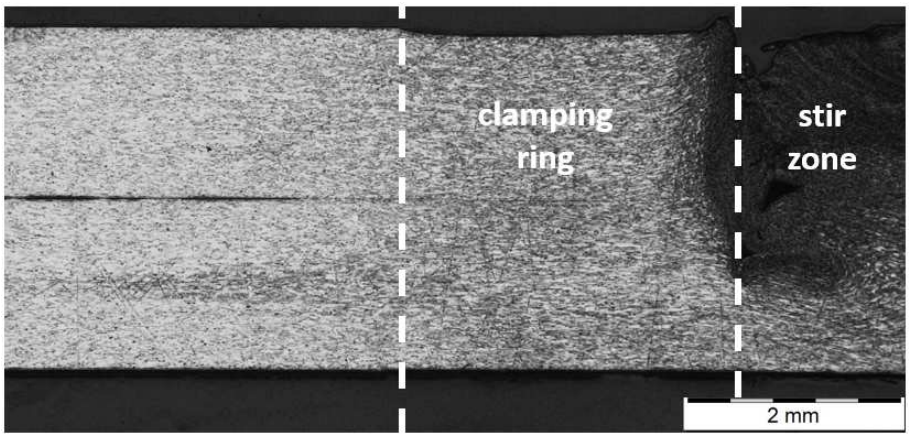

Figure 44: Surface indentation of the clamping ring and underlying affected zone in specimen no. AF-75-R2-6

When the separated sheet interface can penetrate into or through the TMAZ, the formation of a hook is possible. There are two different kinds of hooks, based on their penetration into the weld nugget. The first type of hook penetrates into the TMAZ, but terminates prior to crossing the sleeve plunge path and entering the stir zone. The shape of this type of hook is curved downwards. Figure 45 shows such an interface that ends into a hook (indicated by the arrow). Since the depth of the weld nugget equals the thickness of one sheet, the hooking feature ends at the bottom of the sleeve plunge path (dotted line). Next to the hook, a void located at the maximum plunge depth is visible. A second type of hook is located in the stir zone. This type of hook has an upside-down V-shape. Figure 46 shows two hooks of this type with the recognizable V-shape, located within the stir zone. The bottom hook originates from the separated interfaces and has penetrated into the stir zone. The upper hook is the result of an incomplete refilling stage, during which the sleeve keyhole could not be refilled completely. This is confirmed by the presence of the void from which this hook originates. These two types of hooks found in the present work were also reported in literature for FSpW of EN AW- 6061-T6 sheets [42]. On the contrary, the hook in the TMAZ was reported to have a sharp V-shape, rather than a smooth curved shape. The same conclusions about the origin of the hooks were found.

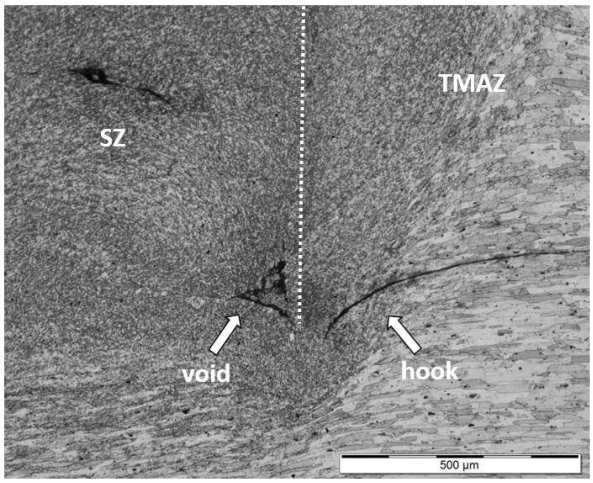

Figure 45: Hook in TMAZ (specimen no. AF-75-R2-3)

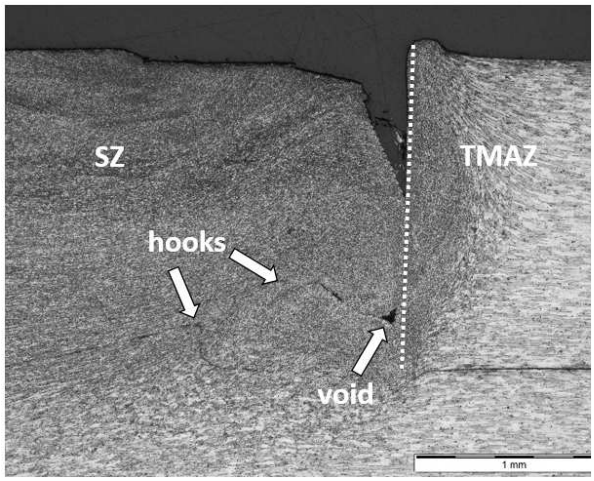

Figure 46: Two hooks in SZ (specimen no. AF-75-R1-6)

Voids and incomplete refills are two large imperfections that were frequently observed in weld cross-sections. Figure 47 shows a non-etched cross-section, in which the dashed rectangle indicates the area subjected to the tool plunging. Voids are frequently located at the bottom of the sleeve plunge path, such as the two voids in the bottom corners of the dashed rectangle. These voids originate upon refilling the sleeve keyhole, as the material flow is insufficient in order to fill the outermost corners of the keyhole. Voids can also be located elsewhere under the sleeve as this entire zone has to be refilled during the third stage of the process. Incomplete refill imperfections are located at the periphery of the weld surface, as observed at the upper side corners of the dashed rectangle. The lack of material at that area is attributed to two factors. Firstly, the weld surface may rise higher than the original sheet surface, and thus insufficient material is available to completely refill the sleeve keyhole. Secondly, material gets extruded into the tolerance gaps between the tool components. In [52], the lack of material was compensated by applying an extra surface indentation of the clamping ring. Voids and incomplete refill imperfections may not necessarily be detrimental to the weld strength, since they do not act like very sharp cracks. However, the presence of large amounts of such imperfections may diminish the load bearing area of the weld.

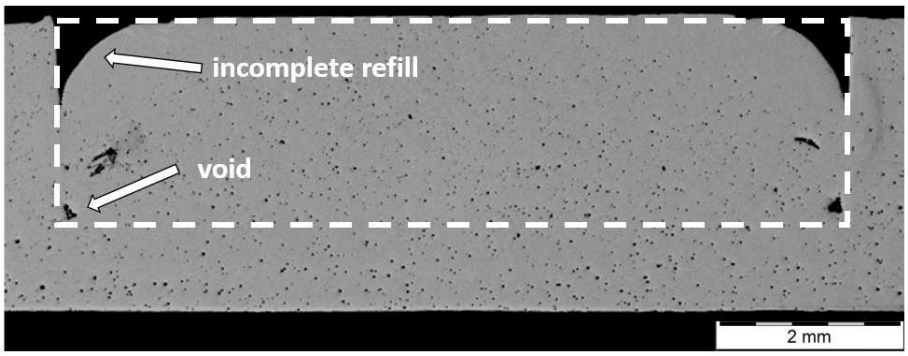

Figure 47: Illustration of incomplete refill and voids present in the area subjected to tool plunging (specimen no.AF-75-R2-5)

Apart from these imperfections found in the sleeve zone, a non-bonded interface is an imperfection observed at the sheet interface. Instead of a strongly bonded region, the interface contains a region where the two sheets are not connected. Two types of non-bonded interfaces are discovered in the inspected welds. Figure 48 shows a type 1 non-bonded interface and a detailed view. A type 1 non-bonded interface separates the sheets over a relatively long curved distance within the stir zone. The material grains have been in close contact during the process, but apparently, the conditions were not sufficient to form a strong bonding ligament. The grain structure present above and below the interface is identical and elongated. Figure 49 shows a type 2 non-bonded interface with a non-etched and etched detail. This type of imperfection typically measures a few millimetres and is always located in the centre along the interface, bounded between 2 bonded interfaces at either side. This type 2 non-bonded interface differs from type 1 in its distinctive shape which is not simply a curved line. In the top overview picture, the bonded interfaces are recognized by the fine-grained curved band. This band is interrupted near the non-bonded interface. The etched detail shows that the microstructure is very heterogeneous in terms of its grain size and orientation around the imperfection. Above the interface, the microstructure is divided into three zones by the blunt V-shape. Below the interface, the microstructure is unidirectional, which indicates the limited interaction between both sheets.

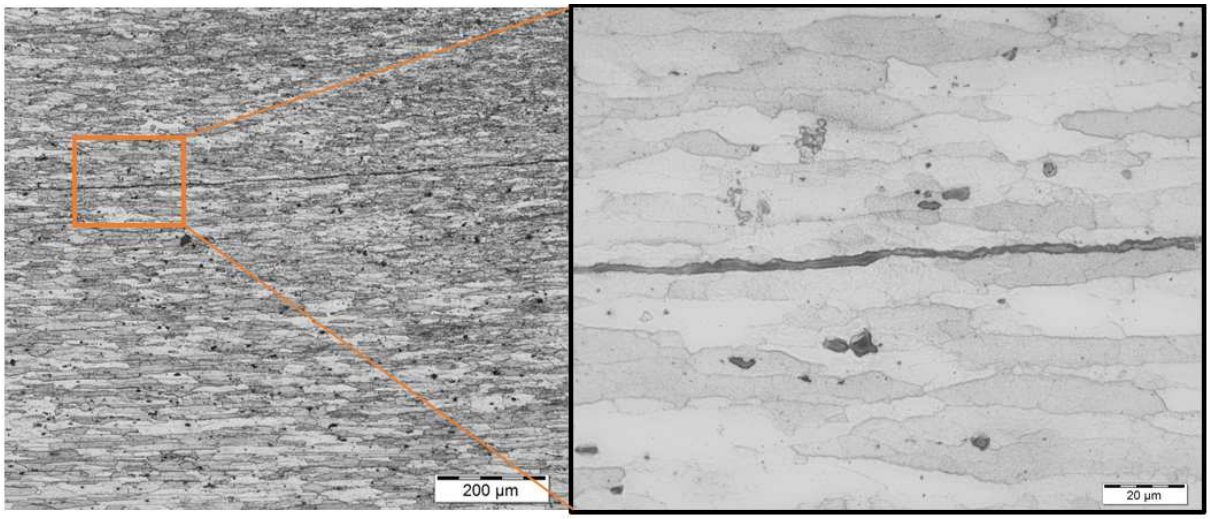

Figure 48: Type 1 non-bonded interface, extending along a long curved distance within the stir zone (specimen no.AF-75-T3-10)

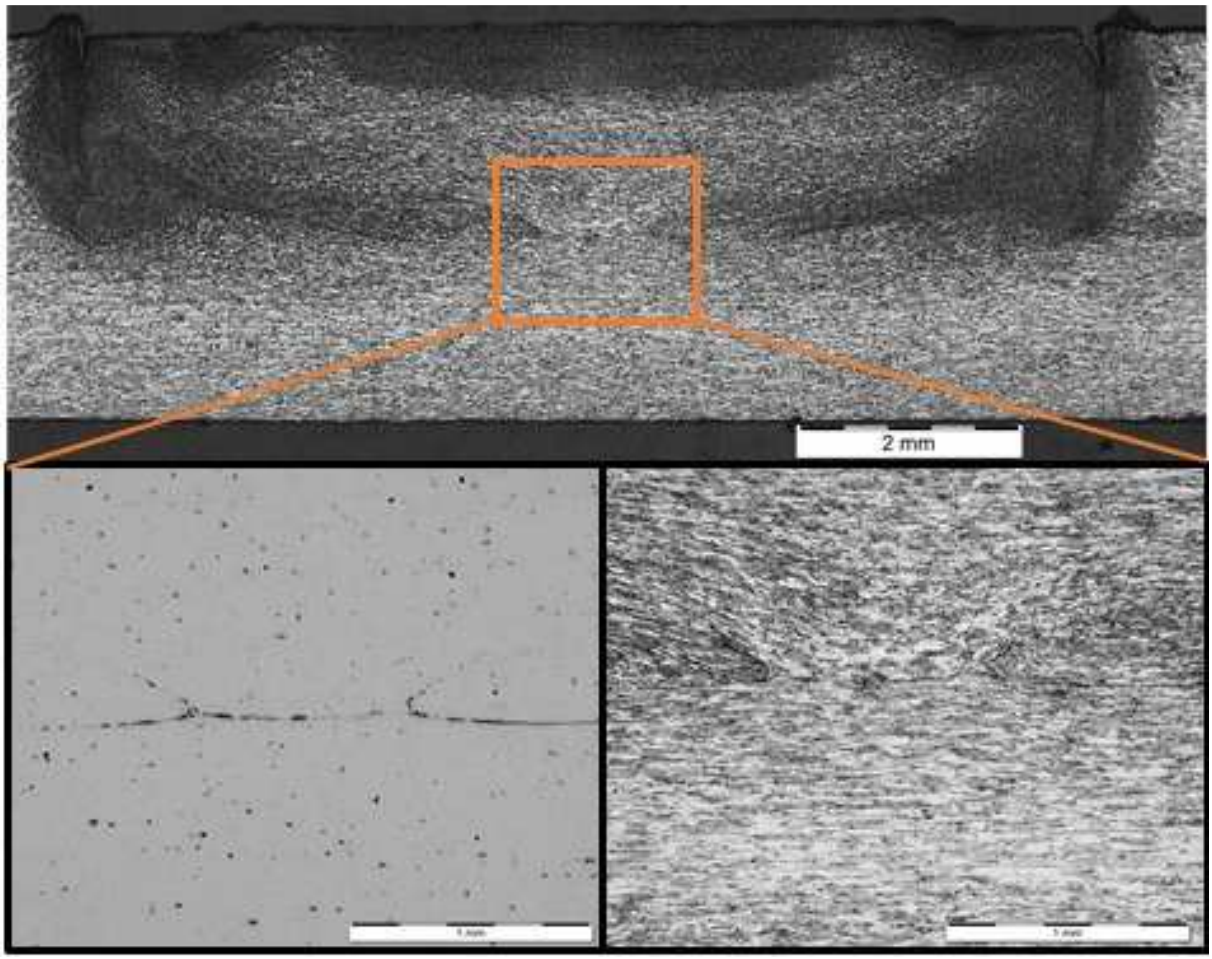

Figure 49: Type 2 non-bonded interface type 2, located in the centre along the interface, between 2 bonded interfaces (specimen no. AF-75-R2-7) (top), non-etched (left) and etched (right) detail.

8.2.2 Influence of welding parameters

The weld appearances discussed above can be related to the welding parameters. Correlations have been found for the three parameters of interest: joining time, plunge depth and rotational speed.

The joining time is closely related to the amount of heat input provided to the weld. An increase in the joining time without changing the other parameters is equivalent to an increase in the dwell time of the tool. Based on the first series of experiments (R1), joining times shorter than 6 s were discarded. These short joining times resulted in weld cross-sections with large incomplete refill imperfections as visualized in Figure 50. The weld nugget is almost not bonded to the upper plate and hence the expected lap shear strength is low. Figure 51 compares three non-etched and etched cross-sections of welds produced at three different joining times of 6, 8 and 10 s, respectively. The fixed parameters are a rotational speed of 2000 rpm and a plunge depth of 1.6 mm. For an increase in joining time, the incomplete refill imperfection disappears, leading to a cross-section with almost no imperfections. However, it is important to notice that the weld produced with a medium joining time (JT = 8 s), contains a non-bonded interface, which is probably more detrimental to the weld strength than the large incomplete refill imperfection, found in the weld produced with a low joining time (JT = 6 s). The etched stir zone appears darker for an increase in joining time, indicating a finer grain size at the nugget centre. The most refined grain size is present at the outer edges of the weld nugget, since the absolute

circumferential velocity of the tool is highest at these locations. For an increase in joining time, the zone with a coarse grain size is reduced. The recrystallized zone also extends further into the lower sheet, although the plunge depth is unchanged. These microstructural changes are consequences of the increased heat input caused by an increase in joining time.

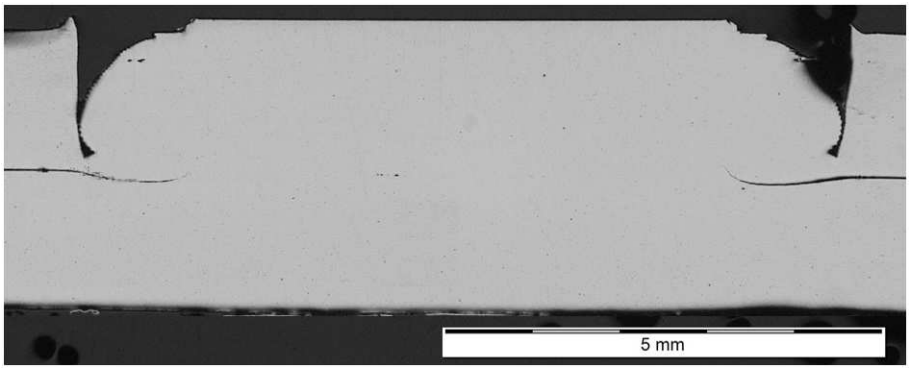

Figure 50: Deep incomplete refill in a weld produced with JT=4 s (specimen no. AF-75-R1-2)

The influence of the joining time on the microstructure of the weld, as illustrated in Figure 51, is a global effect observed for all weld samples. Figure 52 and Figure 53 show the imperfections, in terms of the total area percentage of imperfections and the depth of the incomplete refill (IR), respectively, measured for welds produced at different joining times and rotational speeds. The measurement points at the same rotational speed and the same joining time differ in plunge depth and no replications were made. The measurements show a large variation and therefore a dashed trendline of the mean values is added to the graphs. In general, it can be concluded that both the total area percentage of imperfections and the depth of incomplete refill decrease with an increase in joining time. A significant improvement is clearly observed for an increase in joining time from 6 to 8 s. Only welds produced with the parameter combination of the lowest rotational speed (RS=1000 rpm) together with the shortest joining time (JT=6 s), do not correspond to this overall trend.

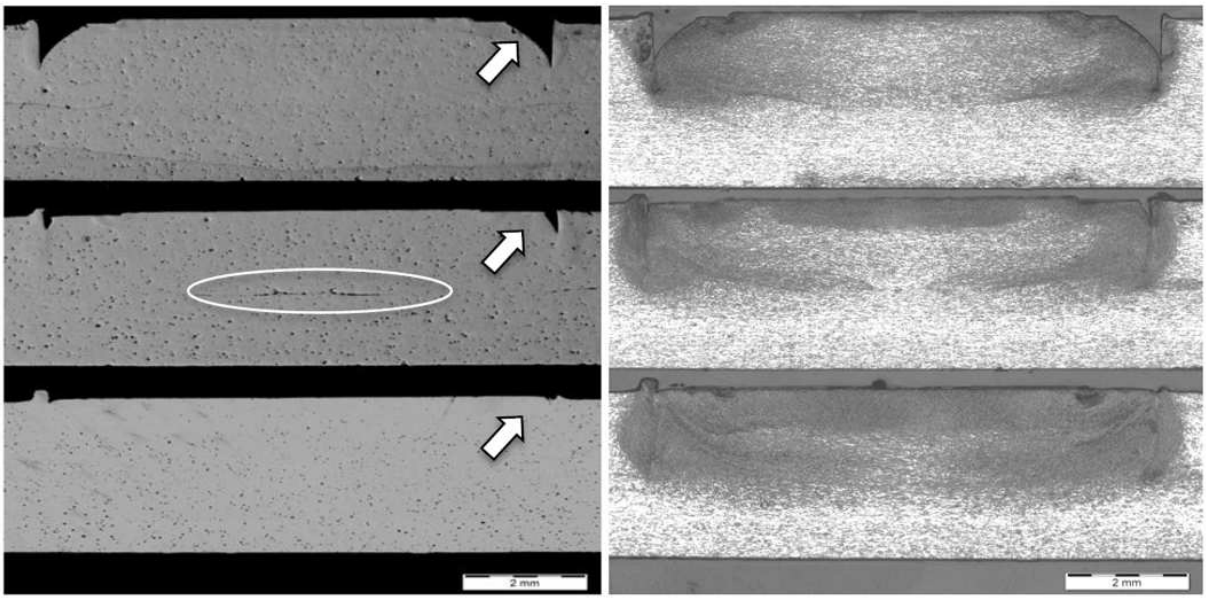

Figure 51: Varying JT: 6 s (top), 8 s (middle), 10 s (bottom); Fixed parameters: RS=2000 rpm, PD=1.6 mm

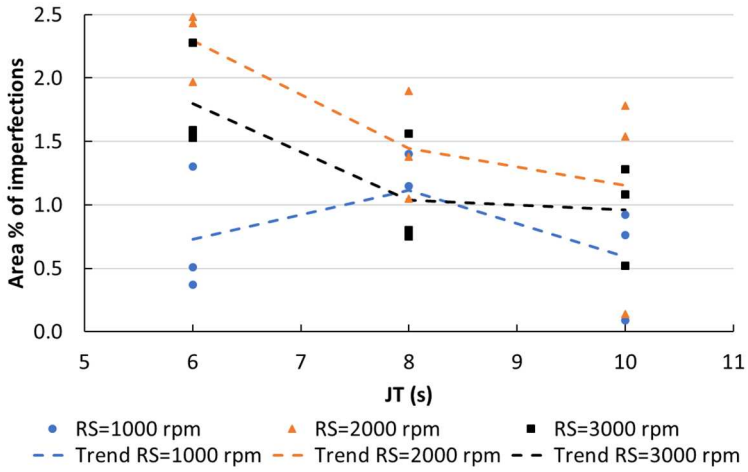

Figure 52 Mean area % of imperfections at varying JT and RS

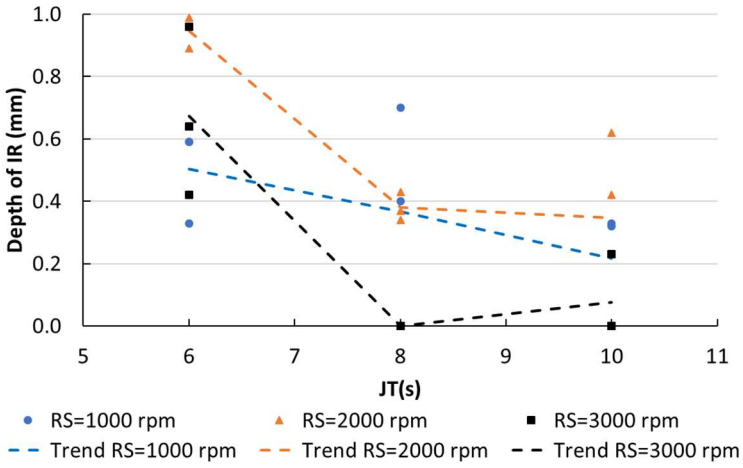

Figure 53: Mean depth of incomplete refill at varying JT and RS

The plunge depth was varied starting from the upper sheet thickness (1.6 mm) up to 50% into the lower sheet (2.4 mm). Welds produced with a plunge depth of 1.6 mm are prone to imperfections at the interface between the sheets. The absence of the tool penetration into the lower sheet does not create a strong interface bond. Welds containing non-bonded interfaces and partial bonding features were always produced with this low plunge depth of 1.6 mm. Figure 54 shows the bottom right-hand corner of a stir zone. The void is located along the sleeve plunge path at the maximal plunge depth. Under the stir zone, the sheet interface is not bonded. Further to the left, the stir zone extends deeper and a bond is formed. Hooking features are typically discovered in the stir zone of welds produced at the lowest plunge depth, since in this case the bottom of the weld nugget is close to the sheet interface. Therefore, partial bonding under the stir zone occurs due to limited plunge depths. At a deeper plunge depth, the hook does not reach into the stir zone. A slight decrease in voids is observed at a deeper plunge depth, but this influence is not significant.

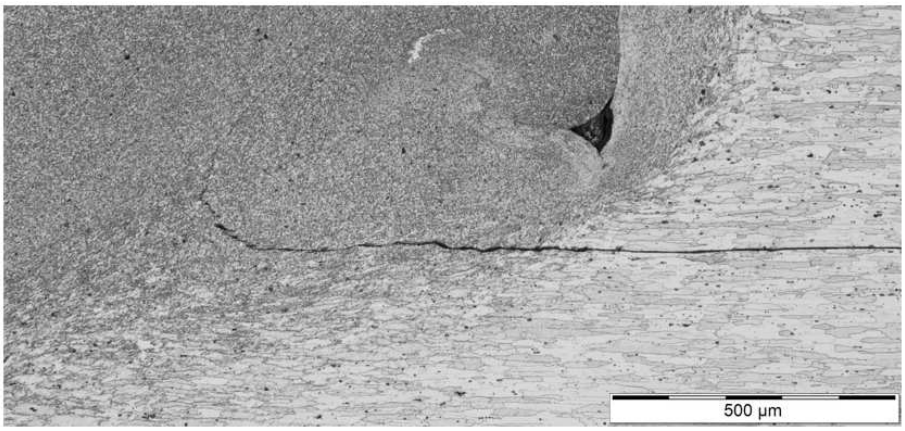

Figure 54: Partial bonding under the stir zone due to the limited plunge depth (specimen no. AF-75-R3-1)

Figure 55 shows three etched cross-sections of welds produced with a joining time of 8 s, a plunge depth of 2 mm and three varying rotational speeds of 1000, 2000 and 3000 rpm. The difference in shape and size of the stir zone is very distinctive. At a lower rotational speed, the affected zone is curved and extends further into the material compared to the plunge depth. At a high rotational speed, the stir zone depth is rectangular-shaped and limited to the plunge depth. Furthermore, the grains are finer at a low rotational speed, with only a vertical zone of coarse grains right underneath the pin zone. At the centre of the pin, the circumferential velocity is zero and the least amount of stirring takes place at that location. At a higher rotational speed, horizontal bands of fine grains become visible. The reason for this difference is not yet completely understood. FSpW machine data showed that more torque was required to produce a weld at a lower rotational speed. Figure 56 shows the maximum actuator current to rotate the spindle measured during a weld cycle. The data points show the mean value for all welding conditions at a certain rotational speed. Welding at the highest rotational speed of 3000 rpm requires the least amount of torque. At the medium rotational speed of 2000 rpm, only an additional torque of 12% is required, but at the lowest rotational speed of 1000 rpm, the additional torque is 68%. This indicates that a higher coefficient of friction between tool and workpiece exists at a low rotational speed. As stated previously, it is not recommended to weld at 1000 rpm when the machine is in a cold state as this has led to overcurrent warnings of the spindle. Rotational speeds of 1300 rpm were also

discouraged in a durability study [19], because they cause unbalanced trends and high torques of the main spindle.

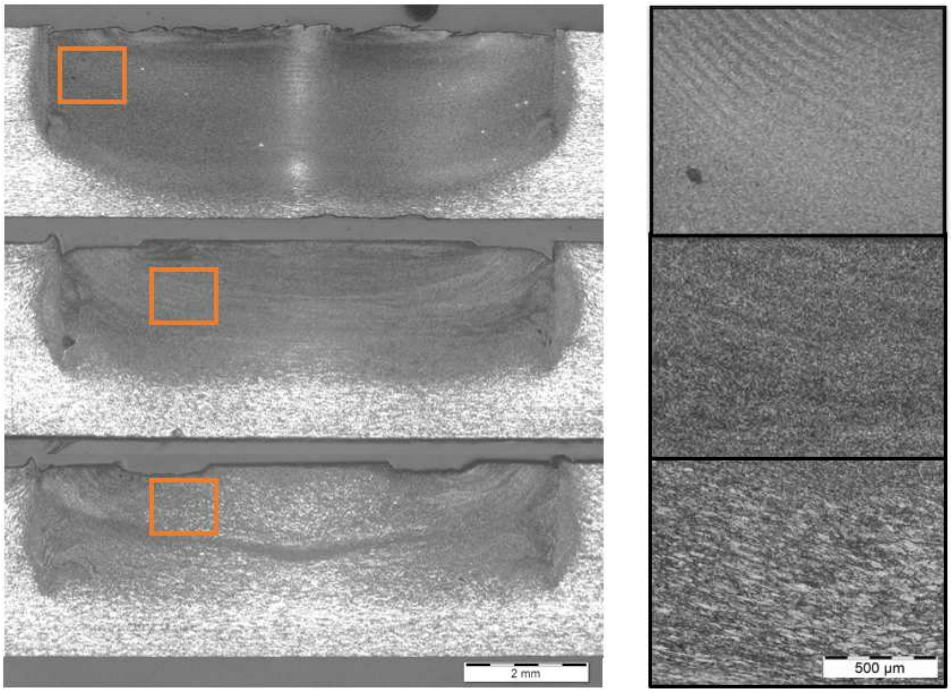

Figure 55: Cross-sectional overview and detail of welds produced at varying RS: 1000 rpm (top), 2000 rpm (middle) and 3000 rpm (bottom); fixed parameters: JT=8 s, PD=2mm

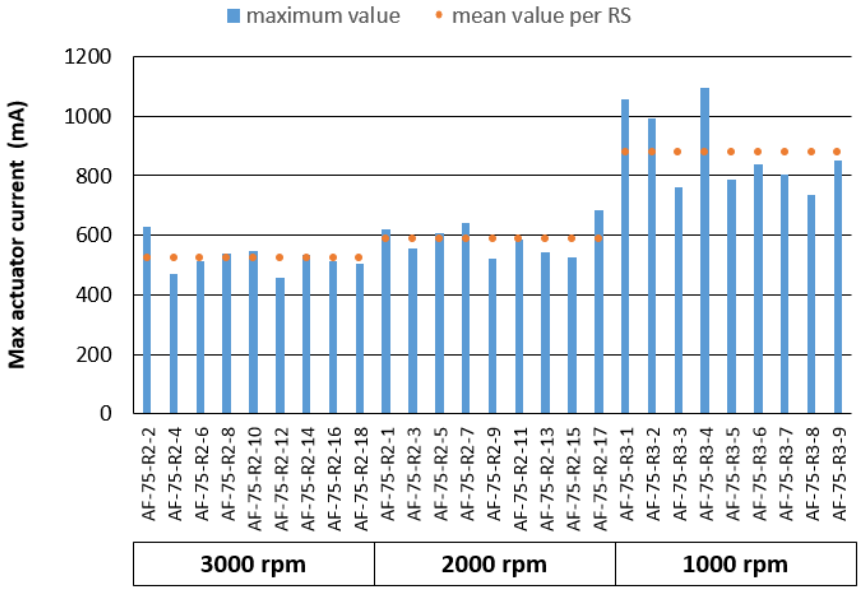

Figure 56: Maximum actuator current of the spindle during a weld cycle, for varying RS

In [59], effects of rotational speed on the microstructure and mechanical properties of friction stir welded EN AW-7075-T6 were investigated. It was found that at an increase of the rotational speed, higher peak temperatures and grain coarsening were present. Higher strain rates result in fine recrystallized grains, but at the same time, higher temperatures improve the grain growth of the recrystallized grains. These two effects counteract the formation of the microstructure. Moreover, the

grain structure is also determined by plastic deformation and (over-)aging of the alloy. Due to the complexity of the process and the alloy, changes in microstructure are hard to explain thoroughly.

As the rotational speed is closely related to the material flow, it has a significant effect on the amount of imperfections. Figure 57 and Figure 58 show the influence of the rotational speed in a similar way as already discussed for the joining time. In both graphs, welds with a rotational speed of 2000 rpm contain the highest amount of imperfections. The incomplete refill imperfection, defined by the depth of the incomplete refill, is smallest at the highest rotational speed combined with medium to long joining times. This is the result of excessive stirring and fluent material flow. On both graphs, the influence of the joining time on the imperfection size can again be identified.

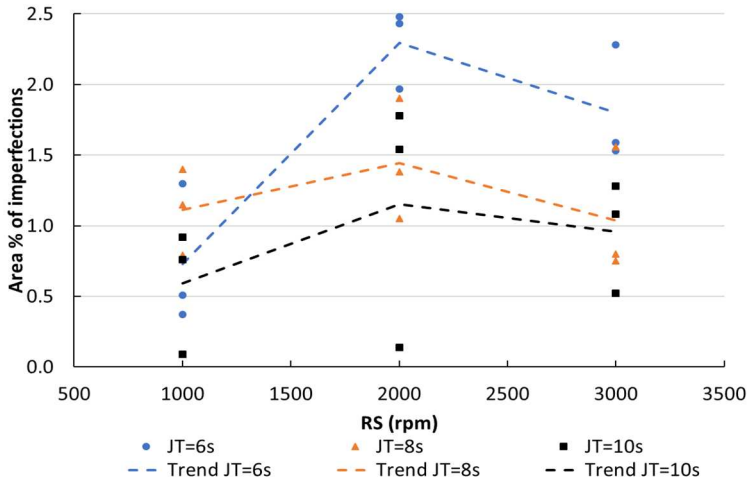

Figure 57: Mean area % of imperfections at varying JT and RS

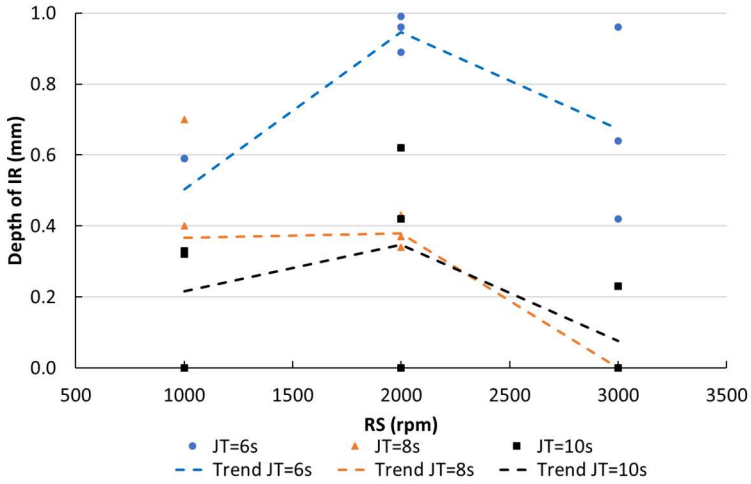

Figure 58: Mean depth of IR at varying JT and RS

8.2.3 Observation of material flow patterns

This section will present some frequently observed material flow patterns. The patterns were always observed at specific locations in the weld cross-section. All patterns are characterized by layers of grains

with different grain sizes. Figure 59 shows two patterns observed near the weld surface. At the left-hand picture, striations in the stir zone are shown. The area depicted is located underneath the sleeve, as the straight sleeve plunge path is visible on the left of the picture. Striations flow from the top surface diagonally to the centre of the stir zone. The different lines are distinctive due to their difference in grain size. This kind of feature is often discovered in welds produced at a low rotational speed of 1000 rpm. At a higher rotational speed, this pattern is not visible anymore. An explanation could be that the different bands are too dispersed due to the extra number of tool revolutions in the same time unit. On the right-hand side figure, a banded zone underneath the sleeve-pin interface is presented. This feature is typically semi-elliptically shaped, with the centre at the sleeve-pin interface. The slight height difference at the weld surface represents the sleeve-pin interface. The feature is curved around this interface and is always located just below the surface. In contrast to the striations, this feature is observed more frequently at a higher rotational speed. The origin of this banded zone is not yet understood.

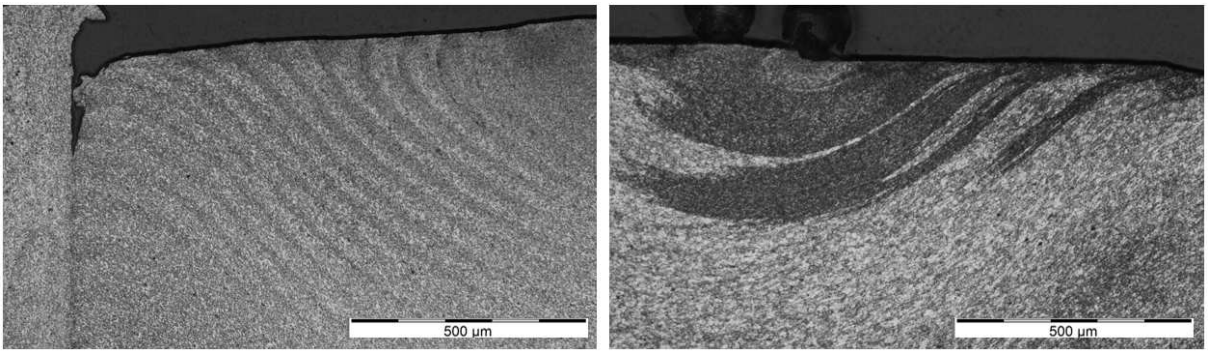

Figure 59: Striations, typically found in welds produced at a low rotational speed (specimen no. AF-75-R3-5) (left), banded zones, typically found in welds produced at a high rotational speed (specimen no. AF-75-R2-15) (right)

8.2.4 Repeatability of the weld quality

The conclusions formulated in the previous subsections are based on a single examination of certain weld combinations. To validate the robustness of the welding process, some welds are repeated three times. A comparison between those replicates allows to evaluate the repeatability of the weld quality and the influence of environmental parameters such as tool contamination. Figure 60 shows non-etched and etched cross-sections of the same welding condition. The welds are produced in sequence from top to bottom. The welding took place with a mechanically cleaned tool, but without intermediate cleaning after every processed weld. Hence, the effect of tool gap filling can be studied. The depth of the incomplete refill imperfections decreases with the production order of the welds. This means that this type of imperfection diminishes when the tool is more contaminated. Since the tolerance gap between the sleeve and clamping ring is already partially filled with workpiece material, less material is extruded in the subsequent produced welds. Other imperfections, like the voids at the sleeve plunge path, remain in every weld replication. The etched cross-section is almost identical in terms of its microstructural zones for all three replications. The typical vertical coarse line at the stir zone centre for welds at a rotational speed of 1000 rpm is visible in all replications. A minor difference is that the stir zone extends further for subsequent produced welds. This could be attributed to heating of the tool head as more frictional heat is produced at the contaminated tool gaps. Another comparison between the replicates

is illustrated in Figure 61. The overall dimension of the stir zone remains similar, but the internal bands of refined grains are different. This means that the material flow was different in all three welds, despite the identical welding parameters. For these two cases, it can be concluded that the overall weld size and appearance is consistent. The exact size of imperfections and material flow is however different.

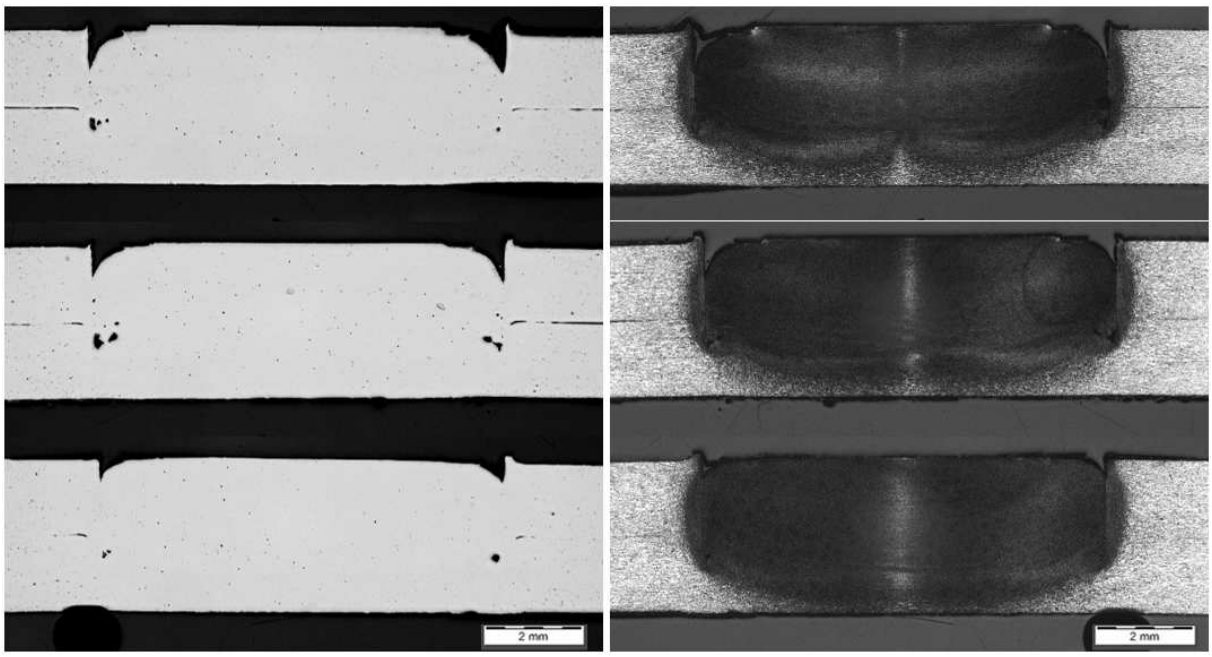

Figure 60: (Non-)etched cross-sectional overview of three repetitions (from top to bottom) of the same welding condition (specimen no. AF-75-R3-6)

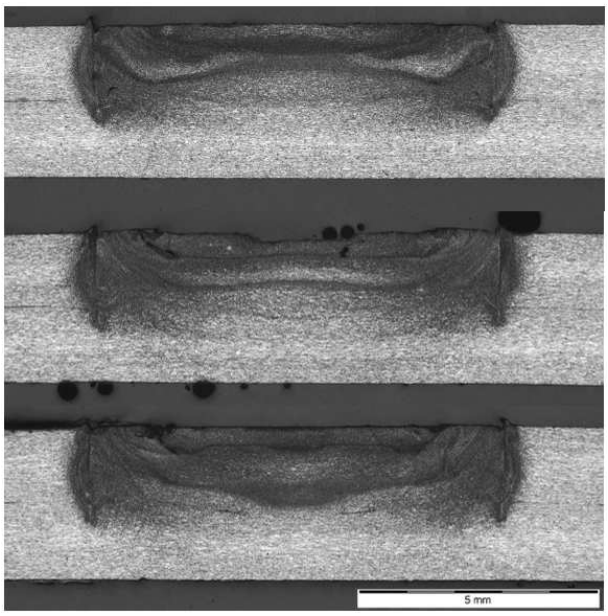

Figure 61: Etched cross-sectional overview of three repetitions of the same welding condition (specimen no. AF 75-R2-10)

8.3 Summary and conclusions

This chapter showed the presence of the typical microstructural regions and features as reported in literature. Special attention was given to possible imperfections in the weld cross-sections: incomplete refill, voids and non-bonded interfaces. These features were attributed to specific parameter choices. Increasing the joining time, decreases the amount and size of the weld imperfections and increases the stir zone dimensions. A plunge depth which is equal to the upper plate thickness, results in imperfections at the sheet interface and should be avoided. Finally, the rotational speed completely determines the microstructural appearance and dimension of the stir zone. The importance and the influence of the weld imperfections on the weld strength is discussed in the following chapter. Since the microstructural changes are partly determined by the thermal cycle, temperature measurements will also be the subject of the next chapter.

Chapter 9 Mechanical properties of the weld

This chapter will discuss the observed mechanical properties achieved for welds produced at the different welding conditions. First, the softening of the weldment is studied by temperature and hardness measurement results. Afterwards, the failure strength and failure modes are presented.

9.1 Softening of the weldment

9.1.1 Temperature measurements

All results in this section were obtained by attaching the K-type thermocouple to the workpiece surface using a bolt and a washer. The maximum temperatures measured do not reach the values published in literature, since the measurement point is relatively far away from the weld centre. In [53], a temperature of 471 °C was measured at 7.1 mm away from the weld centre between the two sheets. In [43], the temperature distribution was simulated on discrete distances from the weld centre. Temperatures of 302 °C and 530 °C were calculated at respectively 9.0 mm from the weld centre and at the weld centre. The maximum temperature observed in this work was 263°C at 14 mm away from the stir zone at the upper sheet surface. Nevertheless, the consistency of the measurement procedure made it possible to compare parameter trends.

Figure 62 shows three temperature profiles, obtained during welding at various joining times, but at a fixed plunge depth and rotational speed. The peak temperature was reached near the end of the process. As long as the tool is in contact with the workpiece, the surface temperature keeps rising. The cooling stage can start as soon as the tool is retracted. The influence of the joining time is clearly visible in this comparison. At a higher joining time, the heat input is larger. Hence, the peak temperature increases and the workpiece remains for a longer time at a higher temperature. It is also observed that the timing of the peak shifts as the joining time is increased, since the process takes longer.

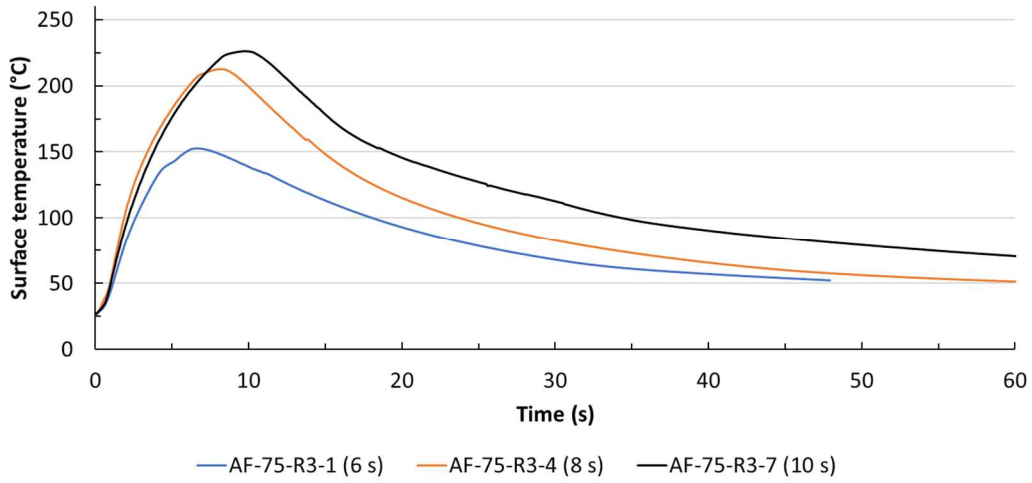

Figure 62: Surface temperature profile at 14 mm away from the weld centre for varying JT; Fixed parameters: PD=1.6 mm, RS=1000 rpm

Figure 63 shows the influence of the rotational speed on the temperature profile. Two different comparisons are visualized, both with the same variation in rotational speed but with other fixed welding parameters. The dashed lines are welds produced with a high heat input (JT=8 s, PD=2.4 mm), while the solid lines represent welds with a low heat input (JT=6 s, PD=1.6 mm). This difference between the welds with a different heat input is clearly identified in the range of the peak temperatures attained. This confirms the previous conclusion regarding the relation between heat input and joining time (see Figure 62). The rotational speed also has an influence on the peak temperature. An increase in rotational speed at a constant joining time corresponds to an increase in the amount of rotations. Every rotation causes friction and plastic deformation and hence the total heat input provided to the weld is higher. This higher heat input during the same process time leads to higher peak temperatures and longer cooling times. This influence was also reported in literature about friction stir spot welding [56]. The slope of the temperature profile is steeper for welds produced at a higher rotational speed. This indicates that the heating rate increases. This can be explained by the fact that more energy is added in one time unit due to the extra revolutions.

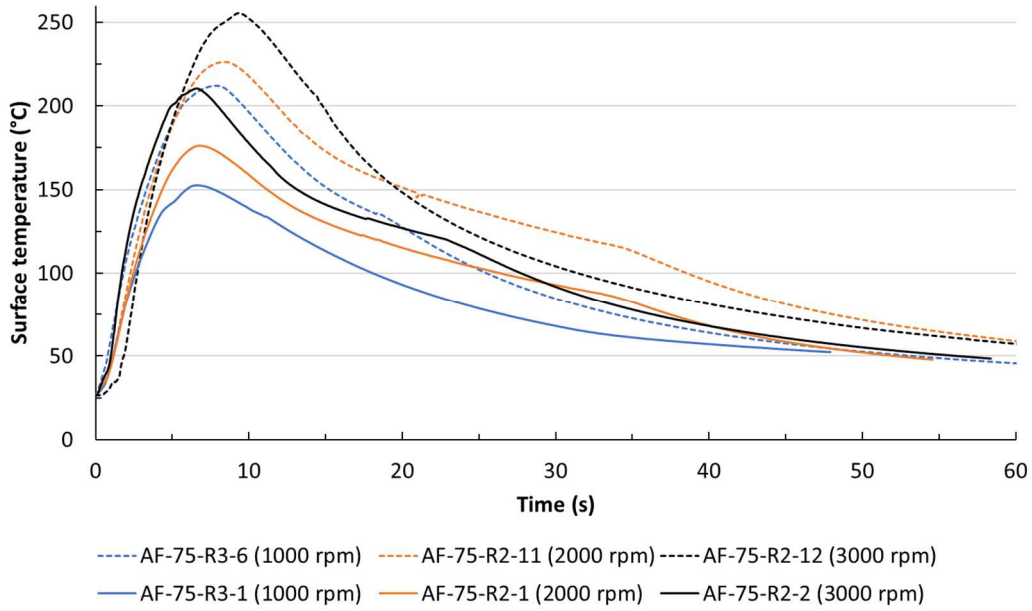

Figure 63: Surface temperature profile at 14 mm away from the weld centre for varying RS. Fixed parameters: dashed line: JT=8 s, PD=2.4 mm; solid Line: JT=6 s, PD=1.6 mm

Finally, Figure 64 shows the influence of the plunge depth on the peak temperature. For welds produced with a deeper plunge depth, this peak temperature increases. More material is displaced in the same amount of joining time and hence a higher sleeve contact surface is created. The extra frictional heat and the larger volume of plastically deformed material result in an increase in heat input provided to the weld.

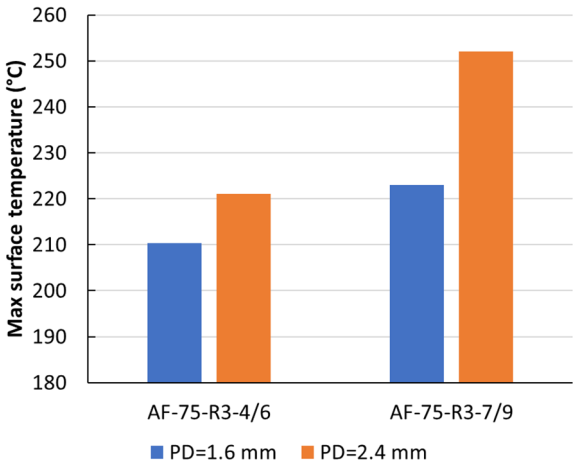

Figure 64: Maximum surface temperature at 14 mm away from the weld centre for varying PD. Fixed parameters: AF-75-R3-4/6: JT=8 s, RS=1000 rpm; AF-75-R3-7/9: JT=10 s, RS=1000 rpm

9.1.2 Hardness reduction

The influence of the temperature and mechanical work on the hardness of the joint is discussed in this section. Figure 65 shows a W-shaped hardness profile which is typical for heat-treated alloys like EN AW-7075-T6 [41], [53]. The complete weld is softened compared to the base material and the hardness profile is symmetrical with respect to the weld centre. As mentioned above, the weld is deliberately positioned asymmetrically on the cross-section, in order to ensure that measurements could be performed at sufficiently large distances away from the weld centre. The base material has a hardness of approximately 180 HV0.5 and is clearly detected by the measurements on the present sample. Approaching the weld, the hardness decreases gradually to a minimum. The location of this minimum hardness is defined as the transition from the HAZ to the TMAZ [6]. In the TMAZ, the hardness increases, up to a rather stable value in the stir zone. The different regions are indicated by the dashed lines and can be compared to the different regions in the metallographic picture. The softening of the HAZ is attributed to the coarsening of precipitates and grains due to the only effect of thermal cycle without any plastic deformation [41, 53]. As from the TMAZ, plastic deformation and grain refinement become significant and result in a hardness increase. The temperature and deformation rate is still too low for dynamic recrystallization [41]. In heat-treated alloys like EN-AW 7075 T6, which is used in the present work, over aging can take place. The heat-treatment T6 has resulted in an alloy with a particular strength Temperatures above this heat treatment temperature will thus diminish its mechanical properties. The stir zone itself consists of fine equiaxed grain structures caused by dynamic recrystallization and probably contains re-precipitated particles due to the high process temperatures [53]. The hardening precipitates were broken into particles and dissolved by stirring of the tool, and the larger precipitates re-precipitated on subsequent cooling [41]. The average hardness reduction in this measurement is 33 %, compared to the base material. According to the European standard on the design of aluminium structures, a strength reduction in the HAZ of 20 to 35 % is common [60]. The measurements in this section were obtained several days after production of the weld. Hence, only a limited amount of natural aging has occurred. After 40 days of natural aging, a larger amount of precipitates should re-precipitate in the stir zone, resulting in a hardness increase of the stir zone to almost the base material hardness [53].

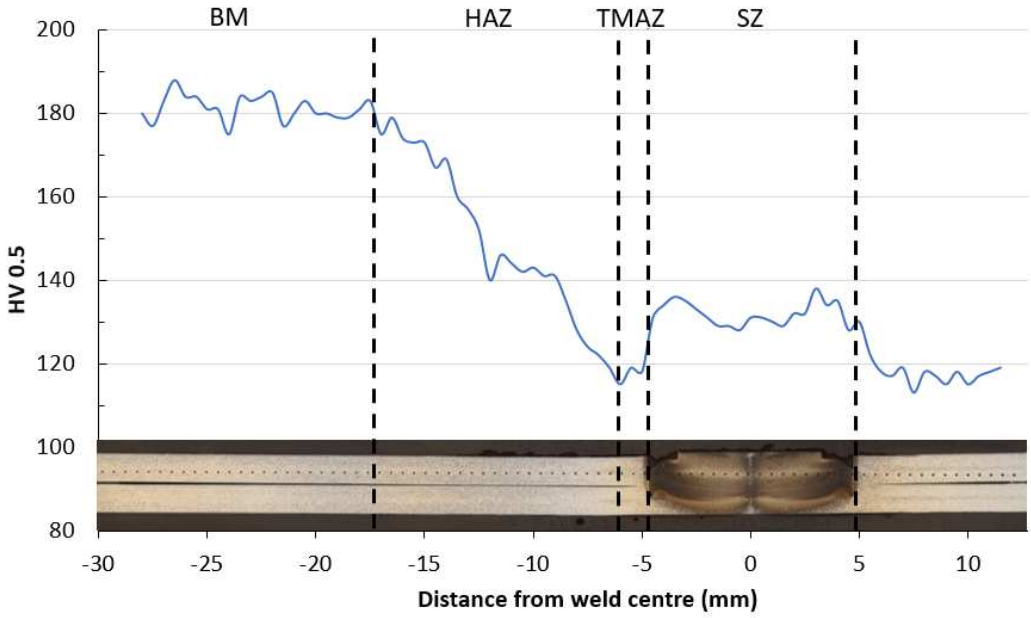

Figure 65: Typical W-shaped transverse hardness profile (specimen no. AF-75-R3-6)

A transverse hardness measurement does not reveal any information about the hardness in the through-thickness direction. Figure 66 shows a full hardness mapping of a weld cross-section, achieved with 700 hardness indents. The location of the stir zone is delimited by the dashed lines. Incorrect measurements are covered with white boxes. These measurements were not representative because the indentation was made too close to the separated sheet interface. The width of the sample was not large enough and thus the base material could not be subjected to the hardness measurements. The hardness distribution within the stir zone is quite homogeneous. The typical curved shape of the stir zone is not reflected in the hardness mapping. This indicates that the grain refinement is not the only factor contributing to the local hardness increase, but amongst others also the plastic deformation

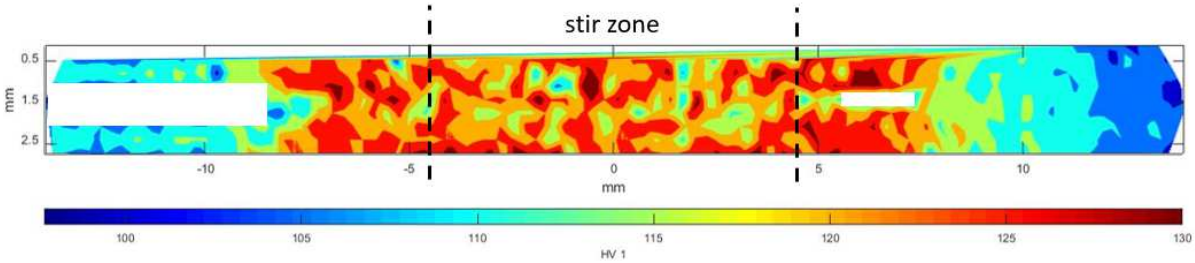

Figure 66: Full hardness mapping (HV1) (specimen no. AF-75-R2-10)

To investigate the influence of the welding parameters, welds with one varying parameter are compared. Figure 67 compares three welds produced at varying joining times. The plunge depth and rotational speed are fixed to 1.6 mm and 1000 rpm, respectively. A first remark is that the hardness in the stir zone does not differ significantly between the different welds. In contrast, a clear increase in peak temperature was observed for an increase in joining time, as illustrated in Figure 62 which compared the temperature profile of the same three welds. Furthermore, when comparing the HAZ of the three welds, the welding condition with the shortest joining time can easily be separated, since the

width of its HAZ is smaller and its minimum hardness is higher. These differences indicate that a lower heat input is provided to the weld produced with the shortest joining time, which corresponds to the temperature measurement conclusions in section 9.1.1. The other two welding combinations are harder to interpret. At a joining time of 8 s, the maximal hardness reduction is higher, but the width of the HAZ is largest for the weld obtained at the longest joining time of 10 s. Overall, with additional results from literature [53], it is safe to conclude that a higher joining time results in a wider and softer HAZ.

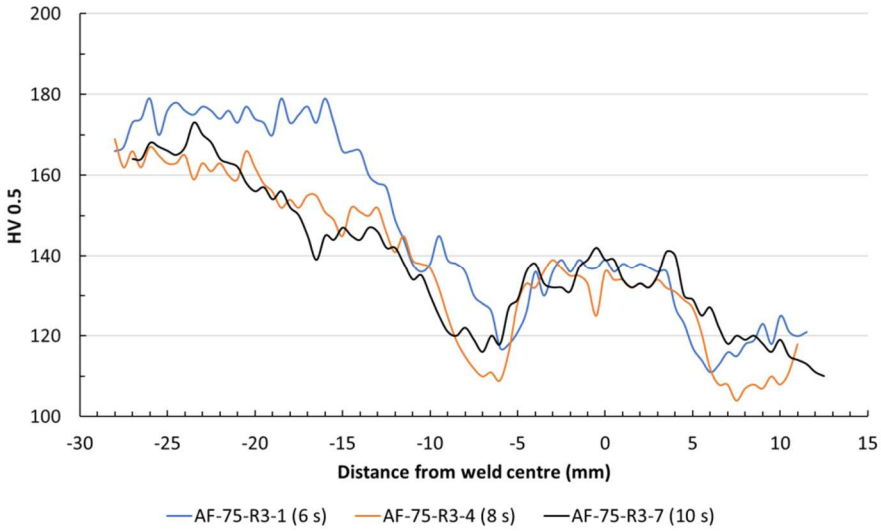

Figure 67: Hardness profile, measured at half of the upper sheet thickness, for varying JT; fixed parameters: PD=1.6 mm, RS=1000 rpm

Figure 68 compares the hardness profiles of welds produced with varying rotational speed and a fixed joining time and plunge depth of 8 s and 2.4 mm, respectively. The same welds were compared in Figure 63, which revealed that a higher peak temperature is reached at a higher rotational speed. The hardness of the stir zone is lower and the HAZ is smaller for the welding condition with the lowest rotational speed. This corresponds to the smallest heat input provided to the weld, as observed in the temperature measurements. The hardness profiles of welds obtained at higher rotational speeds exhibit approximately the same hardness in the stir zone, but this plateau zone of increased hardness is wider than the dimensions of the tool. Apparently, part of the TMAZ has been exposed to sufficiently high temperatures and deformations to maintain an elevated hardness. It is hard to interpret the hardness reduction since all profiles seem to converge to another level of base material hardness. This variance of the base material hardness could be attributed to hardness differences in the large plate material. When calculating the hardness reduction based on the measured base material hardness, reductions of 36.7, 36.4 and 29.6 % are obtained for an increase in rotational speed. This would mean that the lowest rotational speed causes the highest hardness reduction, but at the same time it shows the highest minimum hardness. This result is however influenced by the high measured base material hardness of the sample, which automatically results in a large reduction. To further investigate this influence of varying base material hardness, a mean base material hardness of 175 HV0.5 was measured on a blank sample. Based on this value, the hardness reductions for an increase in rotational speed were 34.3, 38.3 and 35.4 %, respectively. In [59], a similar comparison of hardness profiles for varying rotational speed in EN AW-2024-T4 was made. For an increase in rotational speed, a slight decrease in hardness was caused by the coarsening of the grains and the precipitates.

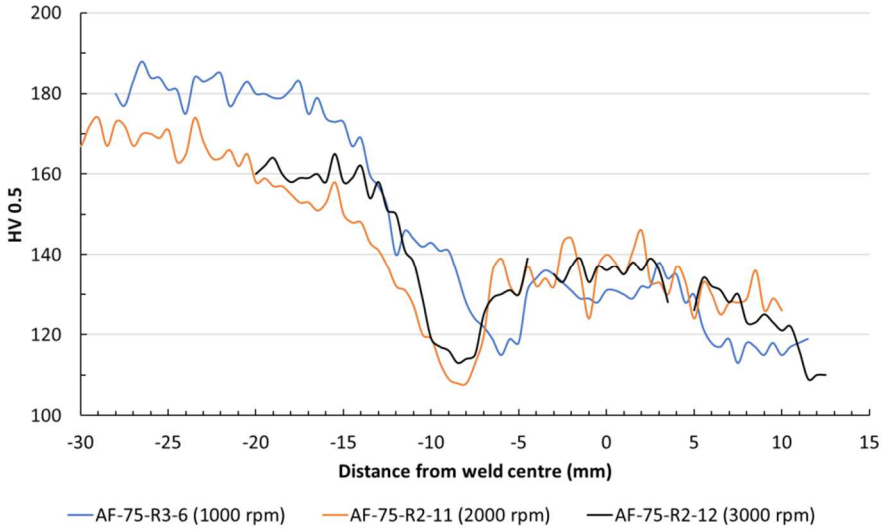

Figure 68: Hardness profile, measured at half of the upper sheet thickness, for varying RS; fixed parameters= JT=8 s, PD=2.4 mm

Finally, Figure 69 compares two hardness profiles of welds produced at a different plunge depth. The same welds were compared in Figure 64, where welds with a deeper plunge depth showed a higher peak temperature. In contrast, no difference is identified in the hardness of their stir zone. Conclusions about the hardness and the width of the HAZ are again difficult to make because of the difference in the base material hardness. Based on the actual hardness measurements, the reduction is 33.5 and 36.7 %, respectively, for an increase in plunge depth. However, when using the mean base material hardness of 175 HV0.5, a hardness reduction of 37.7 and 34.3 % is obtained. Therefore, no firm conclusion is possible. Based on the temperature measurements and different literature sources [42, 53], it is however expected that a higher plunge depth will result in an increase in the heat input, and thus lead to more softening of the weld.

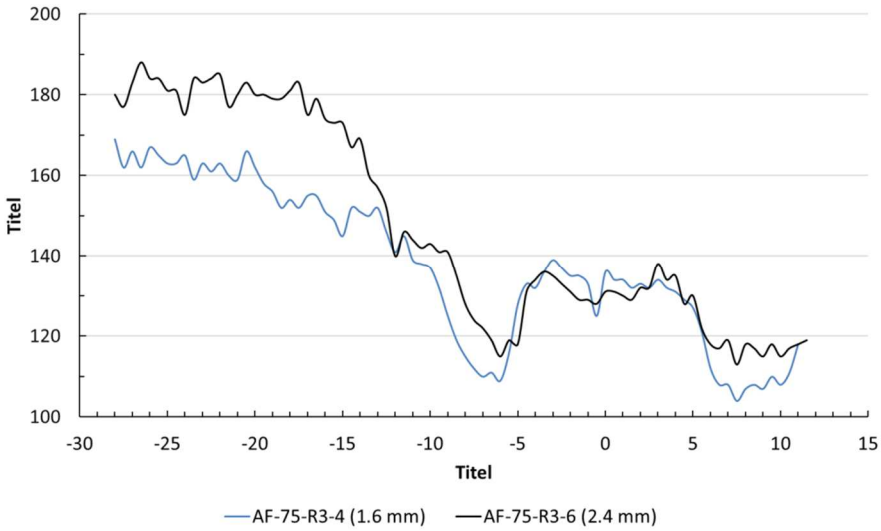

Figure 69: Hardness profile, measured at half of the upper sheet thickness, for varying PD; fixed parameters JT=8 s, RS=1000 rpm

9.1.3 Summary and conclusions

The previous sections discussed the influence of the process parameters on the temperature and the hardness profile. The peak temperature during processing increased upon increasing the joining time, the rotational speed and the plunge depth. The relation with the hardness reduction was not always as clear. This can be attributed to the different values of base material hardness. However, it is concluded that the width of the HAZ increases upon increasing the joining time, the rotational speed and the plunge depth. Hence, the peak temperature is a good indicator for the material softening.

9.2 Lap shear strength

This section will discuss the results of two lap shear test series that were executed and interpreted according to a design of experiments approach. The validity of the results will be checked, after which the main and interaction parameter effects will be identified. The maximum lap shear strength and welding parameters will also be correlated to the failure mode. Chapter 10 will combine and relate the various weld characteristics to the welding parameters.

9.2.1 Design of experiments: full factorial

The first series of strength experiments, T1 series, was performed according to a common factorial design with a rather wide parameter range. A complete overview of the selected welding conditions can be found in Table 13 and Figure 36. Important to remember is that these nine different welding conditions, selected according to a factorial design, are part of the full experimental matrix, illustrated in Figure 35. Eight of these are repeated three times. One of the nine welding conditions is the centre point of the design and is repeated six times. The maximum lap shear strength (LSS) values observed are shown in Figure 70. In the left-hand side figure, the mean values and standard deviation are presented for every welding combination. In the right-hand side figure, the mean values are shown in a cube plot, along with their corresponding welding condition. The variance on the lap shear strength is quite large for some welding conditions, especially for the welds with a higher strength, which are the most interesting. However, it is already noticeable that the welding conditions 7, 8 and 9 are favoured. The cube plot reveals that these conditions correspond to a high joining time and plunge depth. The lap shear strength is compared to the load shear requirement for resistance spot welded sheet specimens in aluminium alloys according to an AWS standard [45]. For an aluminium sheet thickness of 1.6 mm with an ultimate tensile strength of 386 MPa and above, the minimum required shear strength is 2.98 kN and the required average shear strength is 3.64 kN. The lowest weld strength obtained in this series was 3.14 kN for welding condition 4 with an average strength of 4.32 kN. Even this combination matches to the standard, which indicates that friction spot welding has a high potential to serve as an alternative to resistance spot welding.

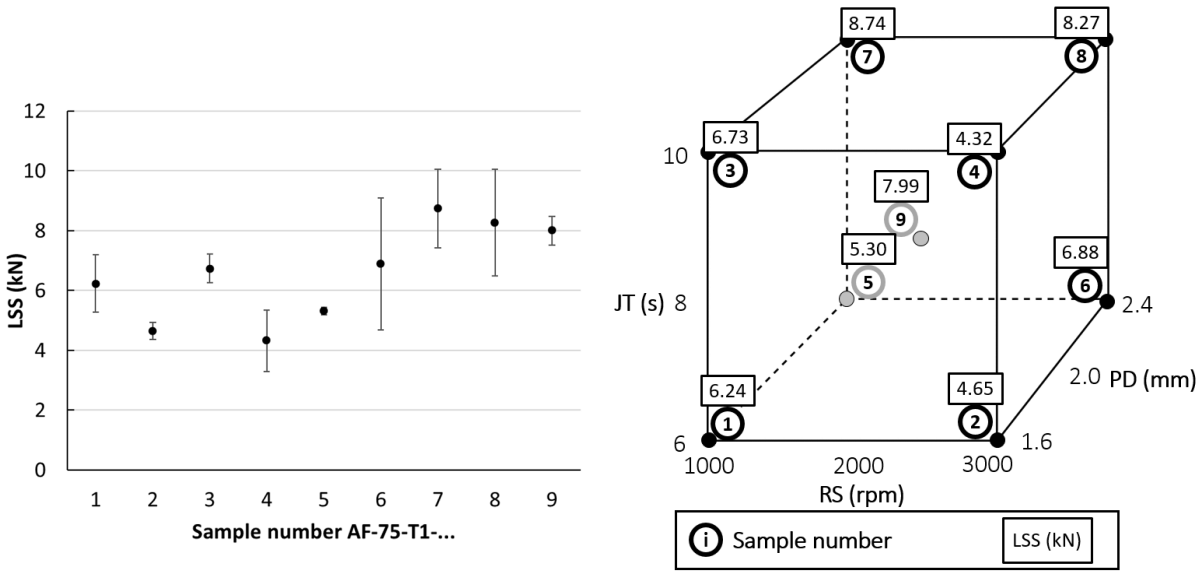

Figure 70: Lap shear strength (kN) results for T1 series: error on the results (left) and mean values (right).

The statistical software Minitab analyses the factorial design and indicates which factors contribute significantly to the response factor, which in the present work corresponds to the lap shear strength. In this case, there are three main factors: rotational speed (A), joining time (B) and plunge depth (C). These can combine to four interactions: AB, AC, BC and ABC. Not all main and interaction influences contribute significantly to the lap shear strength. The significant influences are summarized in Table 15, together with their confidence level. The confidence level defines the importance of the influence. Factors with a confidence level lower than 95 % are not considered significant. From this table, it is clear that the plunge depth has the largest influence, since it appears in every significant interaction and has the highest confidence level. The value for the rotational speed seems only relevant in combination with the plunge depth.

Table 15: Significant factors contributing to the LSS, according to the factorial design of the T1 series

Factor	Confidence level (%)
Plunge depth	99.9
Rotational speed x Plunge depth	99.0
Joining time	98.8
Joining time x Plunge depth	98.2

Figure 71 shows the influence of the joining time and the plunge depth on the lap shear strength. The plotted data points show the mean lap shear strength for all test samples produced at a certain joining time or plunge depth. The error bars indicate the variance around this mean value. Since the data point is the average of strong and weak bonds, the variance is rather large. However, a trendline shows the overall influence. The standard deviation on the centre point (middle data point) is small, because these samples are all produced with identical welding parameters. Both for an increase in joining time and plunge depth, the lap shear strength increases. Since the centre point does not coincide with the trendline, the influences are not linear. In [61], a design of experiments according to the Taguchi approach is performed to optimize the process parameters in friction spot welding of EN AW-7070-T76.

This approach does not take interactions into account and solely focusses on the main effects. It was similarly concluded that a higher joining time and plunge depth had a positive influence on the lap shear strength. The rotational speed was also found to be less significant.

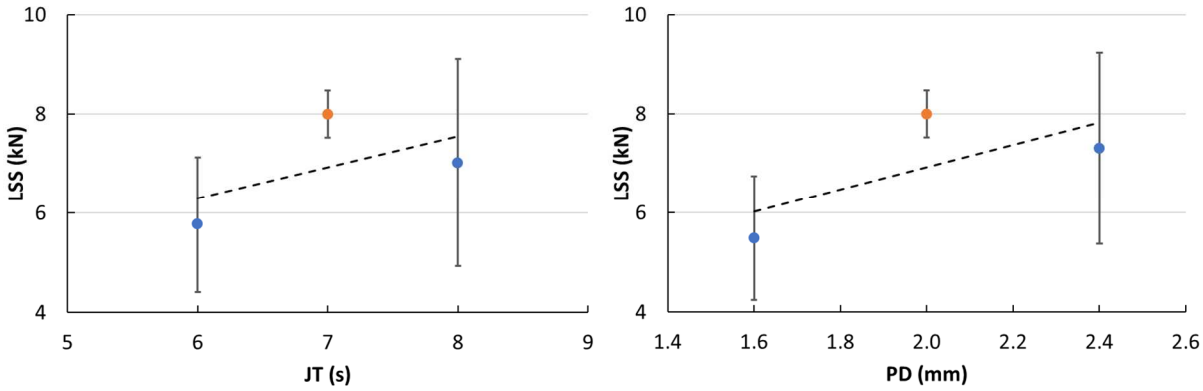

Figure 71: Main influences (JT and PD) on the LSS (kN) of T1 series, according to a full factorial design.

The influences of the interactions between the welding parameters are presented in a 3x3 graph in Figure 72. The two significant interactions (see Table 15) are shown in four subgraphs. The third non-significant interaction is not discussed. The welding parameters are shown on the horizontal axis; and the corresponding lap shear strength on the vertical axis. The legends at the right correspond to the subgraphs of the same row. The centre point (orange cube marker) and the other eight welding conditions are plotted as average data points. Each data point shows the average lap shear strength, achieved for all welding conditions in which only one welding parameter was varied. The other two parameters are fixed by the horizontal axis and the legend. Trendlines are drawn between the extreme data points. The top-right subgraph is explained as an example. It shows the interaction between the rotational speed and the plunge depth and is the second most significant factor influencing the lap shear strength (see Table 15). The left blue dot marker shows the average strength of all welding samples obtained with a plunge depth of 1.6 mm, a rotational speed of 1000 rpm and various joining times. The joining time therefore still varies, but that influence is averaged out. Since there is only one centre point in the design, the middle data point is the average of all replicates of welding condition AF-75-T1-9. This subgraph shows that for an increase in plunge depth, welds exhibit a higher lap shear strength. Nonetheless, the improvement is larger at a higher rotational speed. However, an exception is found for welds produced with a low plunge depth of 1,6 mm. The parameter combination of a low plunge depth with a high rotational speed results in welds with a lower lap shear strength, compared to welds with the parameter combination of a low plunge depth and a low rotational speed. The bottom-left subgraph presents the identical information, but in another format. The interaction between the joining time and plunge depth can be interpreted in a similar way, but the significance of this factor is lower than the interaction between the rotational speed and the plunge depth. Generally, it can be concluded that an increase in plunge depth is always beneficial for the weld strength, but the best results are obtained in combination with a high joining time.

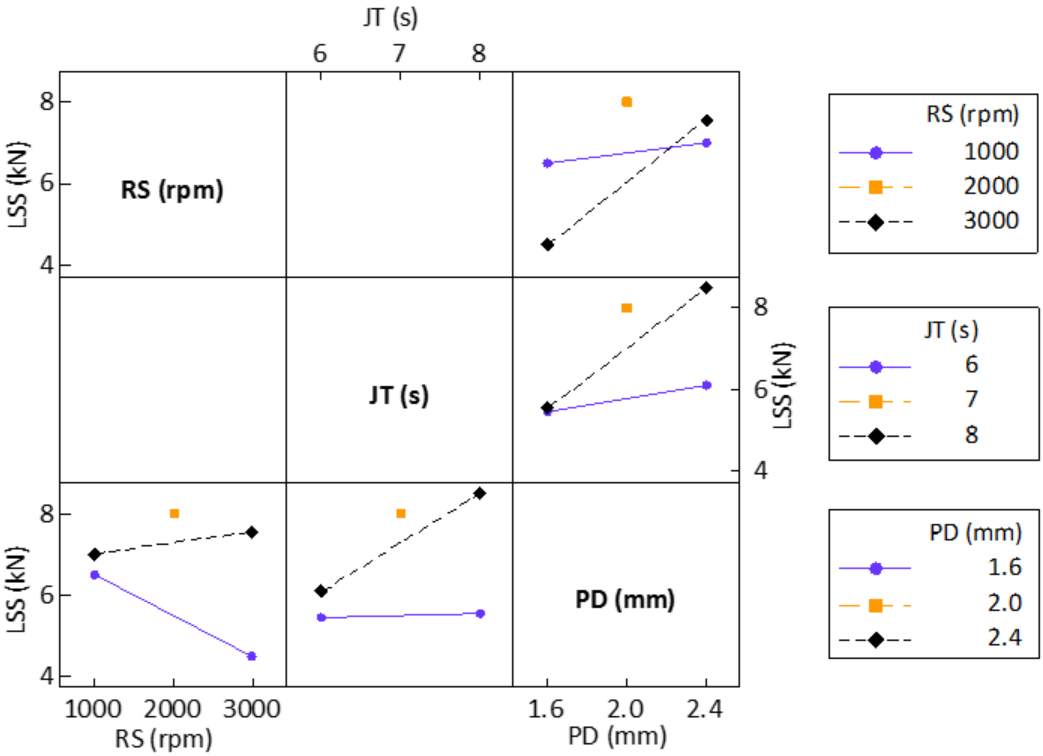

Figure 72: Interaction influences on the LSS (kN) of T1 series, according to a full factorial design

Besides the maximum lap shear strength, also the failure mode was observed. Three main failure modes were distinguished: through-nugget failure (N), plug pull-out at the upper sheet (PU) and plug pull-out at the lower sheet (PL). The general visual appearance of these failure modes was illustrated in Figure 31. The left-hand side of Figure 73 shows the correlation between the lap shear strength and its failure mode. The through-nugget failure shows a large variation and can occur at all weld strengths. Yet, the weakest joints with a lap shear strength below approximately 5 kN fail according to this mode. Plug pull-out at the upper sheet corresponds to welds with a medium weld strength and exhibits less variation. Only a single sample (specimen no. AF-75-T1-7.3) failed in a plug pull-out at the lower sheet and shows the highest lap shear strength of 10.2 kN. Therefore, a pull plug-out failure is preferred, since this indicates that the welded sheet interface is stronger than the softened material around the weld nugget. In contrast, for a through-nugget failure this bonded interface has shown to be the weakest failure path. When a plug pull-out failure occurs, it is more likely to be a pull-out at the upper sheet. The failure path will then follow the softened sleeve plunge path. A pull plug-out at the lower sheet indicates that neither the sheet interface nor the sleeve plunge path acts as the weakest joint location. The joint fails through the bottom sheet material which has not been stirred by the tool over its complete thickness. Remark that the sample (specimen no. AF-75-T1-7.3) which showed this failure mode, was produced with a plunge depth of 2.4 mm and hence the tool has plunged 50% into the lower sheet. The crack has propagated through the lower half of the bottom sheet instead of along the sleeve plunge path in the top sheet. Hence, a strong bond was created.

The bar chart in Figure 73 correlates the plunge depth and the rotational speed to the presence of certain failure modes. For an increase in plunge depth, the failure mode shifts from through-nugget failure to plug pull-out at the upper surface failure. For an increase in rotational speed, the opposite

trend is observed. The relation with the joining time is not visualized, since no correlation to the failure modes was found. A discussion concerning the relation between the weld imperfections and the failure modes can be found in Chapter 10.

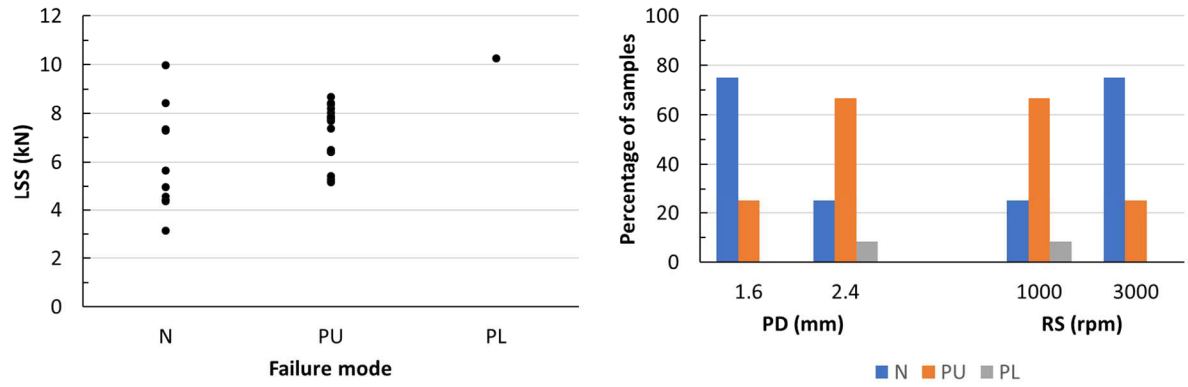

Figure 73: Correlation between failure modes and: LSS (left), welding parameters (right)

9.2.2 Optimized design of experiments: Box-Behnken

Since the common factorial design used in the T1 series revealed a non-linear behaviour, an alternative design of experiments is performed. In this T3 series, a Box-Behnken design is used as explained in Chapter 7, as it allows to analyse experiments which contain non-linear relationships. The ranges of parameters are shifted to more optimal values, based on the results of the T1 series. The lowest plunge depth of 1.6 mm and the lowest joining time of 6 s are omitted, as they resulted in the lowest lap shear strengths. The rotational speed range is not changed, since it was not possible to extract any sound conclusion from the previous design. A complete overview of the thirteen produced welding conditions can be found in Table 14 and Figure 37. Twelve of these are repeated three times. One of the thirteen welding conditions is the centre point of the design and is repeated six times. Furthermore, the concept of blocks is applied (see Chapter 7). The replicates are separated in three blocks, each block containing all different welding conditions. The experiments are executed per block.

Figure 74 gives an overview of the obtained lap shear strengths and their variability. The overall variability is smaller than for the T1 series. Moreover, the overall quality has improved: a minimum observed strength of 6.0 kN is attained, compared to 3.1 kN for the T1 series. This indicates that the parameter range shift was successful and substantial. The right-hand side graph of Figure 74 shows all separate measurements in the order of production of the welds. The experiments are performed successively, block after block. The first two produced welds (circled) showed an abnormally low lap shear strength. This is likely caused by insufficient warming-up of the machine, which started from a “cold” state. The replications of these two welding conditions in the other blocks however, showed an average to good strength. Therefore, these two measurements were deleted from the dataset and replaced by the average of their replications in order to preserve the stability of the Box-Behnken design.

A new trend can be observed when comparing the blocks. The average lap shear strength is higher in block three, compared to the lap shear strength recorded in the first two blocks. The reason for this

trend is unknown, but a few hypotheses are stated. Since all blocks contain an identical set of welding conditions, the cause cannot be attributed to a certain welding parameter and therefore has to be external. One hypothesis is that the tool head heats up when producing welds at a fast rate. The third block has been produced at a faster rate because the welder became more experienced in quickly and securely clamping the workpiece. Contradictory to this hypothesis however is that the tool head is water cooled during operation and that the tool was cleaned mechanically between each block. A second hypothesis is related to the workpiece material. For the production of the T3 series samples, two different batches of EN AW-7075-T6 plates were used. Possibly, slight differences in the mechanical properties of the base material caused this trend.

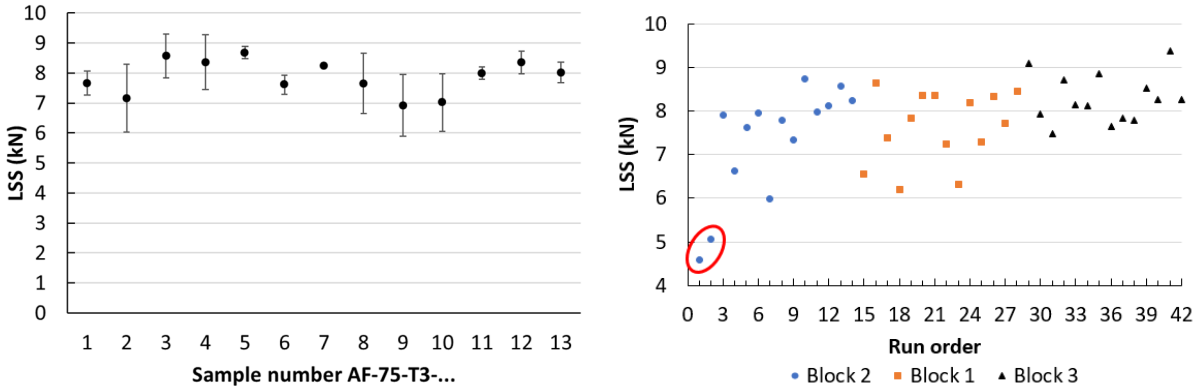

Figure 74: LSS (kN) results for T3 series: error on the results (left) and influence of the blocks (right)

A similar statistical investigation as conducted in test series T1 revealed the significant influence factors, which are summarized in Table 16. The influence of the different blocks is classified as significant, which confirms the observed trend in Figure 74. Moreover, the joining time is again a significant factor contributing to the lap shear strength. Finally, the rotational speed is a significant factor, as opposed to the plunge depth which was more significant in the T1 series. No interactions between any welding parameter were classified as significantly relevant. The limited number of significant factors indicates that the selected parameter ranges approximate an optimal region. The two main significant factors are presented in Figure 75. The joining time shows the same positive trend as in the T1 series (see Figure 71), but the improvement in strength is smaller as an increase of 8 to 9 s only results in an increase of approximately 40 N. This likely indicates that a plateau level of the lap shear strength has been reached. The rotational speed shows a clear trend for the first time. A higher lap shear strength and a lower standard deviation is attained at the slowest rotational speed of 1000 rpm.

Table 16: Significant factors in Box-Behnken design of T3 series

Factor	Confidence level (%)
Joining time	97.9
Blocks	97.8
Rotational speed	96.7

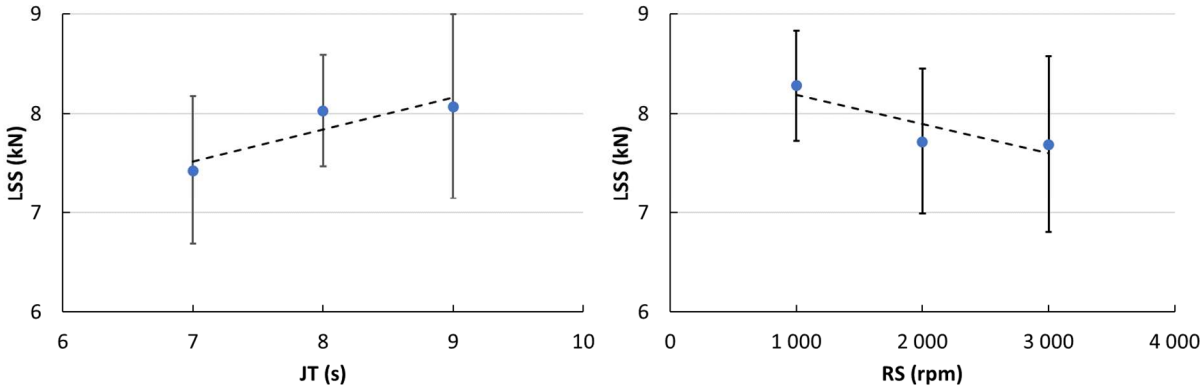

Figure 75: Main influences (JT and RS) on the LSS (kN) of T3 series, according to a Box-Behnken design

The samples were classified into four failure modes: the three conventional ones already observed in the T1 series and an additional new failure mode. The plug pull-out at upper and lower sheet failure (PUL) separates the complete weld nugget from both sheets. Both sheets failed in the through-thickness direction, while the weld nugget remained intact. Figure 76 shows the correlation between the measured lap shear strength and the failure mode. The highest strengths are obtained for a plug pull-out at the lower sheet or in combination with the upper sheet. The lower sheet region should normally be the strongest since the tool has not completely plunged through it. Hence it is plausible that the failure mode of the plug pull-out at the lower sheet occurs for the strongest welds. The bar chart shows the influence of the welding parameters on the failure mode. A deeper plunge depth, a slower rotational speed and a longer joining time all contribute to the PUL failure mode. At a fast rotational speed, the through-nugget failure prevails, while it is absent at a low rotational speed. A discussion concerning the relation between the welding imperfections and failure modes can be found in Chapter 10.

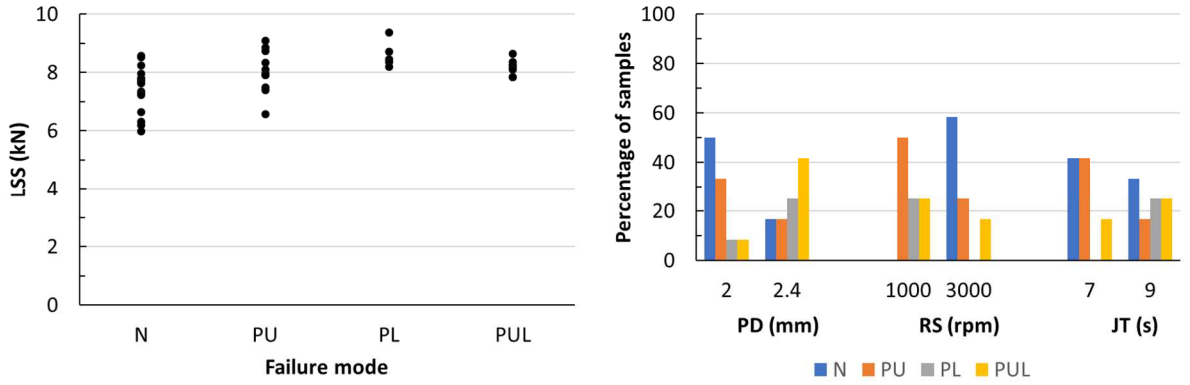

Figure 76: Correlation between failure modes and: LSS (left), welding parameters (right)

9.2.3 Summary and conclusions

The previous sections discussed the lap shear strength of the produced welds, and more importantly the influence of the process parameters. It is revealed that the plunge depth is the most critical parameter and should be higher than the lower plate thickness. This corresponds with the earlier metallographic conclusion. The joining time is preferred to be long, but a plateau level was reached. The

higher hardness reduction for longer joining times, decreases the weld strength for very high heat inputs. The rotational speed only became significant once the plunge depth and the joining time were evaluated in an optimized range. Welds produced at a lower rotational speed show higher lap shear strengths with less variation. Moreover, different failure modes were observed. The plug pull-out in the lower sheet is determined as the strongest and preferred failure mode.

9.3 Cross-tension strength

9.3.1 Design of experiments: full factorial

As an alternative to lap shear testing, cross-tension testing was performed. This T2 series was performed according to the same common factorial design as the lap shear test T1 series. A complete overview of the selected welding conditions can be found in Table 13 and Figure 36. The maximum cross-tension strength (CTS) values recorded are shown in Figure 77. At the left-hand side figure, the mean values and standard deviation are presented for each welding condition. At the right-hand side figure, the mean values are shown in a cube plot along with their corresponding welding condition. These values are much lower than for the lap shear T1 series. This result was expected, since the cross-tension loading is not the preferable loading direction for spot joints in the overlap configuration. The variance on the cross-tension strength values is however smaller than for the lap shear strength results. Unfortunately, the welding conditions with the highest cross-tension strength show the largest standard deviation. Similar to the lap shear tests in the T1 series, welding conditions 7 and 8 lead to welds with the highest strength.

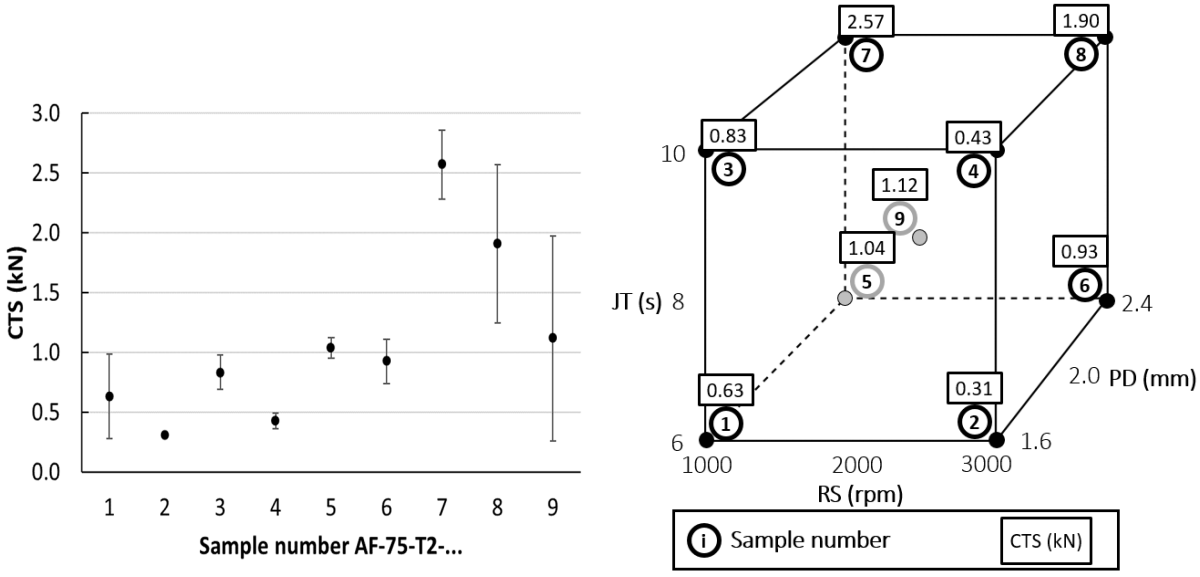

Figure 77: Cross-tension strength (kN) results for T2 series: error on the results (left) and mean values (right).

The same statistical analysis as in the T1 series is performed. Table 17 gives an overview of the significant parameters and interactions. Again, the plunge depth, the joining time and their interaction have a significant influence on the cross-tension strength. The rotational speed is classified as a non-significant factor.

Table 17: Significant factors contributing to the cross-tension strength, according to the factorial design of the T2 series

Factor	Confidence level (%)
Plunge depth	100.0
Joining time	99.4
Joining time x Plunge depth	98.5

Figure 78 shows the influence of the joining time and the plunge depth on the cross-tension strength. The interpretation of this graph is similar as described in the T1 series (see Figure 71). A major difference however is that the centre point now coincides with the trendline. Hence, the parameters show a linear behaviour with the cross-tension strength. For both an increase in joining time and plunge depth, the lap shear strength increases. As it has been shown that the interaction between the joining time and plunge depth is a significant factor (see Table 17), a study of their interaction is essential. The influence of their interaction is depicted in Figure 79. The interpretation of this interaction graph is similar as before (see Figure 72). A deeper plunge depth results in an improvement of the weld strength. This effect is even larger in combination with a longer joining time. Alternatively, a plunge depth equal to the sheet thickness of 1.6 mm does not lead to strong bonds, regardless of the selected joining time.

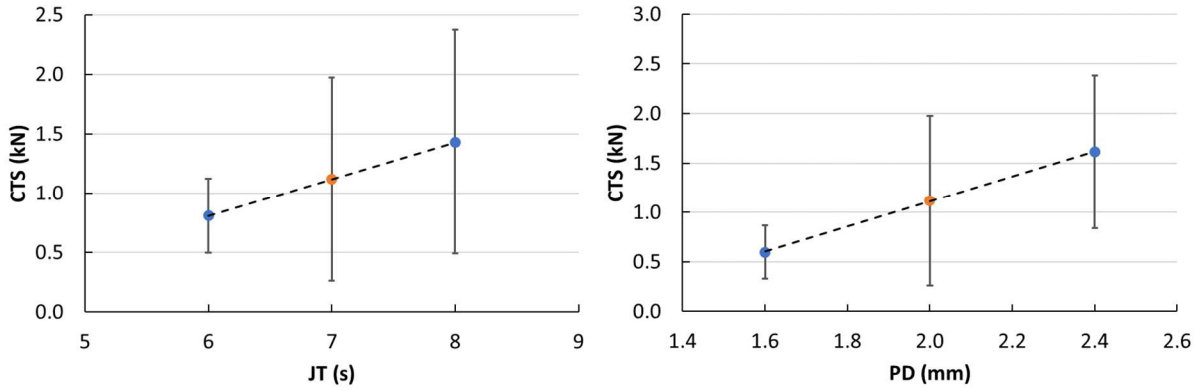

Figure 78: Main influences (JT and PD) on the CTS (kN) of T2 series, according to a full factorial design

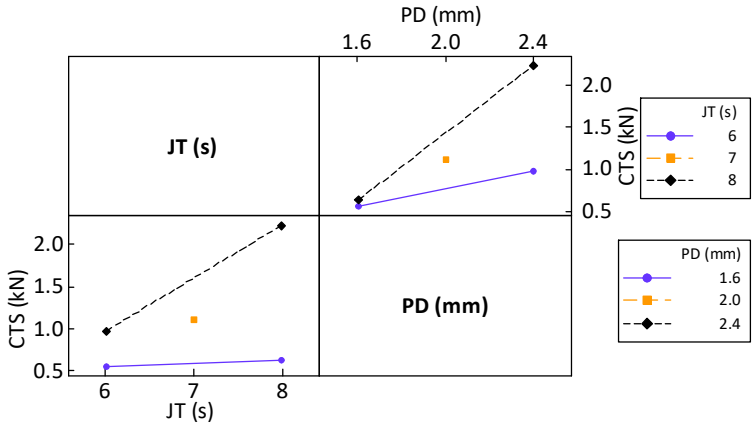

Figure 79: Interaction influences on the CTS (kN) of T2 series, according to a full factorial design

Besides the maximum cross-tension strength, also the failure mode was observed. The same three main failure modes as in the T1 series were distinguished. At the left-hand side of Figure 80, the correlation between the failure mode and the cross-tension strength is shown. The through-nugget failure now occurs for lower weld strengths, approximately below 1.2 kN, with the exception of one sample. The plug pull-out at the upper sheet occurs for almost all weld strengths. Only a single sample (specimen no. AF-75-T2-7.3) failed according to a plug pull-out at the lower sheet and also shows the highest cross-tension strength of 2.79 kN. This is the same welding condition as the weld with the highest lap shear strength in the T1 series. A through-nugget failure mode occurred more often during cross-tension testing (16 times) than during lap shear testing (12 times). This is explained by the fact that the cross-tension loading acts perpendicular on the sheet interface. The bar chart in Figure 80 correlates the plunge depth and the rotational speed to the presence of certain failure modes. For an increase in plunge depth, the failure mode shifts from all through-nugget failures to a large share of plug pull-out at the upper surface failures. Due to the limited penetration of the tool in the bottom sheet at a plunge depth of 1.6 mm, the sheet interface acts as the weakest zone in this loading direction. For an increase in rotational speed, a similar trend as for lap shear testing is observed. However, the through-nugget failure remains dominant in cross-tension loading for all rotational speeds. The relation with the joining time is not visualized, since no correlation with the failure modes was identified. A discussion concerning the relation between the welding imperfections and failure modes can be found in Chapter 10.

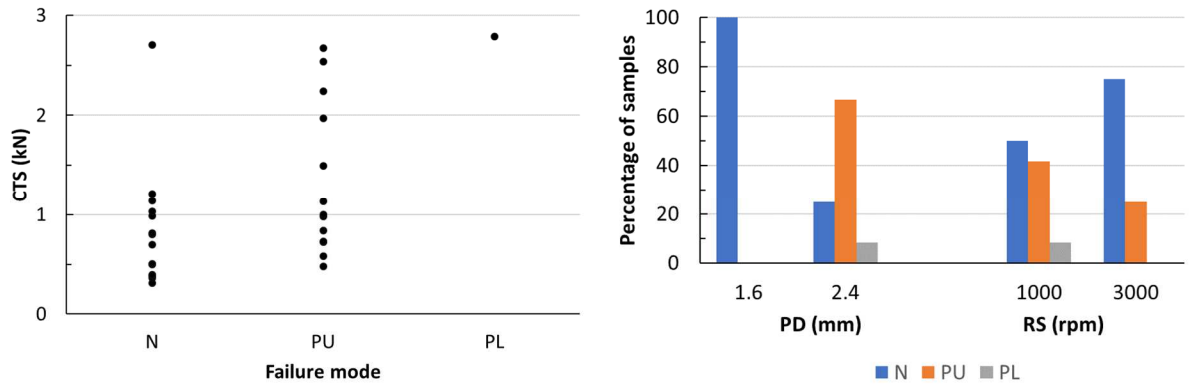

Figure 80: Correlation between failure modes and: CTS (left), welding parameters (right)

9.3.2 Summary and conclusions

Overall, many similarities exist between the lap shear test results and the cross-tension test results. The measured strengths are lower, but the same welding conditions lead to the welds with the highest strength. The joining time and plunge depth are both significant factors and show the same influence on the lap shear strength, whereas the rotational speed is in both cases less significant. Upon an increase in either the plunge depth or the rotational speed, the same transition to another dominant failure modes is observed. However, a higher share of through-nugget failures occurs for the cross-tension samples compared to the lap shear samples.

Chapter 10 Overall parameter influences

This chapter will combine all previous results and correlate them. It will explain the observed trends and in the meantime act as a summary.

10.1 Influence of the joining time

The joining time and heat input are closely correlated in friction spot welding. An increase in the joining time results in a fine and more equiaxed microstructure with a smaller amount of weld imperfections. An increase in heat input softens the workpiece material and the improved material flow diminishes the presence of deep incomplete refill and void imperfections. In contrast, a lack of heat input leads to problems concerning refilling the keyhole. A disadvantage of a longer joining time is that a wider softened heat-affected zone is created, as the workpiece is exposed to a higher elevated temperature for a longer time. Moreover, a long joining time is impractical for industrial applications. Despite these drawbacks, a longer joining time is preferred to achieve strong bonds. All design of experiment series showed a positive and significant influence of the joining time. This can be explained by the lower amount of imperfections and hence a larger load bearing area. Finer grains are also tougher and delay the fracture. However, a plateau value for the weld strength exists. The positive effect of an increase in joining time diminishes when sufficient heat is already applied. An excessive heat input will excessively soften the weld or cause the material to melt. This is also visible in the observed failure modes. At a higher joining time, the failure mode according to a plug pull-out at lower and upper sheet occurs more frequently than the through-nugget. The high heat input provided to the weld has produced a strong nugget, but at the same time softened the nugget circumference (TMAZ and HAZ) to a weaker location than the welded interface. It is expected that the lower sheet material is stronger than the upper sheet since the tool has not reached this area. This was reflected in the welds with high strengths, with corresponding failure in the lower sheet. Eventually, the heat also reaches the lower sheet and hence lower sheet failures can also occur.

10.2 Influence of the plunge depth

It was identified that a plunge depth equal to the upper sheet thickness is not optimal. The absence of tool penetration in the lower sheet creates bonding layer imperfections and other interface irregularities such as partial bonding and hooking. A deeper plunge depth most likely results in a larger nugget area and a longer sleeve plunge path. The larger load bearing area leads to a higher lap shear and cross-tension strength. The heat affected zone becomes wider for a deeper plunge depth. By plunging the tool deeper into the workpiece, a larger frictional area is created, hence resulting in a higher heat input provided to the weld. This is confirmed by the temperature measurements. The failure mode is also strongly affected by the choice of the plunge depth. For the lowest plunge depths, almost all welds fail through the nugget. In that case, many imperfections are located along the sheet interface, such as a non-bonded interface, hooking and voids along the sleeve plunge path. All these nearby imperfections create high stress concentrations along the interface. For a deeper plunge depth, the failure mode shifts to plug pull-out failures. In that case, the interface is strongly bonded and the sleeve plunge path becomes the weakest connection. Plug pull-out failures in the lower sheet occur because

the tool has also plunged and refilled a large part of this sheet. For a low plunge depth, the lower sheet remains rather unaffected of plastic deformations and thus a lower sheet failure will not occur.

10.3 Influence of the rotational speed

The rotational speed is the most challenging parameter to understand. It has an influence on the heat input, the material flow and the nugget area. The weld-cross sections showed the least imperfections at 1000 and 3000 rpm, but an increase of imperfections at 2000 rpm. For a slower rotational speed, the stir zone area becomes larger and contains a finer grain size. This effect cannot be explained by the influence of stirring rate or temperature solely. Additional research on the change in microstructure and the state of strengthening precipitates is required. Temperature measurements showed that welding at a higher rotational speed produced more heat. Hence, the heat affected zone becomes wider and the material flow improves. Welding at a lower rotational speed of 1000 rpm requires more torque from the tool spindle. This is explained by the lack of plasticized material for welds produced at this low rotational speed. Still a low rotational speed showed good results. The combination of the high-quality cross-section which contains only few imperfections, the large load bearing stir zone with the fine-grained microstructure and the decreased temperature and width of the HAZ results in strong joints. The failure mode is also correlated to the choice of the rotational speed. The through-nugget failure occurs more frequently at the highest rotational speed. This indicates a weaker interface bonding at this parameter setting. During the T3 series of lap shear tests, the through-nugget failure was even absent for slow rotational speeds, while it was dominant at a higher rotational speed.

10.4 Best performing weld

The best performing weld produced during this research was AF-75-T1-7.3. The welding parameters are a rotational speed of 1000 rpm, a joining time of 8 s and a plunge depth of 2.4 mm. Figure 81 shows the etched cross-section and details of this weld. The fine and dark stir zone microstructure with the coarser vertical central band, immediately reveals that the rotational speed was set to 1000 rpm. Although the plunge depth was set to 2.4 mm, the stir zone almost made contact with the bottom surface of the lower sheet. This ensures a large load bearing area. The bottom left-hand side picture shows a detail of the incomplete refill imperfection and the TMAZ. Due to the high joining time, the depth of the incomplete refill is only small. Furthermore, the interface of the separated sheets is indicated by the curved line. This non-bonded interface (curved line) is terminated in the TMAZ and cannot penetrate into the stir zone. Due to the deep plunge depth, the void at the end of the sleeve plunge path (circle) is to a large extent separated from the interface imperfections. The bottom-right picture shows a detail of the void imperfection, which is formed upon refilling the sleeve keyhole. The combination of these parameters has led to a weld with a maximum lap shear strength of 8.7 ± 1.3 kN. The strongest sample failed in a plug pull-out at the lower sheet failure, while the replicates failed in a plug pull-out at the upper sheet. The same welding condition also performed best in cross-tension loading. There, the obtained strength was 2.6 ± 0.3 kN. Again, the strongest sample failed in a plug pull-out through the

lower sheet, while the other replicates failed through the upper sheet. A maximum hardness reduction of 34.3 % was measured.

Compared to literature, this is a good result. At a rotational speed of 1500 rpm and a joining time of 3 s, a weld with a lap shear strength of 7 kN was produced in 2 mm thick EN AW-7075-T6 [41]. Unfortunately, the plunge depth was not mentioned. A lap shear strength of 4.7 kN was obtained for EN AW-7075-T6 sheets with a thickness of 0.8 mm, produced at a rotational speed of 2100 rpm, a joining time of 3.5 s and a plunge depth of 1.1 mm [53]. Considering that the sheets are half as thick as in this research, the joining time and plunge depth are similar to the present work.

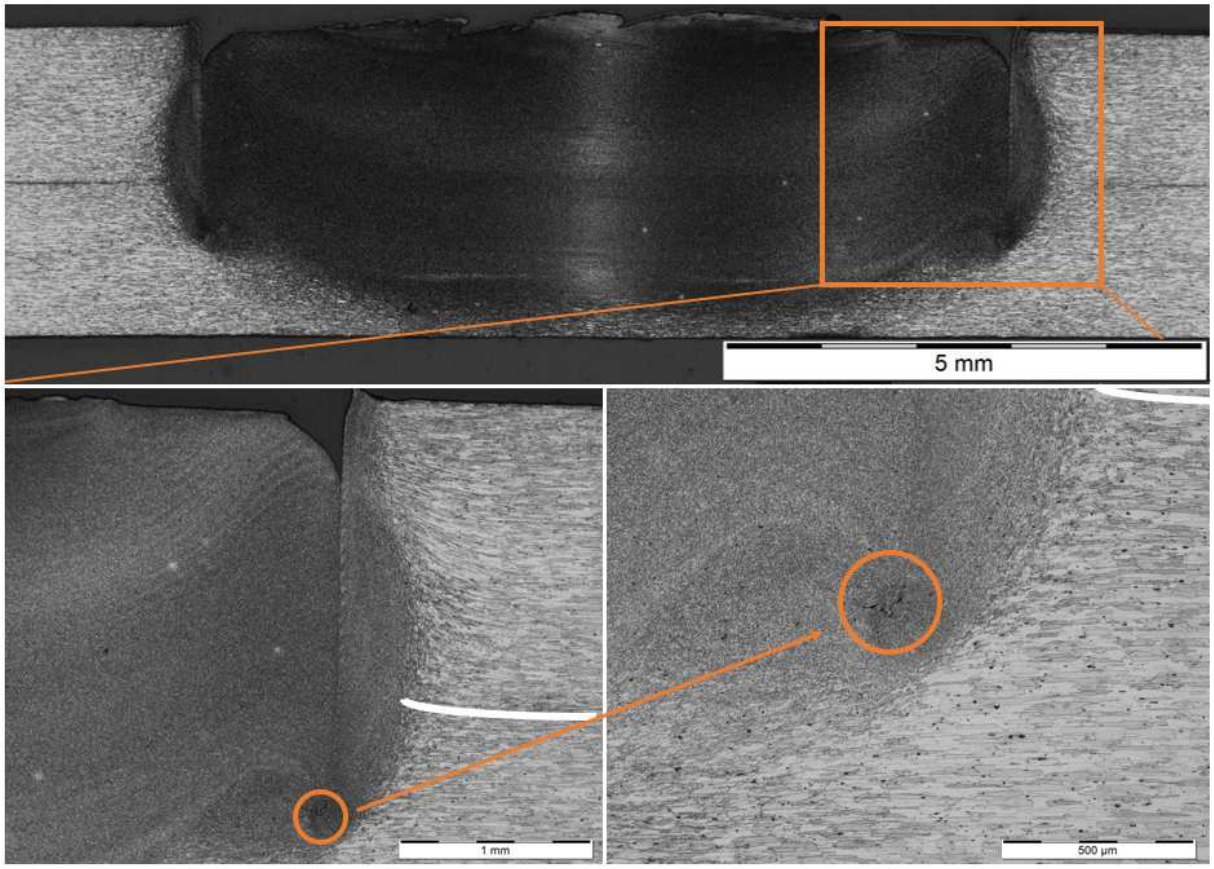

Figure 81: Best performing weld: cross-section and details of interface (curve) and void (circle) in specimen no. AF-75-T1-7

Chapter 11 Future work

The process of friction spot welding is still rather immature, especially for processing of high-strength alloys. This work investigated the weldability of EN-AW 7075-T6, a typical high strength alloy used in aerospace applications. It provided new insights in the process of friction spot welding and is a good onset for further research. The weld was investigated in terms of its microstructure and mechanical properties and useful conclusions were made. Nevertheless, the research on high-strength alloys using friction spot welding is far from completed. Several further research possibilities are discussed below.

The current work could be extended by varying other process parameters which were now kept fixed. The first choice could be to vary the plunge and retraction time, and the respective plunge and retraction rate. These parameters definitely influence the material flow and deformation rate. A good start could be to vary these parameters around the value used in this work: 0.8 mm/s. Moreover, it could be interesting to apply a surface indentation at the end of the process as described in [52]. This compensates for the material loss and should result in welds without incomplete refill imperfections.

Furthermore, it could be sensible to investigate the possibilities of preheating the specimen. Softening the workpiece by first exposing it to a higher temperature, could decrease the required joining time. Hence, a faster production could be obtained. Preheating options are frictional surface stirring and electric or inductive heating.

Many testing methods were already applied during this dissertation, but most of them are destructive. Specific research on non-destructive testing methods is highly recommended. Only a fast and reliable NDT technique can ensure welds of good quality in an industrial environment.

It can also be interesting to build upon the results obtained in this work and to take the investigation to another scale. The complete process of forming a strong bond relies on the change in microstructure and the role of the strengthening precipitates. A thorough investigation of the microstructural changes at higher magnification could contribute to the understanding of the metallurgical bonding. A first attempt to start such a research could be to measure the grain sizes at specific locations in different welds. Probably this is related to different hardness zones. By relating this to the welding parameters, the weld zone could be tailored to the best mechanical properties.

To completely understand the microstructural changes, relevant quantities should be monitored online during processing. Possibilities are the applied pressure, the friction coefficient, thermal properties of the workpiece etc. Quantifying these values make it possible to estimate the total heat input and local temperatures.

The research can also be continued computationally by creating a material flow design using finite elements. This would provide a means to derive the above mentioned relevant quantities without repeating a vast amount of experiments. The simulations could be supported by examining cross-sections of uncompleted welds. By interrupting the welding process at a certain stage, intermediate flow patterns could be investigated. If possible, a marker material can be applied at the sheet interface.

Finally, the inherent problems of the welding technique should not be forgotten. The tool contamination remains one of the most practical issues which hinders the introduction of the process to a large-scale

industry. The occurrence of gap loading will be inevitable with the current tool design. The aluminium adhesion at the tool bottom however could be avoided with the correct tool material choice. Material and coating possibilities where discussed in the literature review of this master dissertation. It is recommended that further research investigates the performance of Ni/Co alloys and diamond-like-carbon coatings.

Chapter 12 Conclusions

This master dissertation investigated the weldability of 1.6 mm EN AW-7075-T6 aluminium alloy using friction spot welding. Chapter 2 introduced the welding process and the controllable welding parameters. Chapter 3 was devoted to the welding tool and the accompanying problems. The typical microstructure and strength values of a friction spot weld were discussed in Chapter 4, while Chapter 5 focussed specifically on published results of some high-strength aluminium alloys. Chapter 6 gave an overview of the measurement procedures and Chapter 7 of the performed welding conditions. Chapter 8 and Chapter 9 respectively discussed the metallographic and mechanical results obtained during this dissertation. Finally, Chapter 10 combined all the previous results in a parameter influence summary. The previous chapter recommended several future research options and this section will list the most important conclusions of this investigation.

- Welds produced with a longer joining time show fewer imperfections, especially a shallower incomplete refill.
- Welds produced with a plunge depth equal to the upper sheet thickness or at a high rotational speed are prone to non-bonded or weak bonded interfaces.
- Welds produced at a lower rotational speed show a larger and finer grained affected stir zone.
- The heat input during welding is positively correlated with the joining time, the rotational speed and the plunge depth.
- Hardness reductions of about 33% were measured at the interface between HAZ and TMAZ.
- Joining time, plunge depth and their interaction are the most significant factors contributing to the weld strength. An increase in the value of both welding parameters improves the weld strength and increases the tendency to fail in a plug pull-out failure.
- The choice of rotational speed is less sensitive, but the weld quality improves at a lower rotational speed.
- The strongest weld was produced at a rotational speed of 1000 rpm, a joining time of 8 s and a plunge depth of 2.4 mm. A lap shear strength of 8.7 ± 1.3 kN and a cross-tension strength of 2.6 ± 0.3 kN were obtained.
- Strong welds fail in a plug pull-out at the lower sheet or by a complete plug pull-out through both sheets.
- The cross-tension specimen has a higher tendency to fail in a through-nugget failure than the lap shear specimen.

References

[1] F. Alshmri, 'Lightweight Material: Aluminium High Silicon Alloys in The Automotive Industry', in *Advanced Technologies in Manufacturing, Engineering and Materials, Pts 1-3*, vol. 774–776, Y. H. Kim and P. Yarlagadda, Eds. Stafa-Zurich: Trans Tech Publications Ltd, 2013, pp. 1271–1276.

[2] R. Dhingra and S. Das, 'Life cycle energy and environmental evaluation of downsized vs. lightweight material automotive engines', *J. Clean. Prod.*, vol. 85, pp. 347–358, Dec. 2014.

[3] K. Grigoriou and A. P. Mouritz, 'Comparative assessment of the fire structural performance of carbon-epoxy composite and aluminium alloy used in aerospace structures', *Mater. Des.*, vol. 108, pp. 699–706, Oct. 2016.

[4] 'Aluminium applications – Transport'. [Online]. Available: http://www.aluminiumleader.com/application/transport/. [Accessed: 30-Nov-2016].

[5] R. Rajan, P. Kah, B. Mvola, and J. Martikainen, 'Trends in Aluminium Alloy Development and Their Joining Methods', *Rev. Adv. Mater. Sci.*, vol. 44, no. 4, pp. 383–397, 2016.

[6] T. Rosendo *et al.*, 'Mechanical and microstructural investigation of friction spot welded AA6181-T4 aluminium alloy', *Mater. Des.*, vol. 32, no. 3, pp. 1094–1100, Mar. 2011.

[7] T. Rosendo, M. Tier, J. Mazzaferro, C. Mazzaferro, T. R. Strohaecker, and J. F. Dos Santos, 'Mechanical performance of AA6181 refill friction spot welds under Lap shear tensile loading', *Fatigue Fract. Eng. Mater. Struct.*, vol. 38, no. 12, pp. 1443–1455, Dec. 2015.

[8] T. Montag, J.-P. Wulfsberg, H. Hameister, and R. Marschner, 'Influence of Tool Wear on Quality Criteria for Refill Friction Stir Spot Welding (RFSSW) Process', *Procedia CIRP*, vol. 24, pp. 108–113, Jan. 2014.

[9] P. L. Threadgill, A. J. Leonard, H. R. Shercliff, and P. J. Withers, 'Friction stir welding of aluminium alloys', *Int. Mater. Rev.*, vol. 54, no. 2, pp. 49–93, Mar. 2009.

[10] X. W. Yang, T. Fu, and W. Y. Li, 'Friction Stir Spot Welding: A Review on Joint Macro- and Microstructure, Property, and Process Modelling', *Adv. Mater. Sci. Eng.*, p. 697170, 2014.

[11] X. W. Yang, T. Fu, and W. Y. Li, 'Friction Stir Spot Welding: A Review on Joint Macro- and Microstructure, Property, and Process Modelling', *Adv. Mater. Sci. Eng.*, p. 697170, 2014.

[12] M. D. Tier *et al.*, 'The influence of refill FSSW parameters on the microstructure and shear strength of 5042 aluminium welds', *J. Mater. Process. Technol.*, vol. 213, no. 6, pp. 997–1005, Jun. 2013.

[13] S. T. Amancio-Filho, A. P. C. Camillo, L. Bergmann, J. F. dos Santos, S. E. Kury, and N. G. A. Machado, 'Preliminary Investigation of the Microstructure and Mechanical Behaviour of 2024 Aluminium Alloy Friction Spot Welds', *Mater. Trans.*, vol. 52, no. 5, pp. 985–991, May 2011.

[14] 'Friction spot welding | www.bil-ibs.be'. [Online]. Available: http://www.bil-ibs.be/en/friction-spot-welding. [Accessed: 02-Nov-2016].

[15] O. Bilouet, 'Soudage par Friction Spot d'assemblages d'alliages d'aluminium', Mons, Belgique, Jan-2016.

[16] J. Shen, M. E. B. Cardillo, and J. dos Santos, 'A preliminary study on FSpW of dissimilar metal joints of Cu and Al.', Helmholtz-Zentrum Geesthacht, Institute of Materials Research, Geesthacht, Germany.

[17] T. Kolba, W. De Waele, and K. Faes, 'Experimental investigation of the weldability of aluminium alloys using friction spot welding', master dissertation at Ghent University, Gent, 2016.

[18] W. Elegeert, F. Vos, and K. Faes, 'The friction spot welding of high-strength Al alloys', master dissertation at KU Leuven, Leuven, 2015.

[19] T. Montag, J.-P. Wulfsberg, H. Hameister, and R. Marschner, 'Influence of setting parameters on tool durability for refill friction stir spot welding (RFSSW) process', presented at the Proceedings of the 10th international Symposium Friction Stir Welding, China, 20-May-2014.

[20] R. S. Mishra and M. W. Mahoney, *Friction Stir Welding and Processing*. ASM International, 2007.

[21] Y. N. Zhang, X. Cao, S. Larose, and P. Wanjara, 'Review of tools for friction stir welding and processing', *Can. Metall. Q.*, vol. 51, no. 3, pp. 250–261, Jul. 2012.

[22] H. MIYAZAKI, Y. UTSUMI, and K. Tsuda, 'Development of a Friction Spot Joining Tool for 980 MPa Tensile Strength Steels Joining', vol. Number 81, Oct. 2015.
[23] 'Thermodur 2344 Superclean/ Thermodur 2344 EFS-datasheet'. Deutsche Edelstahlwerke GmbH, 14-Apr-2016.
[24] 'Uddeholm Hotvar-datasheet'. Uddeholm, Sep-2011.
[25] 'Thermodur 2999 Superclean-datasheet'. Deutsche Edelstahlwerke GmbH, 20-Apr-2016.
[26] S. Cater, *Fundamentals of Friction Stir Welding*, 3rd edition. TWI, 2016.
[27] 'MP 159 alloy-datasheet'. Latrobe Specialty Steel Company.
[28] J. Pujante, M. Vilaseca, D. Casellas, and M. D. Riera, 'The Role of Adhesive Forces and Mechanical Interaction on Material Transfer in Hot Forming of Aluminium', *Tribol. Lett.*, vol. 59, no. 1, p. 10, May 2015.
[29] H. Fukui, J. Okida, N. Omori, H. Moriguchi, and K. Tsuda, 'Cutting performance of DLC coated tools in dry machining aluminum alloys', *Surf. Coat. Technol.*, vol. 187, no. 1, pp. 70–76, Oct. 2004.
[30] J. Jerina and M. Kalin, 'Initiation and evolution of the aluminium-alloy transfer on hot-work tool steel at temperatures from 20 °C to 500 °C', *Wear*, vol. 319, no. 1–2, pp. 234–244, Nov. 2014.
[31] M. Kalin and J. Jerina, 'The effect of temperature and sliding distance on coated (CrN, TiAlN) and uncoated nitrided hot-work tool steels against an aluminium alloy', *Wear*, vol. 330, pp. 371–379, Jun. 2015.
[32] M. Lahres, P. Müller-Hummel, and O. Doerfel, 'Applicability of different hard coatings in dry milling aluminium alloys', *Surf. Coat. Technol.*, vol. 91, no. 1, pp. 116–121, May 1997.
[33] A. R. Riahi and A. T. Alpas, 'Adhesion of AA5182 aluminum sheet to DLC and TiN coatings at 25 degrees C and 420 degrees C', *Surf. Coat. Technol.*, vol. 202, no. 4–7, pp. 1055–1061, Dec. 2007.
[34] S. Bhowmick and A. T. Alpas, 'The performance of hydrogenated and non-hydrogenated diamond-like carbon tool coatings during the dry drilling of 319 Al', *Int. J. Mach. Tools Manuf.*, vol. 48, no. 7–8, pp. 802–814, Jun. 2008.
[35] J. Jerina and M. Kalin, 'Aluminium-alloy transfer to a CrN coating and a hot-work tool steel at room and elevated temperatures', *Wear*, vol. 340, pp. 82–89, Oct. 2015.
[36] B. Wang, G. R. Bourne, A. L. Korenyi-Both, A. K. Monroe, S. P. Midson, and M. J. Kaufman, 'Method to evaluate the adhesion behavior of aluminum-based alloys on various materials and coatings for lube-free die casting', *J. Mater. Process. Technol.*, vol. 237, pp. 386–393, Nov. 2016.
[37] E. K. Tentardini, A. O. Kunrath, C. Aguzzoli, M. Castro, J. J. Moore, and I. J. R. Baumvol, 'Soldering mechanisms in materials and coatings for aluminum die casting', *Surf. Coat. Technol.*, vol. 202, no. 16, pp. 3764–3771, May 2008.
[38] M. Vilaseca, S. Molas, and D. Casellas, 'High temperature tribological behaviour of tool steels during sliding against aluminium', *Wear*, vol. 272, no. 1, pp. 105–109, Oct. 2011.
[39] C. Mitterer, F. Holler, F. Üstel, and D. Heim, 'Application of hard coatings in aluminium die casting — soldering, erosion and thermal fatigue behaviour', *Surf. Coat. Technol.*, vol. 125, no. 1–3, pp. 233–239, Mar. 2000.
[40] A. Gerlich, G. Avramovic-Cingara, and T. H. North, 'Stir zone microstructure and strain rate during Al 7075-T6 friction stir spot welding', *Metall. Mater. Trans. -Phys. Metall. Mater. Sci.*, vol. 37A, no. 9, pp. 2773–2786, Sep. 2006.
[41] Z. Shen, X. Yang, Z. Zhang, L. Cui, and T. Li, 'Microstructure and failure mechanisms of refill friction stir spot welded 7075-T6 aluminum alloy joints', *Mater. Des.*, vol. 44, pp. 476–486, Feb. 2013.
[42] J. Y. Cao, M. Wang, L. Kong, and L. J. Guo, 'Hook formation and mechanical properties of friction spot welding in alloy 6061-T6', *J. Mater. Process. Technol.*, vol. 230, pp. 254–262, Apr. 2016.
[43] Y. Zhao, H. Liu, T. Yang, Z. Lin, and Y. Hu, 'Study of temperature and material flow during friction spot welding of 7B04-T74 aluminum alloy', *Int. J. Adv. Manuf. Technol.*, vol. 83, no. 9–12, pp. 1467–1475, Apr. 2016.
[44] J. A. Esmerio Mazzaferro *et al.*, 'Preliminary Study on the Mechanical Behavior of Friction Spot Welds', *Soldag. Inspecao*, vol. 14, no. 3, pp. 238–247, Sep. 2009.

[45] *AWS D17. 2/D17. 2M-2013, Specification for Resistance Welding for Aerospace Applications*. American Welding Society, 2012.
[46] M. A. D. Tier *et al.*, 'A Study About the Mechanical Properties of Alclad AA2024 Connections Processed by Friction Spot Welding 1', in *ResearchGate*, 2009.
[47] *CES EduPack 2016*. Cambridge, UK: Granta Design Limited.
[48] Z. Li, S. Gao, S. Ji, Y. Yue, and P. Chai, 'Effect of Rotational Speed on Microstructure and Mechanical Properties of Refill Friction Stir Spot Welded 2024 Al Alloy', *J. Mater. Eng. Perform.*, vol. 25, no. 4, pp. 1673–1682, Mar. 2016.
[49] G. Pieta, J. dos Santos, T. R. Strohaecker, and T. Clarke, 'Optimization of Friction Spot Welding Process Parameters for AA2198-T8 Sheets', *Mater. Manuf. Process.*, vol. 29, no. 8, pp. 934–940, Aug. 2014.
[50] 'Total Materia - 's Werelds Meest Uitgebreide Materiaal Database'. [Online]. Available: http://www.totalmateria.com/. [Accessed: 14-Nov-2016].
[51] U. Suhuddin, L. Campanelli, M. Bissolatti, H. Wang, R. Verastegui, and J. F. dos Santos, *A review on microstructural and mechanical properties of friction spot welds in Al-based similar and dissimilar joints*. Cambridge: Woodhead Publ Ltd, 2013.
[52] Y. Q. Zhao, H. J. Liu, S. X. Chen, Z. Lin, and J. C. Hou, 'Effects of sleeve plunge depth on microstructures and mechanical properties of friction spot welded alclad 7B04-T74 aluminum alloy', *Mater. Des.*, vol. 62, pp. 40–46, Oct. 2014.
[53] Z. Shen, Y. Chen, J. S. C. Hou, X. Yang, and A. P. Gerlich, 'Influence of processing parameters on microstructure and mechanical performance of refill friction stir spot welded 7075-T6 aluminium alloy', *Sci. Technol. Weld. Join.*, vol. 20, no. 1, pp. 48–57, Jan. 2015.
[54] T. Azimzadegan and S. Serajzadeh, 'An Investigation into Microstructures and Mechanical Properties of AA7075-T6 during Friction Stir Welding at Relatively High Rotational Speeds', *J. Mater. Eng. Perform.*, vol. 19, no. 9, pp. 1256–1263, Dec. 2010.
[55] A. Gerlich, M. Yamamoto, and T. H. North, 'Local melting and cracking in Al 7075-T6 and Al 2024-T3 friction stir spot welds', *Sci. Technol. Weld. Join.*, vol. 12, no. 6, pp. 472–480, Nov. 2007.
[56] A. Gerlich, M. Yamamoto, and T. H. North, 'Local melting and tool slippage during friction stir spot welding of Al-alloys', *J. Mater. Sci.*, vol. 43, no. 1, pp. 2–11, Jan. 2008.
[57] S. Ji, Y. Wang, J. Zhang, and Z. Li, 'Influence of rotating speed on microstructure and peel strength of friction spot welded 2024-T4 aluminum alloy', *Int. J. Adv. Manuf. Technol.*, Sep. 2016.
[58] 'Minitab'. [Online]. Available: http://www.minitab.com/en-us/. [Accessed: 30-Apr-2017].
[59] H. Rezaei and H. Bisadi, 'Effect of rotational speeds on microstructure and mechanical properties of friction stir-welded 7075-T6 aluminium alloy', *Ournal Mech. Eng. Sci.*, vol. Proceedings of the Institution of Mechanical Engineers Part C, no. vols 203-210, Aug. 2011.
[60] ISO, *NBN EN 1999-1-1: Eurocode 9: Design of aluminium structures-Part 1-1: General structural rules*, 2nd ed. European Committee for standardization, 2007.
[61] P. S. Effertz, L. Quintino, and V. Infante, 'The optimization of process parameters for friction spot welded 7050-T76 aluminium alloy using a Taguchi orthogonal array', *Int. J. Adv. Manuf. Technol.*, Jan. 2017.

Appendix A: Welding conditions

A.1 Metallographic test samples

Sample name	RS (rpm)	JT (s)	PD (mm)
AF-75-R0-1	1750	5	2.0
AF-75-R0-2	2000	5	2.0
AF-75-R0-3	2000	6	2.0
AF-75-R0-4	2000	6	2.4
AF-75-R1-1	1500	4	1.6
AF-75-R1-2	2500	4	1.6
AF-75-R1-3	1500	6	2.4
AF-75-R1-4	2500	6	2.4
AF-75-R1-5	1500	8	1.6
AF-75-R1-6	2500	8	1.6
AF-75-R1-7	1500	10	2.4
AF-75-R1-8	2500	10	2.4
AF-75-R1-9	2000	7	2.0
AF-75-R2-1	2000	6	1.6
AF-75-R2-2	3000	6	1.6
AF-75-R2-3	2000	6	2.0
AF-75-R2-4	3000	6	2.0
AF-75-R2-5	2000	6	2.4
AF-75-R2-6	3000	6	2.4
AF-75-R2-7	2000	8	1.6
AF-75-R2-8	3000	8	1.6
AF-75-R2-9	2000	8	2.0
AF-75-R2-9.1	2000	8	2.0
AF-75-R2-9.2	2000	8	2.0
AF-75-R2-9.3	2000	8	2.0
AF-75-R2-10	3000	8	2.0
AF-75-R2-10.1	3000	8	2.0
AF-75-R2-10.2	3000	8	2.0
AF-75-R2-10.3	3000	8	2.0
AF-75-R2-11	2000	8	2.4
AF-75-R2-12	3000	8	2.4
AF-75-R2-13	2000	10	1.6
AF-75-R2-14	3000	10	1.6
AF-75-R2-15	2000	10	2.0
AF-75-R2-16	3000	10	2.0
AF-75-R2-17	2000	10	2.4
AF-75-R2-18	3000	10	2.4
AF-75-R3-1	1000	6	1.6
AF-75-R3-2	1000	6	2.0

AF-75-R3-3	1000	6	2.4
AF-75-R3-4	1000	8	1.6
AF-75-R3-5	1000	8	2.0
AF-75-R3-5.1	1000	8	2.0
AF-75-R3-5.2	1000	8	2.0
AF-75-R3-5.3	1000	8	2.0
AF-75-R3-6	1000	8	2.4
AF-75-R3-6.1	1000	8	2.4
AF-75-R3-6.2	1000	8	2.4
AF-75-R3-6.3	1000	8	2.4
AF-75-R3-7	1000	10	1.6
AF-75-R3-8	1000	10	2.0
AF-75-R3-9	1000	10	2.4
AF-75-R4-1	2000	7	2.0
AF-75-R4-1.1	2000	7	2.0
AF-75-R4-1.2	2000	7	2.0
AF-75-R4-1.3	2000	7	2.0
AF-75-R4-2	1000	7	2.2
AF-75-R4-3	3000	7	2.2
AF-75-R4-4	1000	9	2.2
AF-75-R4-5	3000	9	2.2
AF-75-R4-6	2000	9	2.0
AF-75-R4-7	2000	7	2.4
AF-75-R4-8	2000	9	2.4
AF-75-R4-9	2000	8	2.2

A.2 Hardness test samples

Sample name	RS (rpm)	JT (s)	PD (mm)	Type	Load
AF-75-H2-1	1000	8	2.4	Transverse	HV 0.5
AF-75-H2-2	2000	8	2.4	Transverse	HV 0.5
AF-75-H2-3	3000	8	2.4	Transverse	HV 0.5
AF-75-H2-4	1000	6	1.6	Transverse	HV 0.5
AF-75-H2-5	1000	8	1.6	Transverse	HV 0.5
AF-75-H2-6	1000	10	1.6	Transverse	HV 0.5
AF-75-H2-7	3000	6	1.6	Transverse	HV 0.5
AF-75-H2-8	3000	10	1.6	Transverse	HV 0.5
AF-75-H2-9	3000	8	2	Full map	HV 1
AF-75-H2-10	2000	8	2.4	Full map	HV 1

A.3 Strength test samples

A.3.1 Lap shear strength test samples

Sample name	RS (rpm)	JT (s)	PD (mm)	Surface class	LSS (kN)	Failure mode
AF-75-T1-1.1	1000	6	1.6	1	7.35	N
AF-75-T1-2.1	3000	6	1.6	1	4.41	N
AF-75-T1-3.1	1000	8	1.6	1	7.29	N
AF-75-T1-4.1	3000	8	1.6	1	3.14	N
AF-75-T1-5.1	1000	6	2.4	1	5.3	PU
AF-75-T1-6.1	3000	6	2.4	2	8.42	N
AF-75-T1-7.1	1000	8	2.4	1	8.2	PU
AF-75-T1-8.1	3000	8	2.4	3	8.42	PU + N
AF-75-T1-9.1	2000	7	2.0	2	7.87	PU
AF-75-T1-9.2	2000	7	2.0	2	7.37	PU
AF-75-T1-1.2	1000	6	1.6	3	5.64	N
AF-75-T1-2.2	3000	6	1.6	2	4.96	N
AF-75-T1-3.2	1000	8	1.6	3	6.43	PU
AF-75-T1-4.2	3000	8	1.6	1	4.97	N
AF-75-T1-5.2	1000	6	2.4	1	5.43	PU
AF-75-T1-6.2	3000	6	2.4	1	7.87	PU
AF-75-T1-7.2	1000	8	2.4	1	7.77	PU + N
AF-75-T1-8.2	3000	8	2.4	3	6.42	PU
AF-75-T1-9.3	2000	7	2.0	1	8.69	PU
AF-75-T1-9.4	2000	7	2.0	1	7.67	PU
AF-75-T1-1.3	1000	6	1.6	3	5.72	PU
AF-75-T1-2.3	3000	6	1.6	1	4.58	N
AF-75-T1-3.3	1000	8	1.6	2	6.49	PU
AF-75-T1-4.3	3000	8	1.6	1	4.85	N
AF-75-T1-5.3	1000	6	2.4	1	5.18	PU
AF-75-T1-6.3	3000	6	2.4	1	4.36	N
AF-75-T1-7.3	1000	8	2.4	2	10.24	PL + N
AF-75-T1-8.3	3000	8	2.4	1	9.97	N
AF-75-T1-9.5	2000	7	2.0	2	8.37	PU
AF-75-T1-9.6	2000	7	2.0	1	8.02	PU
AF-75-T3-1.1	1000	7	2.2	1	7.39	PU
AF-75-T3-2.1	3000	7	2.2	1	7.23	N
AF-75-T3-3.1	1000	9	2.2	1	8.36	PUL
AF-75-T3-4.1	3000	9	2.2	1	8.64	PUL
AF-75-T3-5.1	1000	8	2.0	1	8.46	PL
AF-75-T3-6.1	3000	8	2.0	1	7.28	N
AF-75-T3-7.1	1000	8	2.4	1	8.19	PL

AF-75-T3-8.1	3000	8	2.4	1	6.56	PU
AF-75-T3-9.1	2000	7	2.0	2	6.19	N
AF-75-T3-10.1	2000	9	2.0	1	6.32	N
AF-75-T3-11.1	2000	7	2.4	1	7.84	PUL
AF-75-T3-12.1	2000	9	2.4	1	8.36	PL
AF-75-T3-13.1	2000	8	2.2	1	8.34	PU
AF-75-T3-13.2	2000	8	2.2	2	7.72	N
AF-75-T3-1.2	1000	7	2.2	1	8.11	PU
AF-75-T3-2.2	3000	7	2.2	1	5.99	N
AF-75-T3-3.2	1000	9	2.2	1	7.96	PU
AF-75-T3-4.2	3000	9	2.2	2	7.34	N
AF-75-T3-5.2	1000	8	2.0	1	8.73	PU
AF-75-T3-6.2	3000	8	2.0	2	7.62	N
AF-75-T3-7.2	1000	8	2.4	2	8.24	PUL
AF-75-T3-8.2	3000	8	2.4	1	8.56	N
AF-75-T3-9.2	2000	7	2.0	2	4.59	PU
AF-75-T3-10.2	2000	9	2.0	1	6.63	N
AF-75-T3-11.2	2000	7	2.4	2	5.06	PU
AF-75-T3-12.2	2000	9	2.4	1	7.97	N
AF-75-T3-13.3	2000	8	2.2	1	7.79	N
AF-75-T3-13.4	2000	8	2.2	1	7.91	PU
AF-75-T3-1.3	1000	7	2.2	1	7.48	PU
AF-75-T3-2.3	3000	7	2.2	2	8.25	N
AF-75-T3-3.3	1000	9	2.2	1	9.38	PL
AF-75-T3-4.3	3000	9	2.2	2	9.09	PU
AF-75-T3-5.3	1000	8	2.0	1	8.85	PU
AF-75-T3-6.3	3000	8	2.0	2	7.92	PU
AF-75-T3-7.3	1000	8	2.4	2	8.25	PUL
AF-75-T3-8.3	3000	8	2.4	1	7.83	PUL
AF-75-T3-9.3	2000	7	2.0	1	7.65	N
AF-75-T3-10.3	2000	9	2.0	1	8.11	PUL
AF-75-T3-11.3	2000	7	2.4	1	8.14	PUL
AF-75-T3-12.3	2000	9	2.4	1	8.72	PL
AF-75-T3-13.5	2000	8	2.2	1	8.53	N
AF-75-T3-13.6	2000	8	2.2	1	7.79	N

A.3.2 Cross-tension strength test samples

Sample name	RS (rpm)	JT (s)	PD (mm)	Surface class	CTS (kN)	Failure mode
AF-75-T2-1.1	1000	6	1.6	1	0.36	N
AF-75-T2-2.1	3000	6	1.6	1	/	N
AF-75-T2-3.1	1000	8	1.6	3	0.70	N

AF-75-T2-4.1	3000	8	1.6	2	0.50	N
AF-75-T2-5.1	1000	6	2.4	2	0.98	PU
AF-75-T2-6.1	3000	6	2.4	2	0.84	PU
AF-75-T2-7.1	1000	8	2.4	1	2.24	PU
AF-75-T2-8.1	3000	8	2.4	1	1.97	PU
AF-75-T2-9.1	2000	7	2.0	2	0.58	PU
AF-75-T2-9.2	2000	7	2.0	1	1.49	PU
AF-75-T2-1.2	1000	6	1.6	2	0.50	N
AF-75-T2-2.2	3000	6	1.6	2	0.31	N
AF-75-T2-3.2	1000	8	1.6	1	0.99	N
AF-75-T2-4.2	3000	8	1.6	2	0.40	N
AF-75-T2-5.2	1000	6	2.4	2	1.00	PU
AF-75-T2-6.2	3000	6	2.4	1	1.14	N
AF-75-T2-7.2	1000	8	2.4	2	2.67	PU
AF-75-T2-8.2	3000	8	2.4	3	2.53	PU
AF-75-T2-9.3	2000	7	2.0	2	2.70	N
AF-75-T2-9.4	2000	7	2.0	1	0.72	PU
AF-75-T2-1.3	1000	6	1.6	2	1.03	N
AF-75-T2-2.3	3000	6	1.6	1	/	N
AF-75-T2-3.3	1000	8	1.6	1	0.81	N
AF-75-T2-4.3	3000	8	1.6	1	0.38	N
AF-75-T2-5.3	1000	6	2.4	1	1.14	PU
AF-75-T2-6.3	3000	6	2.4	1	0.80	N
AF-75-T2-7.3	1000	8	2.4	1	2.79	PL
AF-75-T2-8.3	3000	8	2.4	1	1.21	N
AF-75-T2-9.5	2000	7	2.0	1	0.73	PU
AF-75-T2-9.6	2000	7	2.0	1	0.48	PU

A.4 Temperature test samples

Sample name	RS (rpm)	JT (s)	PD (mm)	Max Temp (°C)	Dist from weld centre (mm)
TM-R3-1.1	1000	6	1.6	170	13
TM-R3-1.2	1000	6	1.6	153	14
TM-R2-1.1	2000	6	1.6	196	14
TM-R2-1.2	2000	6	1.6	176	15
TM-R2-2.1	3000	6	1.6	194	14
TM-R2-2.2	3000	6	1.6	210	13
RM-R2-3.1	2000	6	2.0	186	14
RM-R2-3.2	2000	6	2.0	204	13
TM-R2-14.1	3000	10	1.6	262	14
TM-R2-14.2	3000	10	1.6	263	14
TM-R2-18.1	3000	10	2.4	246	14

TM-R3-7.1	1000	10	1.6	220	14
TM-R3-7.3	1000	10	1.6	226	14
TM-R3-9.1	1000	10	2.4	252	14
TM-R3-4.1	1000	8	1.6	225	14
TM-R3-4.2	1000	8	1.6	212	14
TM-R3-4.3	1000	8	1.6	194	14
TM-R3-6.1	1000	8	2.4	236	14
TM-R3-6.2	1000	8	2.4	215	14
TM-R3-6.3	1000	8	2.4	212	14
TM-R2-11.1	2000	8	2.4	226	14
TM-R2-11.2	2000	8	2.4	228	14
TM-R2-11.3	2000	8	2.4	218	14
TM-R2-12.1	3000	8	2.4	226	14
TM-R2-11.2	2000	8	2.4	255	14
TM-R2-11.3	2000	8	2.4	241	14

Appendix B: Cross tension clamps

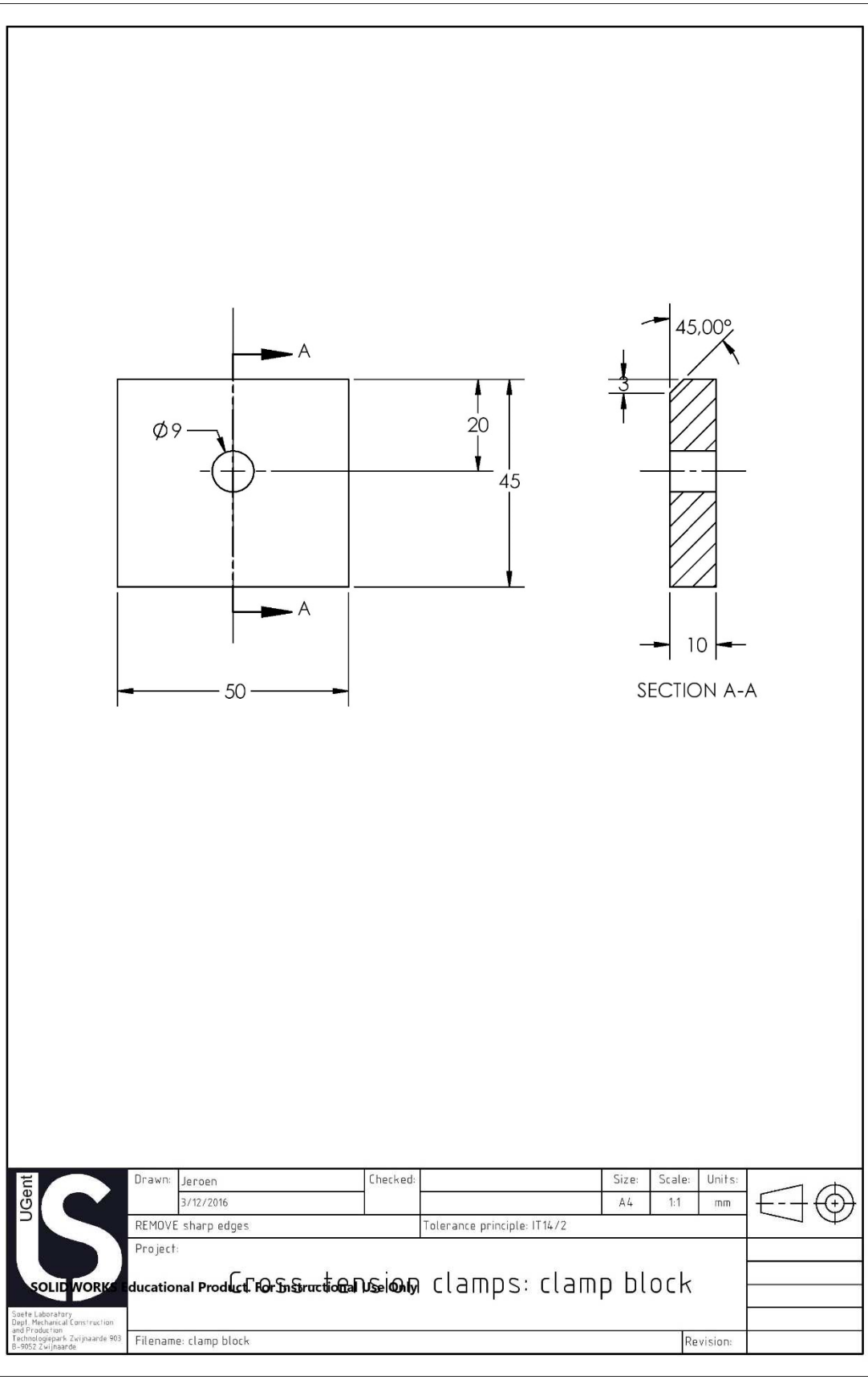

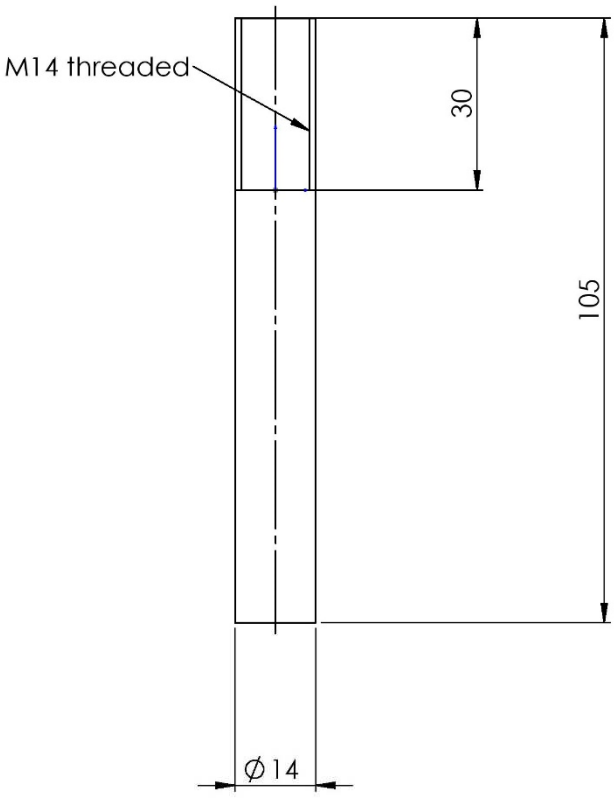

Drawn: Jeroen 6/12/2016	Checked:		Size: A4	Scale: 1:1	Units: mm	
REMOVE sharp edges	Tolerance principle: IT14/2					
Project: Cross tension clamps: pull rod						
Filename: pull rod					Revision:	

UGent
Soete Laboratory
Dept. Mechanical Construction and Production
Technologiepark Zwijnaarde 903
B-9052 Zwijnaarde

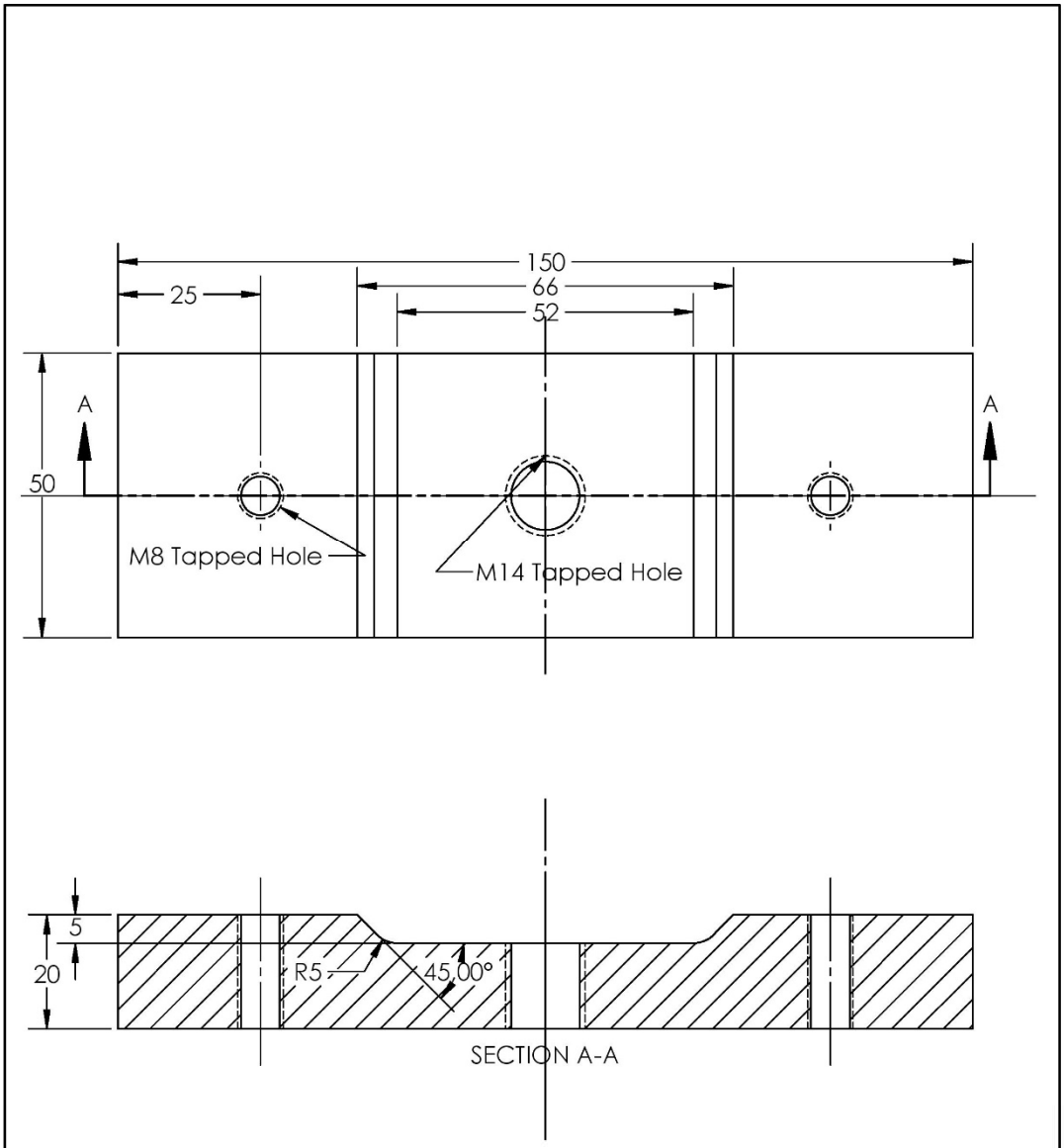

Drawn: Jeroen 3/12/2016	Checked:		Size: A4	Scale: 1:1	Units: mm	
REMOVE sharp edges	Tolerance principle: IT14/2					
Project: Cross tension clamps: pull block						
Filename: pull block					Revision:	

UGent

SOLIDWORKS Educational Product. For Instructional Use Only

Soete Laboratory
Dept. Mechanical Construction and Production
Technologiepark Zwijnaarde 903
B-9052 Zwijnaarde

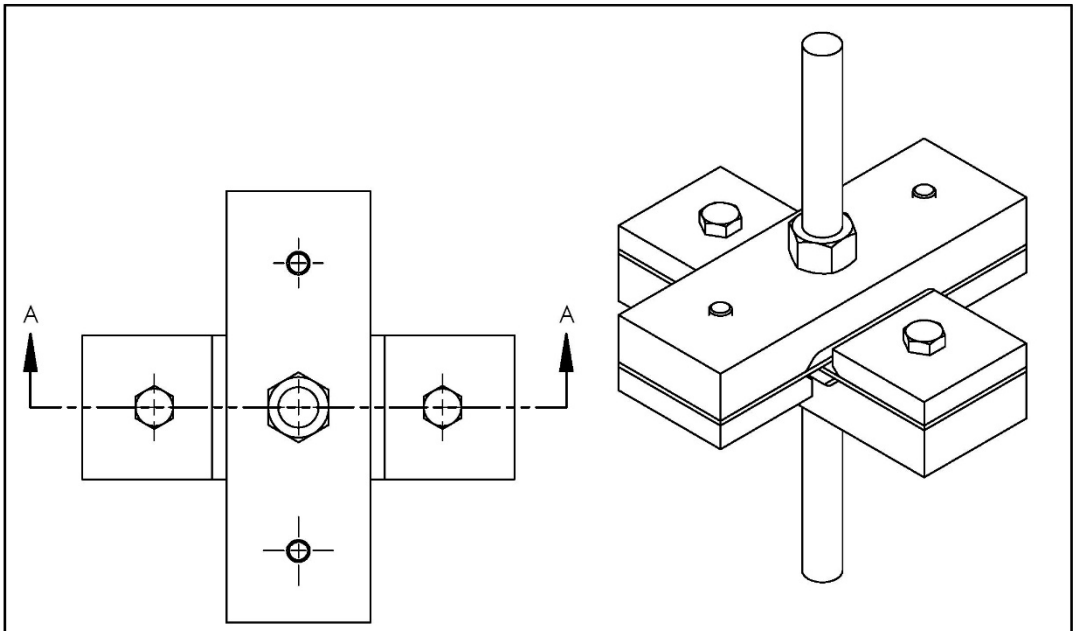

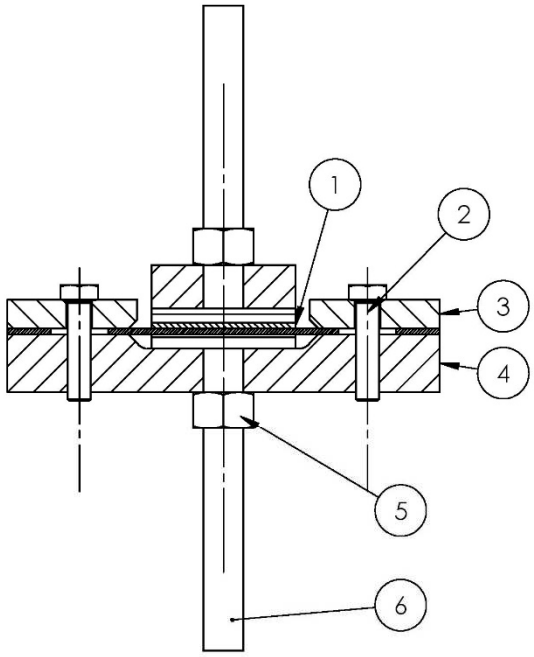

SECTION A-A

1.	test specimen	1
2.	M8x35 bolt	4
3.	clamp block	4
4.	pull block	2
5.	M8 nut	4
6.	M14 nut	2
7.	pull rod	2

UGent

Soete Laboratory
Dept. Mechanical Construction and Production
Technologiepark Zwijnaarde 903
B-9052 Zwijnaarde

Drawn:	Jeroen	Checked:		Size:	Scale:	Units:
	3/12/2016			A4	1:2	mm
REMOVE sharp edges		Tolerance principle: IT14/2				

Project:

clamping system

Filename: clamping system

Revision:

Appendix C: SCAD paper

METALLOGRAPHIC EVALUATION OF THE WELDABILITY OF HIGH STRENGTH ALUMINIUM ALLOYS USING FRICTION SPOT WELDING

J. Vercauteren[1], K. Faes[2] and W. De Waele[3]

[1] Ghent University, Belgium
[2]The Belgian Welding Institute, Belgium
[3] Ghent University, Laboratory Soete, Belgium

Abstract: Friction spot welding is a recent solid-state welding technique well suited for spot-joining lightweight materials in overlap condition. Aerospace and transport industries show great interest in this technique to join high-strength aluminium alloys, but published research is still limited. In this project, the link between process parameters and weld quality is investigated for EN AW-7075-T6 material. Techniques used are metallographic qualification, measurement of hardness reduction and lap shear strength. This paper focusses on the metallographic investigation of the weld region and its imperfections. Increasing joining time and heat input creates an easier material flow resulting in fewer imperfections. Limited plunge depths lead to typical interface imperfections. Variation in the rotational speed shows distinctive stir zone shapes as a consequence of severe stirring and frictional heat.

Keywords: Friction spot welding, EN AW-7075-T6, metallography, microstructure

1 INTRODUCTION

High strength lightweight materials, such as some aluminium alloys, gain importance in industry, especially in automotive and aeronautic fields [1-3]. Joining of these materials is an important step in the production of components or structures. Many joining techniques exist such as fusion welding, riveting, bolting, etc. Nevertheless, researchers keep looking for more efficient alternative techniques as each joining technology has its disadvantages [4]. Fusion welds can for example contain imperfections which deteriorate the mechanical strength of the bond. Furthermore, some high strength lightweight alloys suffer from low weldability issues [5]. Moreover, aluminium alloys are good thermal conductors which means that supplied heat rapidly distributes throughout the specimen. Keeping the specimen above the melting temperature thus requires a high energy input. Mechanical fasteners add non-negligible mass to the structure which is undesirable in lightweight applications.

Friction welding offers a solution to most of the issues concerning lightweight materials. This work focuses on the friction spot welding (FSpW) process, also referred to as refill friction stir spot welding (refill FSSW). It is part of a collective international research project called INNOJOIN [6], an acronym for innovative joining. FSpW is a solid-state welding process well suited for spot-joining lightweight materials in overlap configuration. It differs from the friction stir spot weld (FSSW) process in the ability to refill the keyhole and hence eliminates its major disadvantages: stress concentration and corrosion at the keyhole. Friction spot welding is seen as a green manufacturing method because no additional filler material is required and there is no waste material [4,7]. The welding process has potential for mass production lines as the welding time is relatively short and the process can be automated easily.

The overall goal of this work is the evaluation of the weldability of high-strength aluminium alloys using friction spot welding. In previous work [8] the weldability of alloy EN AW-7475-T761 has been evaluated; this study focuses on aluminium alloy EN AW-7075-T6. This paper mainly focusses on the metallographic investigation and aims to link the most important process parameters to the quality of the weld regarding imperfections.

2 FRICTION SPOT WELDING

2.1 Process description

The friction spot welding process is a solid-state spot joining technology to join sheets in overlap condition. The solid-state property implies that the working temperature does not exceed the melting temperature of the materials. The joint is fully generated by frictional heat and plastic work whereby a metallurgical bond is formed. FSpW is a rather recent technique as it was invented by the GKSS research centre in 1999 [9].

The non-consumable tool consists of three components: a concentric clamping ring, sleeve and pin. All three components can act independently in the axial direction. The pin and sleeve can rotate about their axis in the same direction. The function of the clamping ring is to fix the sheets rigidly in overlap configuration against a backing anvil while the welding process takes place.

The four process stages are depicted in Figure 1. In the first stage, the clamping ring fixes the plates while the pin and sleeve start rotating against the upper plate. As from the second stage the sleeve plunges into the material while rotating at high rotational speed. The pin rises, creating a cavity of the exact required volume for the plasticised material. The sleeve displaces the material underneath and forces it into the cavity provided by the pin rise. Between the second and third stage, the sleeve reaches a pre-defined depth. The frictional heat and mechanical work delivered by the stirring, bond the sheets at their interface. In the third stage, tool and sleeve translation reverse. The plasticised material that accumulated under the pin is pushed back in the keyhole created by the sleeve plunging. When retreating the complete tool in stage four, a flat surface appears. A typical surface view of such a spot weld is shown in Figure 2. Three concentric rings originating from contact with clamping ring, sleeve and pin are clearly visible.

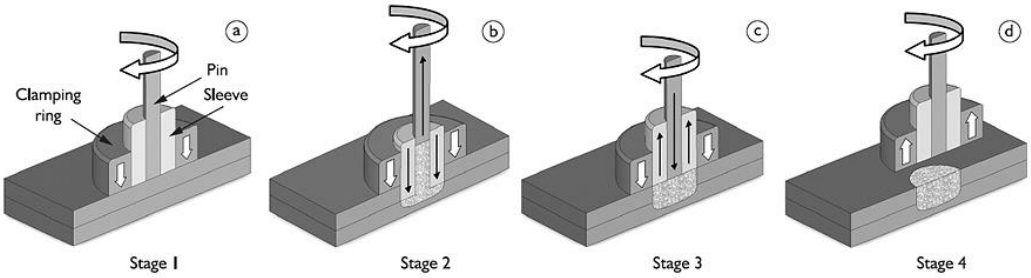

Figure 1: Friction spot welding stages [10]

The process, and thus the weld quality, is controlled by several welding parameters. This work focusses on three parameters: rotational speed, plunge depth and joining time.

The rotational speed (RS) of the pin and sleeve controls the material flow. The upper value is limited by the machine capacity, while the lower value is restricted by a minimum required heat input. The amount of heat input determines the softening of the workpiece. The softer the material, the easier the tool can plunge in. However, this also results in a wider heat affected zone around the weld nugget. A critical, and very material dependent parameter is the plunge depth (PD) [11]. This is the maximum depth the sleeve plunges into the material measured from the top surface of the upper sheet. The plunge depth is often chosen such that the sleeve plunges in the lower sheet for about 25-30 % of the lower plate thickness. This is in good agreement with the common practice in FSW [12]. A third process parameter is the joining time (JT) which consists of three sub-parameters: plunge time (PT), dwell time (DT) and retraction time (RT). These time parameters are graphically visualized in Figure 3. The joining time influences the amount of heat input, the plunge time and retraction time determine the rate of plastic deformation of the weld zone. Related parameters are the plunge rate (PR) and retraction rate (RT).

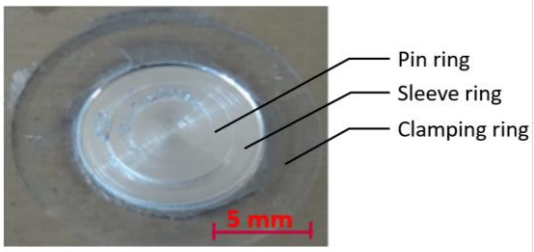

Figure 2: Typical appearance of a friction spot weld in EN AW-7475-T761 [13]

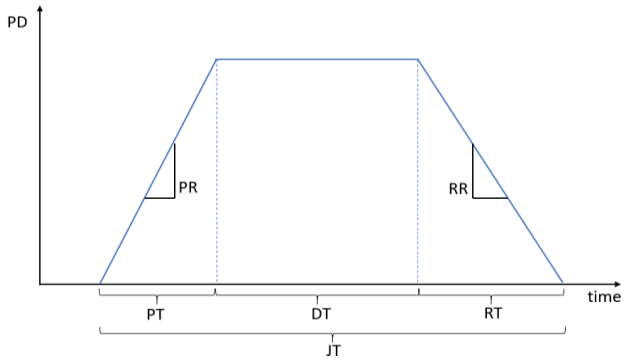

Figure 3: Plunge depth over time and the different time parameters

2.2 Weld cross-section

A friction spot weld consists of different microstructural regions, called weld zones. Figure 4 shows the stir zone (SZ) and the thermo-mechanically affected zone (TMAZ). A third weld zone, the heat-affected zone (HAZ), is not clearly visible on the optical microscope image. All weld zones differ in microstructure and mechanical properties from the base material (BM) as a result of the welding process. The SZ is the centre of the weld and has approximately the same width as the sleeve diameter. It is characterized by refined and equiaxed grains as a result of dynamic recrystallization. This is the effect of the high strain rate and the high local temperatures during the stirring process [14]. Next to the SZ, the TMAZ exists as a transitional region between the SZ and the HAZ. This zone is formed by moderate deformations and temperatures. The microstructure is characterized by elongated and deformed grains caused by the material flow [15]. As the TMAZ is a transition region, it is hard to define the boundaries. The HAZ is the first zone that is not affected by plastic deformations. As the name suggests, the microstructure of this zone is influenced by the conducted heat from the welding process. Grain growth has occurred due to the thermal treatment, but the exact boundary between the TMAZ and the HAZ is difficult to localise microscopically. Far enough from the weld centre, all effects from the welding process on the microstructure disappear. This is where the HAZ ends and the BM starts.

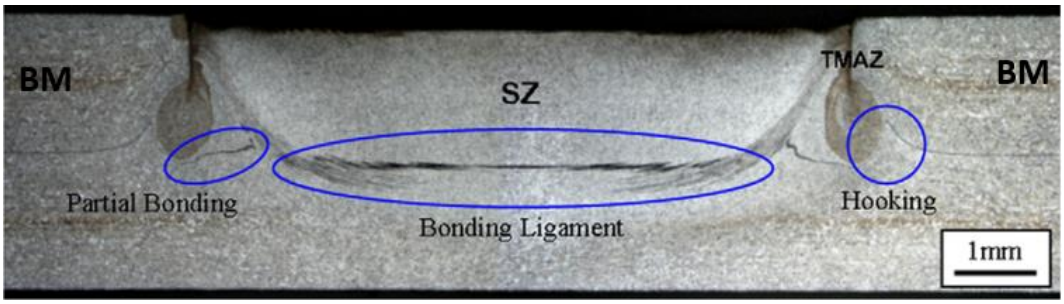

Figure 4: Typical cross-section of a FSpW weld in EN AW-6181-T4 [15].

Three geometrical features are often reported in metallographic inspection: hooking, partial bonding and bonding ligament. The location and appearance of these geometrical features are indicated in Figure 4. The hook feature is a transitional zone between the completely bonded regions and separated interfaces. It is suggested that its formation arises from the plastic upward bending of the interface due to tool penetration into the lower sheet. The importance of hooking lies in the fact that tensile shear strength of a joint decreases monotonically with increasing hook height [16]. The bonding ligament is a region of good adhesion between the upper and lower sheet material [15]. It is located underneath the stir zone and forms the strongest metallurgical bond in the weld. Tier et al. [11] showed that a longer, flatter and stronger bonding ligament can be obtained in EN AW-5042-O for lower rotational speeds. For larger rotational speed, the bonding ligament is curved upwards and the effective bonding ligament length is smaller. However, the presence of the bonding ligament is not always visible in all materials. Finally, the partial bonding zone is a transition region between the hooking and the bonding ligament with minor bonding strength.

Apart from the features described above, imperfections related to improper welding parameter combinations can occur such as lack of mixing, void inclusions or incomplete refill. All these imperfections are located along the path of the sleeve plunge and thus associated with the material flow. Incomplete refill can be partly assigned to the extrusion of material into the tolerance gap between the clamping ring and the sleeve [17].

3 EXPERIMENTAL STUDY

3.1 Material and equipment

In the present investigation, overlap joints were produced using sheets in the aluminium alloy EN AW-7075-T6, which is often used for aerospace applications. The sheets had a thickness of 1.6 mm. The chemical composition of the alloy is given in Table 1.

Table 1: Typical chemical composition of EN AW-7075-T6 in weight % [18]

Al	Cr	Cu	Fe	Mg	Mn	Si	Ti	Zn	Other
87.2-91.4	0.18-0.28	1.2-2	0-0.5	2.1-2.9	0-0.3	0-0.4	0-0.2	5.1-6.1	0-0.15

The experiments were performed using commercial friction spot welding equipment RPS 100 (Harms & Wende, Germany). The welding machine is equipped with a main head, which contains the welding tool. The clamping ring, sleeve and pin have an outer diameter of respectively 14.5, 9.0 and 6.0 mm. The machine is capable of applying axial forces up to 15 kN and rotational speeds up to 3300 rpm. Both the pin and the sleeve are provided with several circumferential grooves. This is done to enhance the material flow during the process [11].

3.2 Measurements

Welds in overlap configuration are produced with different process parameter combinations. After welding, a longitudinal section through the centre of the weld nugget was embedded, ground and polished to investigate using an Olympus MX51 optical microscope. Each sample is first inspected in the non-etched condition as this facilitates the detection of imperfections. The total area percentage of imperfections in the cross-section is calculated afterwards. Figure 5 shows a non-etched cross section with several imperfections and a coloured version with detected imperfections in red. The total area percentage of imperfections is calculated as the percentage red of the complete rectangle. Only imperfections with a minimum area of 0.002 square millimetres are taken into account. The global percentage of imperfections gives an indication of the overall weld quality, but neglects that some imperfections are more dangerous than others. Sharp, fine imperfections like a non-bonded interface lead to higher stress concentrations than spherical voids. Additional measurements were performed on two types of imperfections: the depth of the incomplete refill and the width of the non-bonded interface.

Sequentially, the samples were etched using Keller's reagent to reveal the weld microstructure. Different regions were inspected in detail.

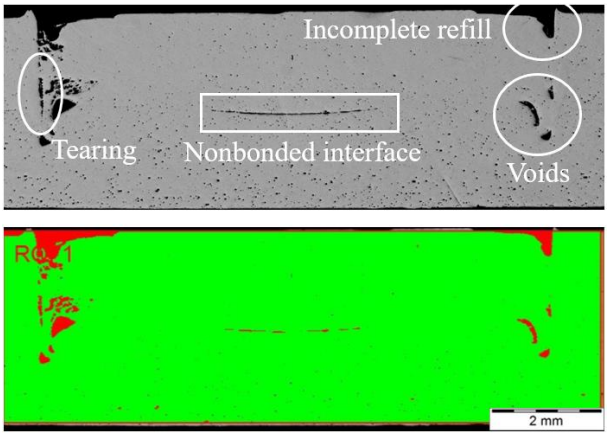

Figure 5: Non-etched cross-section (top) and area percentage of imperfections (bottom)

3.3 Overview of the experiments

The three main process parameters (rotational speed, plunge depth and joining time) were varied on three levels. An overview of the values is given in Table 2. All 27 possible combinations were investigated by metallographic inspection. Plunge rate and retraction rate were kept constant at a rate of 0.8 mm/s. Dwell time follows from the predefined joining time. Clamp pressure was fixed at a level of 3.5 bar.

Table 2: Parameter combinations

RS (rpm)	1000 – 2000 – 3000
PD (mm)	1.6 – 2.0 – 2.4
JT (s)	6 – 8 – 10

4 RESULTS

4.1 Influence of joining time

The joining time is closely related to the amount of heat input into the weld. Recall that the total joining time consists of three different parts. Increasing the joining time without changing the other parameters is equivalent to increasing the dwell time of the tool. Figure 6 compares three (non-)etched cross-sections of welds produced at a rotational speed of 2000 rpm, a plunge depth of 1.6 mm and three different joining times of respectively 6, 8 and 10 s. For increasing joining time the incomplete refill imperfection disappears, leading to an almost perfect cross-section. However, it is important to notice that the weld combination at the middle

(JT = 8s) contains a non-bonded interface which is probably more dangerous than the large incomplete refill imperfection in the upper weld. The etched stir zone becomes darker for longer welding times, indicating a finer grain size at the nugget centre. The recrystallized zone also reaches deeper into the lower sheet, although the plunge depth is unchanged. These are consequences of the increased heat input.

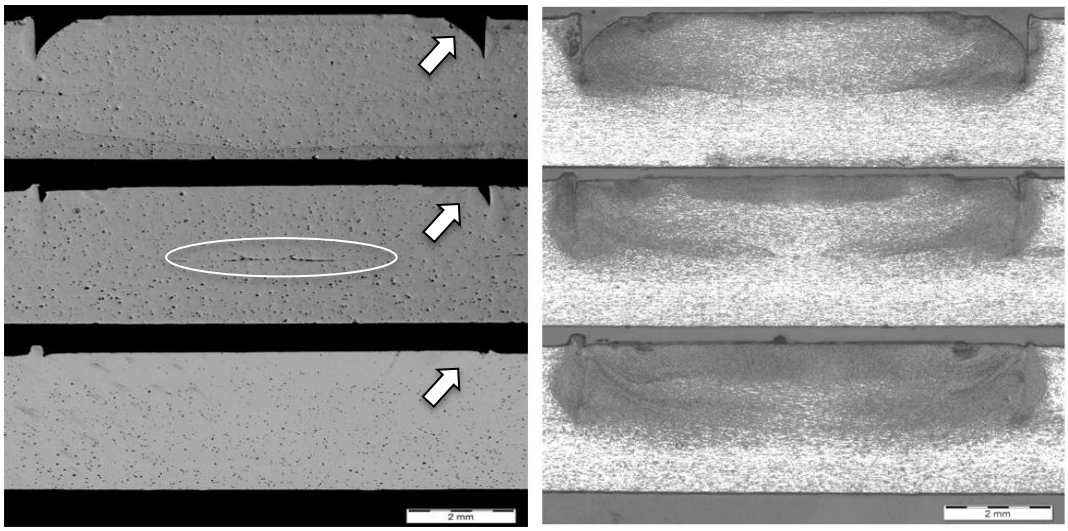

Figure 6: Varying joining time: 6 s (top), 8 s (middle), 10 s (bottom)

The influence of the joining time as illustrated in Figure 6 is a global effect throughout all weld samples. Figure 7 and Figure 8 show imperfection measurements at different joining times and rotational speeds. Measurement points at the same rotational speed and joining time differ in plunge depth, no replications were made. The measurements show a large variation and therefore a dashed trendline of mean values is added to the graphs. It is clear that overall both the total area percentage of imperfections and the depth of incomplete refill decrease with increasing the joining time. Especially the improvement from 6 s to 8 s joining time is significant. Only the parameter combination at the lowest rotational speed (RS=1000 rpm) and the shortest joining time (JT=6 s) does not correspond with the overall trend.

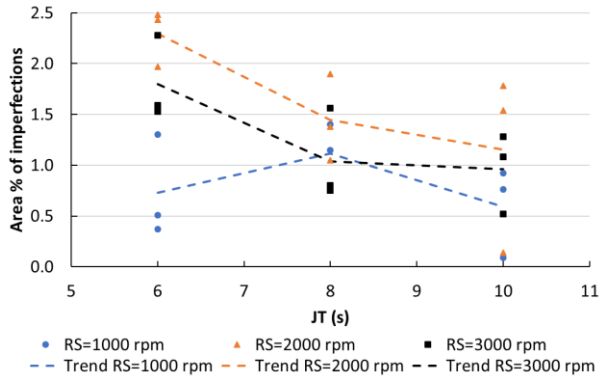

Figure 7: Mean area % of imperfections at varying JT

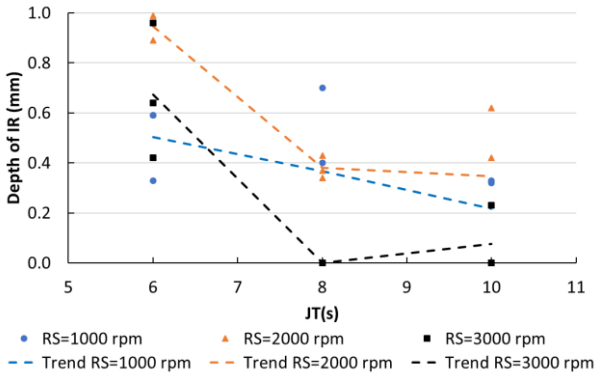

Figure 8: Mean depth of IR at varying JT

4.2 Influence of plunge depth

The plunge depth was varied starting from the upper plate thickness (1.6 mm) up to 50% into the lower plate (2.4 mm). From the experiments, it seems that the plunge depth of 1.6 mm is prone to imperfections at the sheet interface. The absence of the tool penetration into the lower plate does not create a strong interface bond. Welds containing non-bonded interfaces and partial bonding features were always produced with this low plunge depth. Figure 9 shows at the left a non-bonded interface at the centre of the stir zone. This sharp and narrow imperfection can be detrimental in lap shear loading. At the right, a partial bonding is displayed. The wrinkling line starts from the separated surfaces outside the weld nugget and penetrates into the stir zone. On the same picture, a void along the sleeve path is visible. Hooking features were discovered in the stir zone for some of the welds produced at the smallest plunge depth. Figure 10 shows two hook features inside the stir zone. The lower one originates from the sheet interface and is formed during the plastic deformation of the lower plate. The upper hook is formed during the refilling stage. The void in the corner of

the weld shows that the keyhole of the sleeve is not properly refilled. For deeper plunge depths, the hook never reaches into the weld nugget. A slight decrease in voids is observed for deeper plunge depths, but this influence is not significant.

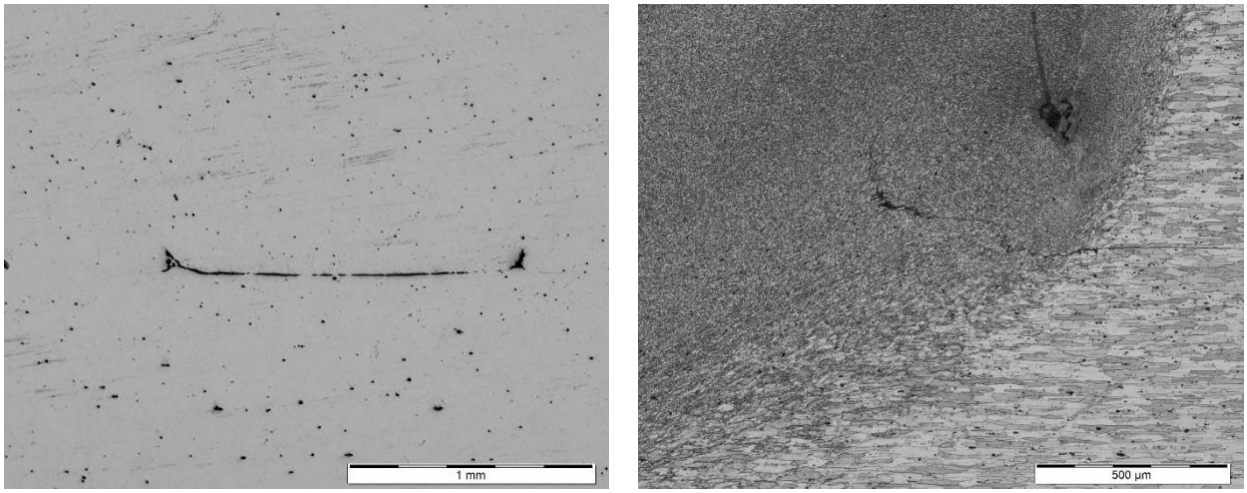

Figure 9 Non-bonded interface (left) and partial bonding (right) at a plunge depth of 1.6 mm

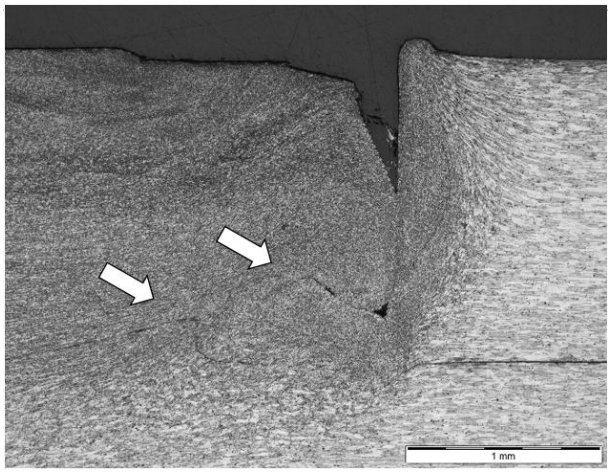

Figure 10: Hook features at a plunge depth of 1.6 mm

4.3 Influence of rotational speed

Figure 11 shows three etched cross-sections of welds produced with a joining time of 8 s, a plunge depth of 2 mm and three varying rotational speeds. The difference in shape and size of the stir zone is very distinctive. At lower rotational speed, the affected zone is curved and reaches much deeper than the plunge depth. At high rotational speed, the stir zone depth is rectangular and limited to the plunge depth. Furthermore, the grains are finer at low rotational speed, with only a vertical zone of coarse grains right underneath the pin zone. At the centre of the pin, the circumferential velocity is zero and the least amount of stirring takes place. At higher rotational speed, horizontal bands of fine grains become visible. The reason for this difference is not yet completely understood. FSpW machine data showed that 60% more torque was required to produce a weld at 1000 rpm compared with welds at 2000 and 3000 rpm, indicating a higher coefficient of friction between tool and workpiece. It is not recommended to weld at 1000 rpm when the machine is in a cold state as this has led to overcurrent warnings of the spindle.

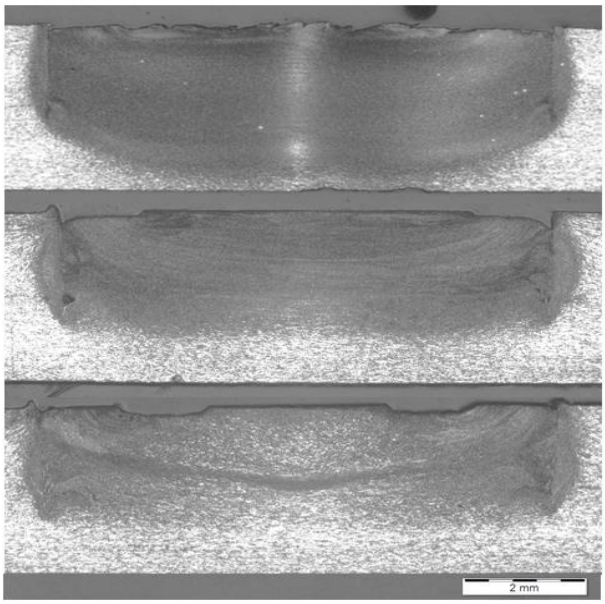

Figure 11:Varying RS: 1000 rpm (top), 2000 rpm (middle) and 3000 rpm (bottom)

In [19], effects of rotational speed on the microstructure and mechanical properties of friction stir welded 7075-T6 Al alloys were investigated. It was found that with increasing the rotational speed, higher peak temperatures and grain coarsening were present. Higher strain rates result in fine recrystallized grains, but higher temperatures improve the grain growth of the recrystallized grains [19]. It is a trade-off between these two effects that determines the final grain size.

As the rotational speed is closely related to the material flow, it has a significant effect on the amount of imperfections. Figure 12 and Figure 13 show the influence of the rotational speed in a similar way as for the joining time in section 4.1. In both graphs, welds with a rotational speed of 2000 rpm perform worst. The incomplete refill imperfection is smallest at the highest rotational speed combined with medium to long joining times, as a result of excessive stirring and a fluent material flow. On both graphs, the earlier discussed influence of the joining time on imperfection size is again visible.

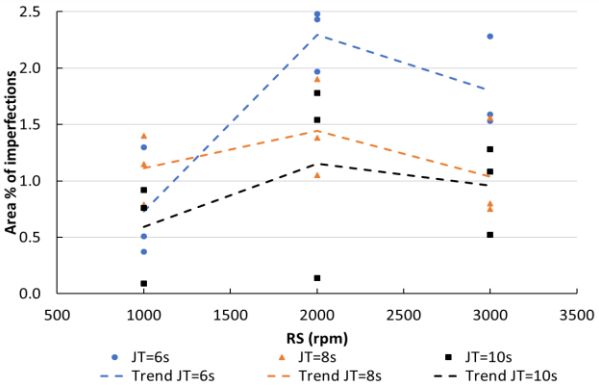

Figure 12: Mean area % of imperfections at varying RS

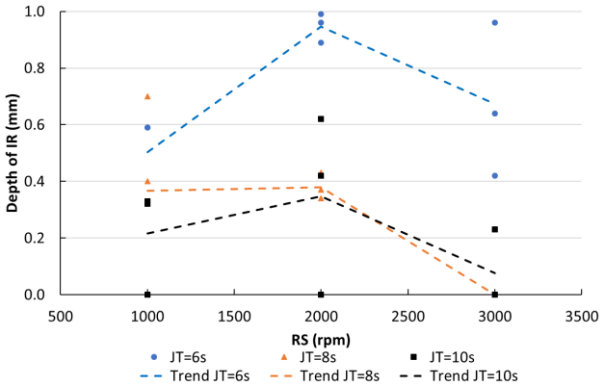

Figure 13: Mean depth of IR at varying RS

5 CONCLUSIONS

FSpW is a recent solid-state joining technique with a lot of potential. This work studied the effect of three main welding parameters (JT, PD and RS) on the metallographic quality of the weld cross-section. Lap joints were produced in 1.6 mm EN AW-7075-T6 aluminium alloy. Overall imperfection percentage of the weld decreased for increasing joining time and thus heat input. Most imperfections were formed at a rotational speed of 2000 rpm, while the incomplete refill imperfection was minimal at a rotational speed of 3000 rpm. Low plunge depths, equal to the sheet thickness, should be avoided as this frequently results in imperfections at the interface such as non-bonded interfaces, partial bonding and hooking. Especially the rotational speed determines the final shape of the stir zone and its grain size. It is believed that a trade-off between dynamic recrystallization and grain growth is the cause of this phenomenon. The metallographic observations will be linked to mechanical properties as hardness and strength in next research steps.

6 ACKNOWLEDGEMENTS

The authors would like to acknowledge the support of the employees of the Belgian Welding Institute (BWI) for the metallographic training and support.

7 REFERENCES

[1] F. Alshmri, 'Lightweight Material: Aluminium High Silicon Alloys in The Automotive Industry', in *Advanced Technologies in Manufacturing, Engineering and Materials, Pts 1-3*, vol. 774–776, Y. H. Kim and P. Yarlagadda, Eds. Stafa-Zurich: Trans Tech Publications Ltd, 2013, pp. 1271–1276.
[2] R. Dhingra and S. Das, 'Life cycle energy and environmental evaluation of downsized vs. lightweight material automotive engines', *J. Clean Prod.*, vol. 85, pp. 347–358, Dec. 2014.
[3] K. Grigoriou and A. P. Mouritz, 'Comparative assessment of the fire structural performance of carbon-epoxy composite and aluminium alloy used in aerospace structures', *Mater. Des.*, vol. 108, pp. 699–706, Oct. 2016.
[4] R. Rajan, P. Kah, B. Mvola, and J. Martikainen, 'Trends in Aluminium Alloy Development and Their Joining Methods', *Rev. Adv. Mater. Sci.*, vol. 44, no. 4, pp. 383–397, 2016.
[5] T. Rosendo *et al.*, 'Mechanical and microstructural investigation of friction spot welded AA6181-T4 aluminium alloy', *Mater. Des.*, vol. 32, no. 3, pp. 1094–1100, Mar. 2011.
[6] 'INNOJOIN: Development and evaluation of advanced welding technologies for multi-material design with dissimilar sheet metals | www.bil-ibs.be'. [Online]. Available: http://www.bil-ibs.be/en/onderzoeksproject/innojoin-development-and-evaluation-advanced-welding-technologies-multi-material-d. [Accessed: 27-Apr-2017].
[7] T. Rosendo, M. Tier, J. Mazzaferro, C. Mazzaferro, T. R. Strohaecker, and J. F. Dos Santos, 'Mechanical performance of AA6181 refill friction spot welds under Lap shear tensile loading', *Fatigue Fract. Eng. Mater. Struct.*, vol. 38, no. 12, pp. 1443–1455, Dec. 2015.
[8] T. Kolba, K. Faes, and W. De Waele, 'Experimental investigation of the weldability of high strength aluminium using friction spot welding'. [Online]. Available: http://ojs.ugent.be/SCAD/article/view/3638.
[9] T. Montag, J.-P. Wulfsberg, H. Hameister, and R. Marschner, 'Influence of Tool Wear on Quality Criteria for Refill Friction Stir Spot Welding (RFSSW) Process', *Procedia CIRP*, vol. 24, pp. 108–113, Jan. 2014.
[10] 'Friction spot welding | www.bil-ibs.be'. [Online]. Available: http://www.bil-ibs.be/en/friction-spot-welding. [Accessed: 02-Nov-2016].
[11] M. D. Tier *et al.*, 'The influence of refill FSSW parameters on the microstructure and shear strength of 5042 aluminium welds', *J. Mater. Process. Technol.*, vol. 213, no. 6, pp. 997–1005, Jun. 2013.
[12] M. A. D. Tier *et al.*, 'A Study About the Mechanical Properties of Alclad AA2024 Connections Processed by Friction Spot Welding 1', in *ResearchGate*, 2009.
[13] O. Bilouet, 'Soudage par Friction Spot d'assemblages d'alliages d'aluminium', Mons, Belgique, Jan-2016.
[14] A. Gerlich, G. Avramovic-Cingara, and T. H. North, 'Stir zone microstructure and strain rate during Al 7075-T6 friction stir spot welding', *Metall. Mater. Trans. A-Phys. Metall. Mater. Sci.*, vol. 37A, no. 9, pp. 2773–2786, Sep. 2006.
[15] T. Rosendo *et al.*, 'Mechanical and microstructural investigation of friction spot welded AA6181-T4 aluminium alloy', *Mater. Des.*, vol. 32, no. 3, pp. 1094–1100, Mar. 2011.
[16] J. Y. Cao, M. Wang, L. Kong, and L. J. Guo, 'Hook formation and mechanical properties of friction spot welding in alloy 6061-T6', *J. Mater. Process. Technol.*, vol. 230, pp. 254–262, Apr. 2016.
[17] Y. Q. Zhao, H. J. Liu, S. X. Chen, Z. Lin, and J. C. Hou, 'Effects of sleeve plunge depth on microstructures and mechanical properties of friction spot welded alclad 7B04-T74 aluminum alloy', *Mater. Des.*, vol. 62, pp. 40–46, Oct. 2014.
[18] *CES EduPack 2016*. Cambridge, UK: Granta Design Limited.
[19] H. Rezaei and H. Bisadi, 'Effect of rotational speeds on microstructure and mechanical properties of friction stir-welded 7075-T6 aluminium alloy', *ournal of Mechanical Engineering Science*, vol. Proceedings of the Institution of Mechanical Engineers Part C, no. vols 203-210, Aug. 2011.